Aus der/dem Abteilung/Funktionsbereich für molekulare Kardiologie

(Leiter/in: Univ. - Prof. Dr. Jens Fielitz)

der/dem Klinik und Poliklinik / Institut für Innere Medizin B, Kardiologie

(Direktor/in: Univ.- Prof. Dr. Stephan B. Felix)

der Universitätsmedizin der Universität Greifswald

Thema: MuRF1 und MuRF3 steuern koordinativ die Energiehomöostase des Herz- und Skelettmuskels, durch Regulation der mitochondrialen Funktion/MuRF1 and MuRF3 coordinately regulate the energy homeostasis of heart and skeletal muscle by regulation of mitochondrial function

Inaugural - Dissertation

zur

Erlangung des akademischen

Grades

Doktor der Wissenschaften in der Medizin

(Dr. rer. med.)

der

Universitätsmedizin

der

Universität Greifswald

2023

vorgelegt von:

Elisa Martin

geb. am: 28.12.1991

in: Mainz

Dekan/in: Prof. Dr. Karlhans Endlich

1. Gutachter/in: Prof. Dr. Jens Fielitz

2. Gutachter/in: Prof. Dr. Volker Adams

(3. Gutachter/in:)

Ort, Raum: Forschungscluster III, Seminarraum A5.1.15

Tag der Disputation: 26.03.2024

Meinen Eltern

1. Summary

The maintenance of protein homeostasis in muscle by degradation systems, e.g. the autophagy lysosomal pathway (ALP) and the ubiquitin-proteasome system (UPS), is of great importance. It prevents the accumulation of nonfunctioning and not properly folded proteins, which can lead to protein aggregate myopathies (PAMs) and several other protein storage diseases. Degradation by the UPS depends on the transfer of ubiquitin to a target protein. This happens in a cascade of E1-E2-E3 proteins. This process is also involved in protein location and regulation of protein activity. E3 ligases are often tissue specific. Muscle RING-finger proteins (MuRFs) are a family of really interesting new gene (RING)-Finger E3 ubiquitin ligases, that are almost exclusively expressed in the striated muscle. They play a role in muscle wasting, but are also important for the maintenance of the structure of striated muscle. MuRF proteins are also involved in the regulation of the striated muscle energy metabolism. Previous work has demonstrated that MuRF1/MuRF3 DKO mice show a protein surplus myopathy characterized by an accumulation of myosin heavy chain proteins in striated muscles and a reduction in function of both heart and skeletal muscle. The aim of this study was to test the hypothesis that the myopathic phenotype of MuRF1/MuRF3 DKO mice is mediated by a disturbed energy homeostasis in the heart and skeletal muscle, with focus on mitochondrial function. Because sex-specific differences have not been investigated in these mice so far, a further aim was to investigate any differences between male and female mice.

To test these hypotheses, we measured the weight of the heart and the hindlimb muscles tibialis anterior and soleus to detect a possible hypertrophy in the DKO mice. Hematoxylin and eosin staining of histological cross sections of the tibialis anterior were performed to investigate protein accumulations. Muscle function was quantitated via grip strength and specific force measurements. Possible changes in protein amounts were detected via mass spectrometry analyses and western blot analyses. Changes in gene expression were investigated by qRT-PCR. Coimmunoprecipitation was used to determine direct interactions between proteins. Protein stability and ubiquitination were investigated by cycloheximide (CHX) and ubiquitination assays, respectively.

DKO mice showed an increase in heart and skeletal muscle weights. Grip strength assays revealed limb weakness of DKO mice. H&E staining of histological cross sections of the tibialis anterior muscle (TA) showed protein aggregates within myofibers. Mass spectrometry analyses of proteins isolated from TA and heart muscle revealed an increase of muscle stress markers and structural proteins in DKO mice, while proteins involved in the energy metabolism were reduced. Especially interesting here were the proteins of the mitochondrial electron transport chain (ETC), which play a major role in the energy production of the mitochondria by catalyzing the phosphorylation of ADP to ATP, the universal energy carrier in all living organisms. These changes were more pronounced in TA compared to heart. Western blot and qRT-PCR results of ETC subunits supported our proteome data. They also revealed a sex-specific difference, in which the reduction ETC subunits was more pronounced in females than males. In female

TA NDUFB8, SDHB, UQCRC2, MTCO1 and ATP5 were significantly reduced compared to controls, while only UQCRC2 and ATP5 were decreased in male TA compared to controls. A significant reduction in gene expression of *Ndufb8*, *Sdhb*, *Mtco1* and *Atp5* was detected in TA of female mice compared to controls, while only *Ndufb8*, *Sdhb* and *Atp5* were decreased in male TA compared to controls. We observed the same pattern in Heart of male (protein: NDUFB8; mRNA: *Mtco1*) and female (protein: UQCRC2, MTCO1, ATP5; mRNA: *Sdhb*, *Mtco1*) DKO mice compared to their controls. The reduction in ETC subunits was paralleled by a reduction in complex I and complex III activity in the TA of DKO mice, but not in heart. However, this was only significant in the TA of female but not male mice. Mechanistical analyses using coimmunoprecipitation, cycloheximide chase and ubiquitination assays showed that MuRF1 physically interacted with the transcriptional repressor histone deacetylase 5 (HDAC5), mediated its ubiquitination as well as its UPS-dependent degradation. The absence of MuRF1 and MuRF3 in DKO mice let to an increase in the amounts of HDAC5 in TA. Because HDAC5 binds to PGC-1α, the master regulator of mitochondrial biogenesis (encoded by *Ppargc1a*), we investigated its gene expression in DKO muscle and found it to be reduced.

These data connect MuRF1 and MuRF3 directly to the striated muscle energy metabolism, by regulating mitochondrial function. The results provide insights into the development of PAMs and possibly other protein storage diseases, where a decrease of mitochondrial function has already been described.

Key words: MuRF1, MuRF3, HDAC5, protein accumulation, mitochondrial dysfunction

2. Contents

3. Abbreviations

Ac-CoA	Coenzyme A
ATP	Adenosine triphosphate
ATP5	ATP synthase subunit 5
BSA	Bovine serum albumin
Ca2+	Calcium ion
CS	Citrate synthase
DKO	Double knockout
DM	Differentiation medium
DMD	Duchenne muscular dystrophy
DMEM	Dulbecco's Modified Eagle Medium
e.g.	For example (exempli gratia)
E1	Ubiquitin activating enzyme
E2	Ubiquitin conjugating enzyme
E3	Ubiquitin protein ligase
ECL	Enhanced chemiluminescence
EDL	Extensor digitorum longus
ERα	Estrogen receptor alpha
ETC	Electron transport chain
GAPDH	Glyceraldehyde-3-phosphate dehydrogenase
GM	Growth medium
H&E stain	Hematoxylin and eosin stain
HDAC5	Histone deacetylase 5
HECT	Homologous to E6-AP carboxyl terminus
ICU	Intensive care unit
IMFM	Intermyofibrillar mitochondria
IMJs	Intermitochondrial junctions
IMM	Mitochondrial inner membrane
IRI	Cardiac ischemia–reperfusion injury
MEF2	Myocyte enhancer factor-2
MFM	Myofibrillar myopathies
MPTP	Mitochondrial permeability transition pore
MSM	Myosin storage myopathies
MTCO1	Cytochrome c oxidase subunit 1

mtDNA	Mitochondrial DNA
MuRF	Muscle Specific RING finger protein
NADH	Nicotinamide adenine dinucleotide
nDNA	Nuclear DNA
NDUFB8	NADH dehydrogenase (ubiquinone) 1 beta subcomplex subunit 8
OMM	Mitochondrial outer membrane
PAMs	Protein aggregate myopathies
PBS	Phosphate-buffered saline
PCR	polymerase chain reaction
PGC1-α	Peroxisome proliferator-activated receptor gamma coactivator 1-alpha
PPARα	Peroxisome proliferator-activated receptor alpha
PVDF membrane	Polyvinylidenfluoride membrane
qRT-PCR	Quantitative real-time PCR
RBR	Ring between ring
RING	Really interesting new gene
RIPA Buffer	Radioimmunoprecipitation assay buffer
ROS	Reactive oxygen species
rpm	revolutions per minute
SDHB	Succinate dehydrogenase (ubiquinone) iron-sulfur subunit
SDS-PAGE	Sodium dodecylsulfate polyacrylamide gel electrophoresis
SOL	Soleus
SSM	Subsarcolemmal mitochondria
TA	Tibialis anterior
TCA cycle	tricarboxylic acid cycle
UFD	Ubiquitin fold domain
UPS	Ubiquitin-Proteasome System
UQCRC2	Cytochrome b-c1 complex subunit 2
UT buffer	Thiourea/urea lysis buffer

4. Introduction

4.1. The striated muscle

Muscle tissue is divided in smooth and transverse striated muscle, due to its light microscopic appearance (Betts et al., 2017a). The regular stripe pattern is caused by a repetitive arrangement of large protein complexes within muscle cells (myocytes), which enables them to contract and relax, therefore granting the ability for conscious and unconscious movement (Betts et al., 2017b; Ulfig, 2005a). This protein complex, the smallest contractile unit in muscle, is the sarcomere, the basic contractile element of muscle cells. Multiple sarcomeres-built myofibrils, and multiple myofibrils form a myofibril bundle, which takes up most of the interior space of a myocyte. Between the sarcomeres are filamentous protein complexes, consisting of actin and myosin filaments, and they are framed by two Z-disks. Actin filaments consist of globular actin molecules, tropomyosin and troponin complexes (troponin I, troponin C and troponin T). They are bound to the Z-disks and regulate contraction. One myosin heavy chain (MyHC), divided in head, neck and tail domain, and two myosin light chains (MLC), one structural one regulatory, built one myosin filament. Two myosin filaments form a dimer, by wrapping the helical tail domains of the two heavy chains around each other. Approximately 150 of those dimers assemble to one bipolar myosin filament. Bipolar means here that on one half of the filament the heads point into one direction, while on the other half they point into the other. Myosin filaments originate from the M-line (from the german "Mittel-Scheibe"), the center of the sarcomere, and overlap with actin filaments within the A-band (anisotropic), where the heads enable interaction between the filaments. They are connected to the Z-disk (from the german "Zwischen-Scheibe") via titin. There are no actin filaments in the H-zone (Hensen zone, named after Victor Hensen), while in the I-band (isotropic) are no myosin filaments (Figure 1). Muscle contraction is the result of an ATP- and Ca^{2+} dependent conformational change of myosin, which pulls actin filaments closer and shortens the sarcomere, therefore leading muscle contraction (Betts et al., 2017b; Ulfig, 2005a; Wehner & Gehring, 2007a).
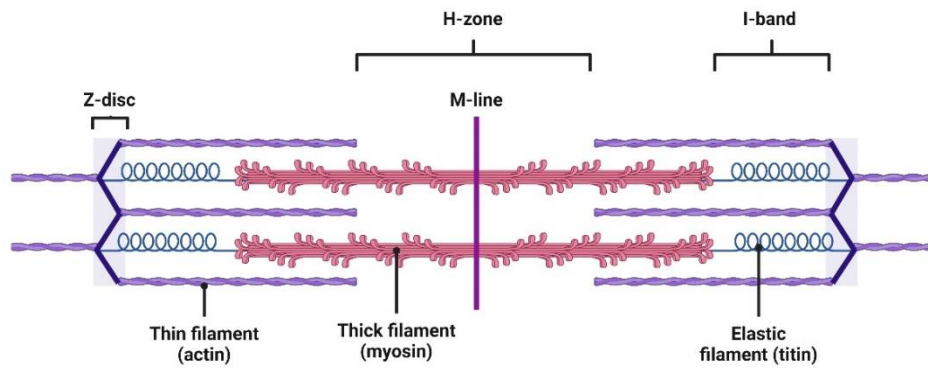
Figure 1. Structure of a sarcomere. The sarcomere is the contractile element of myocytes. Myosin originates from the M-line and is connected to the Z-discs via titin. It overlaps in the A-band with actin, which is directly connected to the Z-discs, which allows contraction. While the H-zone is free of actin, the I-band is free of myosin. Created with BioRender.com.

4.1.1 The skeletal muscle

Movement of Organisms, auxiliary respiratory musculature and the stabilization of posture are major functions of the skeletal muscle system, though they also play an important role in heat production and as a metabolic organ, for example by serving as an amino acid reserve. The striated muscle is separated in heart and skeletal muscle. Myocytes, cells elongated in shape with multiple marginalized nuclei and multiple myofibrils, are the smallest unit of the skeletal muscle, who originate from myoblasts, that are spindle-shaped muscle progenitor cells with centrally located nuclei, by fusion. They are also called myofibrils and are incased by the first layer of connective tissue, the endomysium. Multiple fibers are bundled to the fascicle by the perimysium, a second layer of connective tissue. These bundles build the whole muscle, delineated externally by the epimysium, and encased by the last layer of connective tissue the fascia. A tendon than connects the muscle to the bone (Figure 2) (Betts et al., 2017b; Ulfig, 2005a)(Betts et al., 2017b; Ulfig, 2005a).
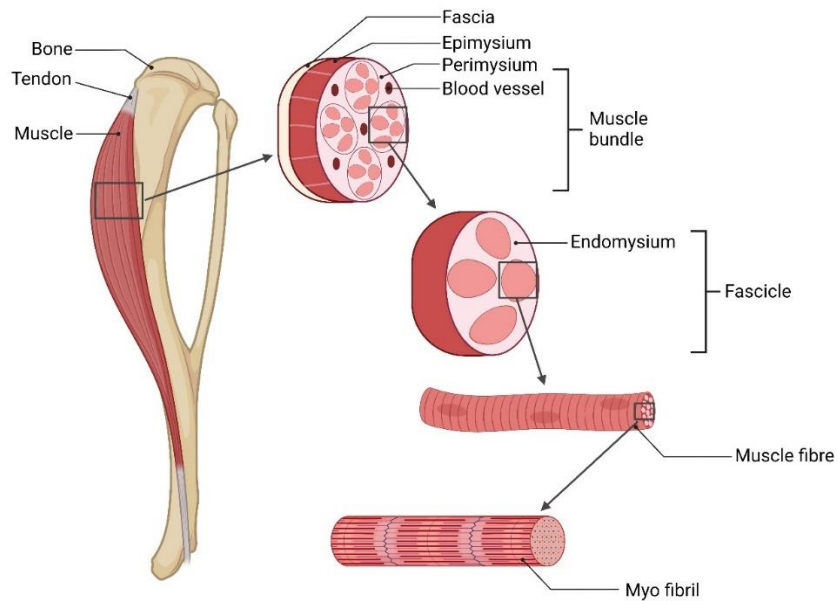
Figure 2. Built up of a skeletal muscle. Muscle fibres contain multiple myofibrils and are encased by the first connective tissue layer the endomysium. They are bundled by the perimysium, the next connective tissue layer, to the fascicle. Fascicles then built the muscle bundle, encased by the last layer of connective tissue the epimysium and the fascia. A tendon than connects the muscle to the bone. Created with BioRender.com.

4.1.2 Composition of skeletal muscle fibre types in the mouse hindlimb

There are 11 known genes, which encode for different MyHC isoforms in mammals. Four of these isoforms, MYH1 (MyHC-IIX), MYH2 (MyHC-IIA), MYH4 (MyHC-IIB) and MYH7 (MyHC-β), can be found in the adult skeletal muscle (Schiaffino & Reggiani, 2011). Depending on which isoform is mainly expressed in a muscle fibre, they can be divided in type-I (MyHC-I/β), type-IIA (MyHC-IIA), type-IIX/D (MyHC-IIx) and type-IIB (MyHC-IIB). Visually they can be distinct by the fact that MyHC-IIB tend to be larger compared to the smaller MyHC-I/β fibers (Augusto et al., 2004; Kammoun et al., 2014). Type-IIB are also glycolytic, while type-I/β depend on oxidative phosphorylation for energy production (Westerblad et al., 2010). There are fibers who contain two different MyHC, who are then referred to as type-IC/IIC (type-I/type-IIA), type-IIAD (type-IIA/type-IID) and type-IIDB (type-IID/type-IIB)(Staron & Hikida, 1992; Staron & Pette, 1986, 1993). Their composition in the muscle depends on species, function and sex. For example, human skeletal muscle does not express MyHC-IIB, while murine skeletal muscle does (Harrison et al., 2011). In both sexes the murine masseter displays a high number of type-IIX fibers, though female mice compared to males had less type-IIB fibers and more type-IIA (Eason et al., 2000). The fibre type composition of the

four hindlimb muscles of the mouse, *Tibials anterior* (TA), *extensor digitorum longus* (EDL), *gastrocnemius and plantaris* (GP) and *soleus* (SOL) are displayed in table 1.

Table 1. Fiber type of different skeletal muscle.

Fibre Type	SOL	EDL	GP	TA
Type-I	37.42%	0.44%	0.17%	5.74%
Type-IC/IIC	0%	3.55%	0.008%	0%
Type-IIA	38.62%	0.46%	1.12%	5.73%
Type-IIAD	18.74%	7.56%	3.42%	12.40%
Type-IID	5.69%	0.46%	2.25%	2.26%
Type-IIDB	0%	21.48%	33.83%	19.37%
Type-IIB	0%	66.01%	59.68%	54.42%

Fiber type composition of the hindlimb muscles soleus SOL, EDL, GP and TA in (%). The data is taken from C57BI6J mice (Asmussen et al., 2003; Augusto et al., 2004; Kammoun et al., 2014).

4.1.3 The heart muscle

Main task of the heart is to supply the body with blood and oxygen, but it also transports nutrients, hormones, waste products and heat (Betts et al., 2017b) (Figure 3). The heart is hollow muscle consisting of four areas: two atria and two ventricles. The interior is lined with the endocardium, a connective tissue, which is then followed by the muscle layer, the myocardium. As opposed to skeletal myocytes cardiomyocytes are shorter and have a single central nucleus (Betts et al., 2017b). The last connective tissue layer, the epicardium, is enclosed by the pericardium (Betts et al., 2017c; Ulfig, 2005b). Between those layers is the pericardial cavity, which is filled with serous fluid necessary for the smooth movement of the heart. Four valves, the tricuspid valve, the mitral valve, the aortic valve and the pulmonary valve, assure a unidirectional blood flow which is important for proper cardiac function. The left and the right atrium as well as the left and the right ventricle are separated by the interatrial and intraventricular septum, respectively (Figure 3). This setup enables two circulatory systems, the pulmonary and the systemic circulation. Deoxygenated blood gets pumped into the pulmonary trunk by the right ventricle, leading to the left and right pulmonary arteries. Those arteries branch into the pulmonary capillaries, where carbon dioxide exits and oxygen enters the blood. Via the pulmonary veins oxygenated blood reaches the left atrium, where it is pumped into the left ventricle. It then flows into the aorta, therefore reaching the systemic circuit. In the systemic capillaries oxygen exits and carbon dioxide enters the blood. Those capillaries form venules, then veins, which then form the two major systemic veins, superior vena cava and inferior vena cava. The major systemic veins lead the blood to the right atrium, were the

circulation starts again. Two valves, the aortic and the pulmonary, prohibit a back flow of the blood (Betts et al., 2017c).
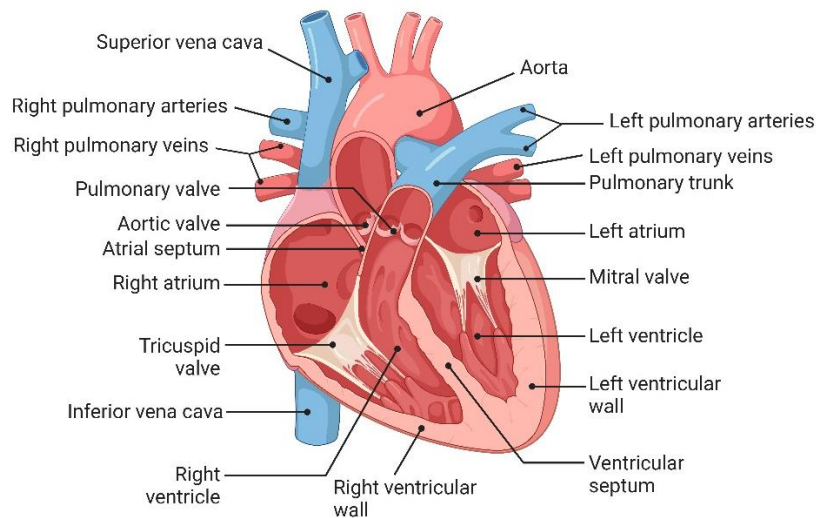
Figure 3. Anatomy of the heart muscle. The four chambers of the heart (left atrium, left ventricle, right atrium, right ventricle) are separated by the interventricular and interatrial septum, while the mitral and tricuspid valve prevent the blood from flowing back into the left and right atrium, respectively. This allows for two circulatory systems, the pulmonary and the systemic circulation. The aorta leads oxygenated blood into systemic circuit, while the superior vena cava and inferior vena cava lead the blood back to the right atrium. Pulmonary trunk and arteries connect the heart with the lung, where oxygen enters the blood. Created with BioRender.com.

4.1.4. Adaption of the heart to stress

In response to chronic cardiac stress or injury, for example volume overload or myocardial infarction (MI), the heart increases in size and mass to reduce wall stress (Grossman et al., 1975). Since cardiomyocytes are unable to proliferate, the increase in heart size is achieved by enlarging the cells themselves (Porrello et al., 2011; Soonpaa & Field, 1998). Over time this compensatory response, referred to as pathological cardiac hypertrophy, however leads to ventricular dilation, an impaired contractile function and finally to heart failure (HF) (Artham et al., 2009; Kannel et al., 1987). This process is accompanied by several molecular changes. One is the activation of the fetal gene program (FGP), that includes for example the regulation of sarco/endoplasmic reticulum Ca2+-ATPase (SERCA2a), which's decrease is believed to support the development of diastolic dysfunction in diabetic cardiomyopathy (Abe et al., 2002; Zhong et al., 2001), myofilament proteins (e.g. skeletal a-actin, cardiac titin isoform N2BA)(Driesen et al., 2009; Opitz & Linke, 2005), peptide hormones (e.g. atrial natriuretic peptide (ANP), B-type natriuretic peptide (BNP)(Dietz, 2005; Rosenkranz et al., 2003) and transcription factors (e.g. transcription factor GATA-4 (GATA4), myocyte enhancer factor 2 (MEF2), transcription factor Sp1 (SP1), Homeobox protein Nkx-2.5

(NKX2.5)(Azakie et al., 2006))(Cox & Marsh, 2014). The FGP is therefore a common marker to detect cardiac hypertrophy. Hypertrophy also leads to a substrate shift in the heart from fatty acid oxidation to glucose oxidation and to the depletion of the cardiac energy reserve, due to an increased energy demand (Liao et al., 1996; Taegtmeyer, 2002). Another concomitant factor is interstitial and perivascular fibrosis, the accumulation of ECM proteins, for example collagens and fibronectin, matrix metalloproteinases (MMPs) and tissue inhibitor of matrix metalloproteinases (TIMPs). It is a common process of pathological conditions in the heart (Ho et al., 2010; Small et al., 2010). Not only fibroblasts are involved here, but also cells who secret fibrogenic mediators like macrophages and mast cells (Gruber, 2003; Lafuse et al., 2021). Fibrosis is important for tissue repair and wound healing (Martin & Blaxall, 2012), but under chronic stress can lead to diastolic and systolic dysfunction (Segura et al., 2014). The diastole is the time period where the myocardium returns to its unstressed length and force, the heart relaxes and fills with blood. A diastolic dysfunction occurs when this process is prolonged, slowed down or incomplete. This can lead to diastolic heart failure, in which the blood intake of the heart during the diastole is decreased, while the percental amount of blood pumped out of the ventricles (ejection fraction (EF)) remains the same (Zile & Brutsaert, 2002). It is therefore also referred to as heart failure with preserved ejection fraction (HFpEF) (Lekavich et al., 2015). The systole is the time period where the myocardium shortens and creates force, the heart contracts and pumps blood into the body. Systolic dysfunction occurs when this process perturbed, leading to a decrease in EF. It can lead to systolic heart failure, in which the EF during the systole is decreased, while the blood intake of the heart remains the same (Goldberg & Jessup, 2006). Therefore, it is also referred to as heart failure with reduced ejection fraction (HFrEF)(Jin et al., 2022). Pressure overload and MI have also been shown to induce inflammation in the heart (Baumgarten et al., 2002; Vanderheyden et al., 2005). In fact, pathological cardiac remodeling was observed to be increased by toll-like receptors (TLR) and cytokines, which are both connected to inflammatory pathways, causing an impaired contractile function as well as an increase in reactive oxygen species (ROS), apoptosis and fibrosis (González et al., 2015; Kleinbongard et al., 2011; Mann, 2011). Therefore, chronic inflammation leads to tissue damage, maladaptive cardiac remodeling and HF (Mann, 2011).

4.2. Mitochondria and striated muscle

In skeletal and heart muscle mitochondria can be divided in two distinct subgroups: the subsarcolemmal (SSM) and the intermyofibrillar (IMFM) mitochondria. SSM are found below the sarcolemmal membrane, close to the capillary and nuclei and are more spherical. IMFM are located between the myofibrils adjacent to the Z-line of the sarcomere (Picard et al., 2013). Their shape is elongated and they providing ATP to the contractile filaments (Cogswell et al., 1993; Ferreira et al., 2010). Both subgroups built interconnected networks, referred to as the reticulum, with a continuity existing between them

(Kirkwood et al., 1986; Picard et al., 2013). Compared to glycolytic type-II fibers, oxidative type-I fibers display a more structured network with a higher number of mitochondria (Dahl et al., 2015). Under basal conditions type-I fibers fusion rates are also higher (Mishra et al., 2015). Muscle mitochondria are particularly capable to adapt their morphology dependent on metabolic demands. High-intensity interval training for example increases mitochondrial content and chronic exercise increases the fission-fusion rates of mitochondria (Iqbal et al., 2013; Jacobs et al., 2013; Russell et al., 2014).

Mitochondrial function is mainly regulated by the transcriptional coactivator Peroxisome proliferator-activated receptor-γ coactivator 1α (PGC1-α). PGC1-α upregulates nuclear respiratory factor 1 (NRF1) and NRF2 activity. (Athale et al., 2012; Z. Wu et al., 1999). An increase of NRF1 and NRF2 leads to mitochondrial biogenesis e.g. via the increased transcription of ETC proteins (Pandit et al., 2009). PGC1-α also controls fatty acid oxidation (FAO). It enhances the transcriptional activity of nuclear receptor peroxisome proliferator-activated receptor alpha (PPARAα) and estrogen-related receptor α (ERRα). This leads to an increase of proteins needed for FAO e.g. medium-chain specific acyl-CoA dehydrogenase, mitochondrial (MCAD) or [pyruvate dehydrogenase (acetyl-transferring)] kinase isozyme 4, mitochondrial (PDK4) (Kitamura et al., 2020; Pérez-Schindler et al., 2012; Vega et al., 2000). Class IIa histone deacetylases (HDACs) were observed to have an inhibitory effect on PGC1-α (Czubryt et al., 2003). This leads to an impaired mitochondrial function, possible cause by a reduction of e.g. NRF1 and Peroxisome proliferator-activated receptor gamma (PPARγ) activity (Czubryt et al., 2003; Gaur et al., 2016). The observed decrease of e.g. ETC complex subunits and FOA proteins like ATP synthase F1 subunit delta (Atp5d) and MCAD, which are needed for a proper mitochondrial function, are the direct consequence (Czubryt et al., 2003; Gaur et al., 2016)

In neurodegenerative diseases like Alzheimer disease (Manczak et al., 2011), Huntington's disease (Costa et al., 2010) and amyotrophic lateral sclerosis (ASL) (E. F. Smith et al., 2019) the mitochondrial reticulum is often fragmented (Romanello et al., 2010). Dysfunctional mitochondria also often display ultrastructural changes, e.g. increased compartmentalization or concentric cristae (Vincent, Ng, et al., 2016). This can be directly caused by pathogenic genetic variants in the mitochondrial DNA (mtDNA) or nuclear DNA (nDNA) (1171 known, 442 predicted mitochondrial proteins), which leads to an impaired function of the ETC (Kirby et al., 2004; Shoffner et al., 1989; A. C. Smith & Robinson, 2016). Due to its high energy demands, this can lead to adult-onset skeletal myopathies. Muscle histologies of patients suffering from mitochondrial myopathies often display ragged-red fibers (modified Gomori Trichrome staining), mitochondrial aggregates (succinate dehydrogenase (SDH, complex II) histochemistry) and COX-negative fibers (COX/SDH, complex IV/II histochemistry) (Bua et al., 2006; Campbell et al., 2014; Moraes et al., 1992). SDH histochemistry, a staining depending on ETC complex II activity, is used to localize mitochondria (Miles et al., 2012; Sciacco et al., 2001; Winter et al., 2015). It can also be used to identify

mitochondria aggregates, a common sign of mitochondrial dysfunction in muscle tissue (Miles et al., 2012; Winter et al., 2015; Zhou et al., 2019). Ragged-red fibers are defined by subsarcolemmal accumulation and aggregation of mitochondria (Ahuja, 2018; DiMauro & Williams, 2006; Milone & Wong, 2013; Reichmann et al., 1996). This leads to a ragged appearance of the fiber in the modified Gomori Trichrome staining. They are also partly COX-negative, meaning they are not stained by COX histochemistry (Reichmann et al., 1996). Since COX histochemistry depends on ETC complex IV activity, this is an indicator for a complex IV deficiency, often caused by a reduction in ETC subunits (Crugnola et al., 2010; Milone & Wong, 2013; Reichmann et al., 1996; Ross, 2011; Sciacco et al., 1994). The sequential double-labeling with SDH, COX/SDH histochemistry, provides an easier localization of cells with mitochondrial dysfunction (Ross, 2011). It was also shown that cardiac ischemia–reperfusion injury (IRI) causes mitochondrial dysfunction, via mitochondrial Ca^{2+} overload. In correlation with increased ROS production a non-selective inner membrane channel, the mitochondrial permeability transition pore (MPTP), opens, which leads to mitochondrial depolarization, swelling, rupture, and cell death causing disease progression (Jennings & Reimer, 1991; Kwong & Molkentin, 2015; Murphy & Steenbergen, 2008). Reduced mitochondrial function in skeletal muscle was also detected in patients suffering from protein storage diseases like Parkinson's, Alzheimer's and Huntington's disease (Blin et al., 1994; Chaturvedi et al., 2009; Manczak et al., 2004). In fact, an impaired energy metabolism, especially mitochondrial dysfunction, is integral for disease development and can even predate the clinical onset of other symptoms.

4.2.1 The Mitochondria

The mitochondrion is the power house of the cell, though they also play in important role in other cellular processes like Ca^{2+} homeostasis (de Stefani et al., 2011; Eisner et al., 2014), regulation of gene expression (Picard et al., 2014) redox signaling (Giorgio et al., 2005; Salmeen et al., 2003) and muscle function (Picard et al., 2012). They are elongated cylinders of 0.5 to 1 m in diameter. In the cytoplasm, mitochondria are often aligned along microtubules. A mitochondrion consists of two membranes, creating four compartments: the outer mitochondrial membrane (OMM), the intermembrane space, the inner mitochondrial membrane (IMM) and the mitochondrial matrix. The OMM consists of a lipid bilayer. It contains enzymes of lipid metabolism and transport proteins that allow molecules of up to 10 kDa to pass into the intermembrane space by forming a hydrophilic channel (Berg et al., 2013a; Wehner & Gehring, 2007b). By bending inwards, the IMM builds three regions the inner boundary membrane, the crista junctions and the cristae membrane (Frey & Mannella, 2000)(Figure 4).
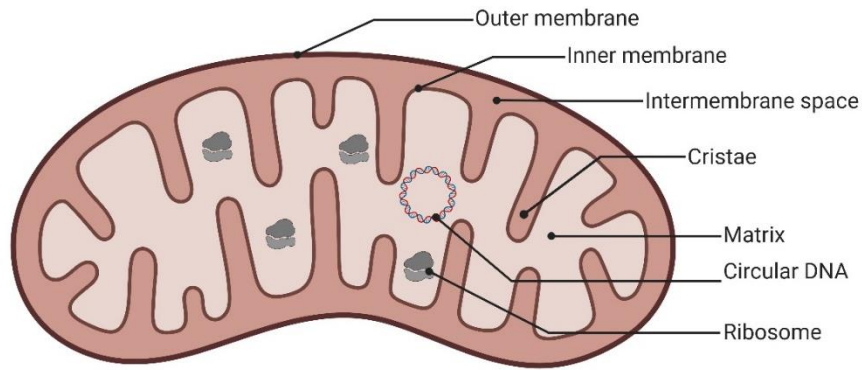
Figure 4. Mitochondrial structure. A mitochondrion consists of two membranes, the outer and inner membrane. Between them is the intermembrane space. The inner membrane bends inwards, forming the cristae, were the ETC is located. In the matrix, the inner space of the mitochondrion, circular mtDNA and ribosomes are found. Created with BioRender.com.

The IMM is impermeable to most proteins, contains the enzymes of the ETC and the ATP synthase complex, and transport proteins that move metabolites in and out of the mitochondrial matrix. The matrix contains enzymes for the oxidation of pyruvate and fatty acids, for the biosynthesis of amino acids, multiple copies of the circular mtDNA, mitochondrial ribosomes, mitochondrial tRNA, and all the enzymes needed for the expression as well as replication of mitochondrial genes (Berg et al., 2013a; Wehner & Gehring, 2007b). Mitochondria rarely occur singly but form a dynamic reticular network from which mitochondria can uncouple but also fuse again, while oscillating between a tubular and a spherical morphology (Ogata & Yamasaki, 1997). This process is called fission and fusion. During fission the dynamin related protein (Drp1) associates to a linear filament, after being activated by Guanosine-5'-triphosphate (GTP). Hydrolysis of GTP by Drp1 then leads to a curling of the DRP1 filament into constricted and closed ring, diving a part from the mitochondrial network (Kalia et al., 2018; Smirnova et al., 1998). Fusion is a multi-step process, in which multiple proteins are required to synchronize the fusion of the IMM and OMM. Mitofusin 1 and 2 are needed for OMM fusion and are early involved in the process, while optic atrophy 1 (OPA1) is essential for IMM fusion (Cipolat et al., 2004; Santel & Fuller, 2001; Song et al., 2009). Fission and fusion allow mitochondria to share components and damaged components to be degraded by mitophagy. Under physiological conditions, mitochondrial biosynthesis and degradation are in equilibrium (Griparic et al., 2004; Papanicolaou et al., 2011). To limit the spread of local dysfunction electron-dense structures, so called intermitochondrial junctions (IMJs), are placed between connected mitochondria (Glancy et al., 2017; Picard et al., 2013).

4.2.2 Mitochondrial energy production via the ETC

In the oxidative metabolism, the cellular energy utilization of a glucose molecule is divided into three steps: Glycolysis (cytosol), citrate cycle (matrix) and the oxidative phosphorylation (OXPHOS). In the ETC, NADH is oxidized by atmospheric oxygen. Glycolysis and citrate cycle are anaerobic reaction pathways, so they do not rely on oxygen, whereas OXPHOS does. Their main function in oxidative metabolism is the cleavage of H_2 from the starting product and the transfer of H_2 to NAD, reducing NAD and producing NADH and 4 molecules of ATP per one molecule glucose. NAD, like ATP, is an energy transport molecule. They also produce 4 molecules of ATP per one molecule glucose (Berg et al., 2013a; Wehner & Gehring, 2007c).

However, the hydrogen bound by NAD is not directly transferred to oxygen, but is split into electrons and protons. The two electrons pass through the ETC, which consists of NADH-Q reductase (complex I), cytochrome reductase (complex III) and cytochrome oxidase (complex IV), and the transport molecule ubiquinone (Acín-Pérez et al., 2008; Schägger & Pfeiffer, 2000; M. Wu et al., 2016). Instead of NADH succinate can also be used for oxidation via the Succinate reductase (complex II), which is rate limiting here (Blanchi et al., 2004). Electron transporting groups here are flavins, iron-sulfur clusters, heme, and copper ions (Letts et al., 2016; M. Wu et al., 2016). The last complex, ATP synthase (complex V), consists mainly of F0 units forming a proton channel (Figure 5).

This creates an electrochemical gradient, which is used by the ATP synthase to generate ATP from ADP. This whole process is referred to as oxidative phosphorylation, short OxPhos.

Cytoplasm

Outer membrane

Intermembrane space

$4H^+$ $4H^+$ $2H^+$ nH^+

CoQ

Cyt c

I   III   IV   ATP synthase

Inner membrane

$2e^-$ $2e^-$

II

Mitochondrial matrix

NADH $NAD^+ + 2H^+$ $FADH_2$ $FAD + 2H^+$ $\left[2H^+ + 1/2O_2 + 2e^- \longrightarrow H_2O \right] \times 2$

ADP   ATP

Electron Transport Chain
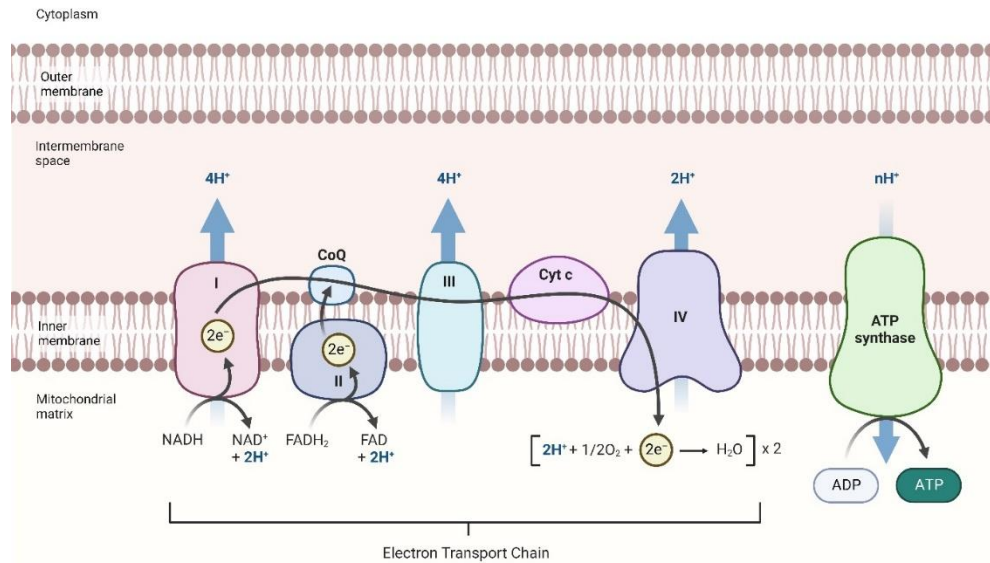
Figure 5. The electron transport chain. Located in the inner membrane cristae, complex I, cytochrome complex III, complex IV, and the transport molecule ubiquinone transport two electrons, while pumping H_2 protons into the intermembrane space. This creates an electrochemical gradient, causing protons to flow back into the matrix via the ATP synthase, which produces ATP and H_2O. Created with BioRender.com.

In the last step of the ETC, ATP and H_2O are produced from ADP (Rubinstein et al., 2003). ADP and ATP do not diffuse freely across the membrane, but need the help of the ATP-ADP translocase. In this process, ADP only enters the mitochondrial interior when ATP exits and vice versa. This exchange is energetically costly, which is why a quarter of the energy yield is required for the regeneration of the membrane potential. The production of ATP can result in the generation of radical oxygen, which is why superoxide dismutase is an important adaptation to the planet's oxygen atmosphere. This protein converts radical oxygen to H_2O_2, minimizing potential cell damage.

Phosphorylation of ADP is coupled to ATP consumption. No electron flows through the ETC unless ADP is simultaneously phosphorylated to ATP, making the rate dependent on the level of ADP. The same pathway is used to regulate the speed of the citrate cycle. Regulation by ADP level is also known as respiratory control. Thus, 30 molecules of ATP can be obtained from one molecule of glucose by complete degradation to CO_2 and H_2O by mitochondria (Berg et al., 2013a; Wehner & Gehring, 2007c).

4.3. The UPS in striated muscle

To maintain protein homeostasis multiple of protein quality control mechanisms are required. The reason for this is the insufficient thermodynamic stability of some conformations or damages caused by for example mutation, ROS or heat. Chaperons and degradation systems, e.g. the ALP and the UPS, therefore constantly monitor the proper folding of proteins, to reduce dysfunction and the threat of protein aggregation, which can lead to diseases like Alzheimer's, Parkinson's and Huntington's disease. They also target damaged or functionless proteins, in the case of ALP even whole cell organelles (Amm et al., 2014; Kleiger & Mayor, 2014).

In the UPS proteins are tagged by ubiquitin, a highly conserved 76 amino acid polypeptide, on a lysin residue via an isopeptide bond between the carboxyl end of ubiquitin and the lysine primary amine (Hershko et al., 1979, 1980). To ubiquitinate a protein a cascade of E1, E2 and E3 proteins is needed (Berg et al., 2013b; Hershko et al., 1983)(Figure 6).
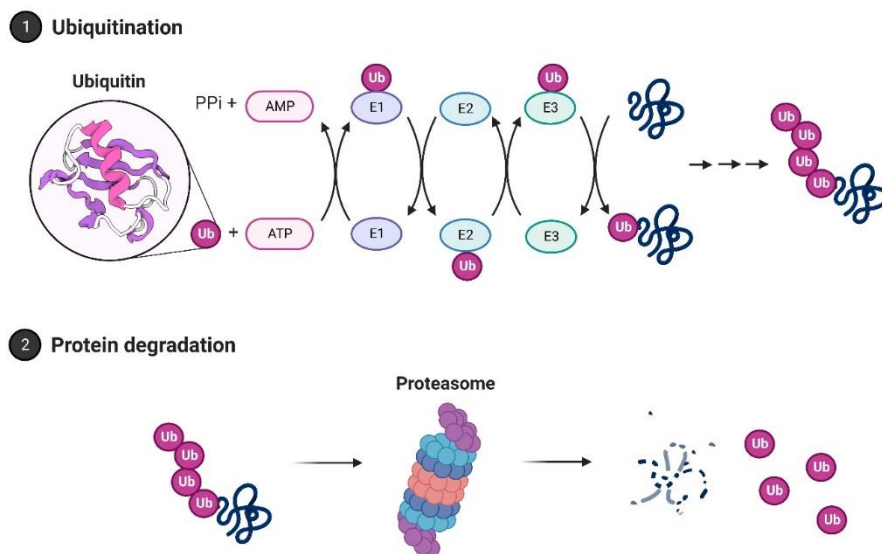
Figure 6. The Ubiquitin-Proteasome system. 1. A protein gets marked for degradation by ubiquitin via E1, E2 and E3 proteins. Ubiquitin (Ub) is first activated by the E1 ubiquitin activating enzyme in an ATP-dependent manner. Then the E1 transfers the activated Ub to the E2 ubiquitin conjugating enzyme. E2 and E3 ubiquitin ligase together than transfer ubiquitin to the substrate. Substrate specificity is assured by the E3. 2. The targeted protein gets degraded by the 26S proteasome, while ubiquitin gets released. Created with BioRender.com.

In an ATP dependent manner E1 ubiquitin activating enzymes, 8 known in human, adenylate the C-terminal carboxyl group of ubiquitin, forming a thioester bond between E1's catalytic cysteine residue and the C-terminus of ubiquitin, which is then transferred onto the catalytic cysteine of the E2 ubiquitin conjugating enzyme (Berg et al., 2013b; Groettrup et al., 2008). The E2-binding domain of E1s, also called ubiquitin fold domain (UFD), is very flexible, possible assisting the ability to bind multiple E2s (Huang et al., 2009; Olsen & Lima, 2013). E2s (approximately 35 in human), together with the E3 ubiquitin ligases (more than 600 in human), change the conformation of ubiquitin bound to the E2 to promote the transfer to the substrate (Berg et al., 2013b; W. Li et al., 2008; Wijk & Timmers, 2010). The formation of a thioester bond between the C-terminal end of ubiquitin and the conserved E2 cysteine residue is catalyzed by E2s, while E3s act as protein scaffolds, bringing the substrate and E2 ubiquitin into proximity (Berg et al., 2013b; Dou et al., 2012; Kleiger & Mayor, 2014; Plechanovov et al., 2012)

Since ubiquitin has seven lysine residues and free amino ends, it is an acceptor for ubiquitination itself, enabling the built of poly-ubiquitin chains (Peng et al., 2003; Tokunaga et al., 2009; Xu et al., 2009). Those ubiquitin chains are built by the same E1-E2-E3 cascade as described before. The resulting ubiquitin code does not always mark proteins for degradation, but also regulate e.g. transcription, cell cycle progression and DNA damage response (Garnett et al., 2009; K.-B. Lee et al., 2002; Pham & Sauer, 2000). Ubiquitin linkage types are e.g. K6 (DNA damage response), K11 (human cell cycle control), K27 (nuclear translocation), K29 (degradation), K33 (T-cell receptor signaling), K48 (proteasomal degradation), K63 (protein trafficking) and M1 (angiogenesis). Polyubiquitination can be achieved by conjugating one of ubiquitin's free lysine residues (K6, K11, K27, K29, K33, K48 and K63) or the N-terminal methionine residue (M1). If a ubiquitin chain contains a single linkage type, it is referred to as homotypic. Ubiquitin chains, which utilize a mix of linkages are heterotypic. Heterotypic chains can also branch, when one ubiquitin molecule is ubiquitinated on more than one site. Post-translational modifications, like acetylation and phosphorylation, of ubiquitin molecules diversify poly-ubiquitin chains even more (Akutsu et al., 2016).

In skeletal and heart muscle RING E3 ubiquitin ligases are the most abundant and regulate a variety of processes like cell proliferation, transcription, and development (Han et al., 2020; Lopez et al., 2011; Min et al., 2021). The majority of myofibrillar proteins are degraded via the UPS, regulated by muscle specific RING finger 1 (MuRF1, encoded by *Trim63*) and the muscle atrophy F-Box (Atrogin-1/MAFbx, encoded by *Fbxo32*) protein. Important is here the balance between protein synthesis and degradation. An increase in MuRF1 and Atrogin-1 levels leads to muscle atrophy, via an increased proteasome activity (Bodine et al., 2001; Gomes et al., 2001; Sandri et al., 2004). Especially in age related muscle atrophy (sarcopenia) or intensive care unit (ICU) acquired weakness (ICUAW) type-II glycolytic muscle fibers are more affected compared to type-I oxidative fibers (Bierbrauer et al., 2012; Nilwik et al., 2013; Sandri et al., 2006).

Though, a decrease in proteasome activity is likely correlated to age-associated deteriorations in striated muscle (Ferrington et al., 2005; Kitajima et al., 2020).

Mutations in E3 ligases or target proteins are the cause of serious hereditary diseases. Dysfunctional E3s lead to PAMs, which are characterized by protein accumulations in myofibers, often containing sarcomeric proteins like myosin. This was for example shown in a patient suffering from *TRIM63* and *TRIM54* mutations (Olivé et al., 2015). Similar to patients suffering from *MyHC7* mutations, who also develop protein accumulations, they display a progressive weakness of the limbs and in some cases a hypertrophic cardiomyopathy (HCM) (Laing et al., 2005; Marsiglia et al., 2013; Olivé et al., 2015; Tajsharghi et al., 2003). Mutations in *cardiac myosin-binding protein C* gene (*MYBPC3*) are also known to cause HCM (Bahrudin et al., 2008). Another prominent example for muscle dystrophies caused by a mutation in the target protein, in this case dystrophin, is the Duchenne muscular dystrophy (DMD). Patients develop a rapid decrease in limb strength and a severe cardiomyopathy (Falzarano et al., 2015). Desmin-related myopathies (DRMs) are examples of how an impaired UPS function caused by mutations in chaperon proteins like αB-crystallin decreases heart and skeletal muscle function (J. Liu et al., 2006; Vicart et al., 1998).

Only in presence of E3s can maximal E2 activity be achieved (Kleiger et al., 2009). E3s transfer multiple ubiquitins onto a substrate before it's released (Pierce et al., 2009). Degradation of the ubiquitin-tagged protein takes place in the 26S proteasome. It is a two multisubunit enzyme complex built by the 20S core, a highly symmetrical, hollow barrel-like structure, and two 19S regulatory particles, which assemble on both ends of the core. Rpn10 (proteasome regulatory particle base subunit) and Rpn13 (also Adrm1, adhesion regulating molecule), receptors bound to the 19S regulatory particle, allow ubiquitinated proteins to dock to the proteasome (Berg et al., 2013b; Elsasser et al., 2004; Husnjak et al., 2008). The ubiquitin chain is then cleaved by Rpn11/Poh1, recycling the ubiquitin and enabling protein to enter the 20S core, where it is degraded (Verma et al., 2002; Yao & Cohen, 2002).

4.4. The MuRF E3 ligases

E3 ubiquitin ligases can be separated into three groups: RING (really interesting new gene)-, HECT (homologous to E6-AP carboxyl terminus)- or RBR (ring between ring)-proteins. Most belong to the RING and RING-related E3s, approximately 95 % in human, which transfer ubiquitin directly from the E2 to the substrate (W. Li et al., 2008). In contrast HECT and RBR E3s require an additional transthioesterification step, where ubiquitin is transferred from E2 to E3 (Duda et al., 2013; Kamadurai et al., 2013)((Figure 7).
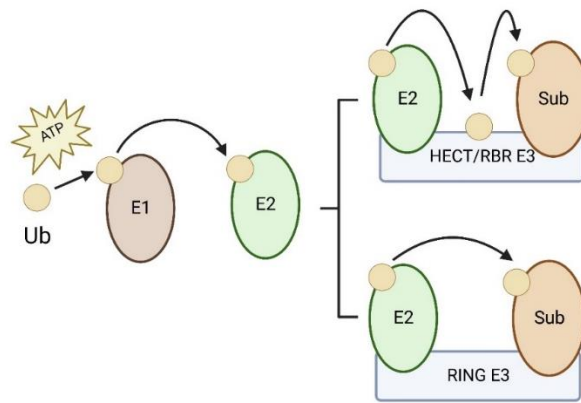
Figure 7. RING, HECT and RBR E3 ligase. While RING E3 ligases directly transfer ubiquitin (Ub) from the E2 to the substrate (Sub), HECT and RBR E3 ligases require an extra step, where ubiquitin is transferred from E2 to E3. Created with BioRender.com.

A canonical RING-finger domain is a domain consisting of specifically spaced cysteine and histidine residues (Cys-X2-Cys-X(9-39)-Cys-X(1-3)-HisX(2-3)-Cys-X2-Cys-X(4-48)-Cys-X2-Cys, X = any amino acid) (Freemont et al., 1991; Lorick et al., 1999). It enables E2-dependent ubiquitylation, while the RING-finger domain or surrounding regions allow formation of hetero- and homodimers (Liew et al., 2010; Linke et al., 2008). In the case of heterodimerization of E3s it is often observed that one E3 lacks ligase activity, therefore maybe conforming and/or stabilizing the active E2-binding RING domain (Linke et al., 2008; Metzger et al., 2014).

MuRF1 (*Trim63*), MuRF2 (*Trim55*) and MuRF3 (*Trim54*) belong to the TRIM (tripartite motif) family of E3 ubiquitin ligases, characterized by three zinc-binding domains: RING, B-box (type 1 and/or Type 2) and the coiled-coil domain. Specific for this family that in mammals consists of 37 proteins, is the B-box (Reddy et al., 1992). MuRFs are localized at the M-line, Z-line, nucleus or microtubules (Short & Cox, 2006). They are mostly known for targeting structural proteins for degradation via the UPS, like titin (Lange et al., 2005; Mrosek et al., 2007; Pizon et al., 2002; S. H. Witt et al., 2005), nebulin (S. H. Witt et al., 2005), myozenin 1 and 2 (Moriscot et al., 2010), FHL2 (C. C. Witt et al., 2008) and γ- filamin (Fielitz, Kim, et al., 2007), in tandem with E2 ubiquitin conjugating enzymes like Ubiquitin-conjugating enzyme E2 D1 (UbcH5a),-b and c, as well as Ubiquitin-conjugating enzyme E2 E1 (UBE2E1), E2 G1 (UBE2G1), E2 J1 (UBE2J1), E2 J2 (UBEJ2) and E2L3 (UBEJ2)(Fielitz, Kim, et al., 2007; Polge et al., 2018). Especially MuRF1 has been the focus of research, because of its prominent role in muscle wasting (Bodine et al., 2001). Samples taken from patients suffering from ICUAW display a significantly increased amount of MuRF1 and the germ line deletion of *Trim63* in mice has been shown to have a protective effect against muscle wasting (Bodine et al., 2001; Wollersheim et al., 2014). On the other side MuRFs are integral for striated muscle development and maintenance. In vitro KO of *Trim55* (MuRF2) delays myogenic differentiation and myotube formation, as well as the structure of stable microtubule populations, DES, vimentin, and

the M-line region (McElhinny et al., 2004; Perera et al., 2012). It was also shown that the DKO of *Trim55* and *Trim54* leads to a decrease in heart and skeletal muscle function (Lodka et al., 2016). Furthermore, *Trim63* and *Trim55* redundantly regulate E2F transcription factors, which are essential for cardiac development (Willis et al., 2014).

4.4.1. MuRFs and energy metabolism

MuRF proteins are involved in striated muscle metabolism (Banerjee et al., 2015; Hirner et al., 2008; Koyama et al., 2008; Lodka et al., 2016; C. C. Witt et al., 2008). For example, non-targeted metabolomics analysis of *Trim63*, *Trim55* and *Trim54* single KO hearts revealed significant changes in taurine metabolism and primary acid biosynthesis (*Trim63* KO) as well as ascorbic acid and aldarate metabolism (*Trim55* KO)(Banerjee et al., 2015). Overexpression of MuRF1 in the heart leads to a decrease in nuclear PPARα, therefore inhibiting fatty acid oxidation (Rodríguez et al., 2015). It was also shown to link skeletal muscle metabolism with liver and pancreas, by regulating the carbohydrate metabolism, under metabolic stress (Hirner et al., 2008). Likely via targeting creatine kinase M-type (M-CK) for degradation MuRF1 keeps the homeostasis of energy- and amino acid metabolism during muscle-atrophy-inducing conditions (Koyama et al., 2008). M-CK transfers phosphoryl groups from phosphocreatine (Pcr) to ADP, therefore creating ATP. This reaction plays an important role in tissue with a high but also fluctuating energy demand like skeletal and heart muscle (Barclay, 2017; Saks et al., 2006). Mitochondrial function was brought into connection with MuRFs via yeast-two-hybrid (YTH or Y2H) screens performed for *Trim63* and *Trim55*, where 6 proteins of the mitochondrial energy metabolism were identified as possible interaction partners, as well a significant decrease of mitochondrial proteins in *Trim55/Trim54* DKO mice (Lodka et al., 2016; C. C. Witt et al., 2008).

4.4.2 MuRF1/MuRF3 DKO Phenotype

With focus on mitochondrial function, we are going to continue the previous work on MuRF1/MuRF3 DKO mice. This phenotype was established by Fielitz et al. in 2007. MuRFs function in a redundantly way, therefore only DKO mice develop a phenotype (Willis et al., 2014; S. H. Witt et al., 2005). Compared to littermates, MuRF1/MuRF3 DKOs are smaller in size and are lighter in body weight, while their skeletal muscle mass is significantly increased. They also display cardiac hypertrophy. This increase in striated muscle weight is caused by subsarcolemmal accumulation of proteins, such as type-I and type-IIA MyHC, which are located along the entire length of the myofiber surrounding a central myofiber core. Mitochondria are redistributed along the centralized myofiber core and there is an increase of, often centralized, nuclei per myofiber. Atrophic and split myofibers with no fiber type preference could be observed. Affected fibers had disoriented sarcomeres with an intact M-line, but greatly diminished Z-

lines, sometimes with Z-line streaming. This leads to a decrease in maximum force development and an enlargement of the LV end-systolic dimension as well as a decreased left ventricular systolic function. Since this phenotype closely resembles patients suffering from myosin storage myopathies (MSM), it makes it a suitable model to study those diseases. In fact, a patient was described, who carried a homozygous null mutation in *TRIM63* and a heterozygous missense mutation in *TRIM54*, that changed one amino acid leading to a loss of function and a decreased protein stability, that displayed the same symptoms (Olivé et al., 2015). The patient was diagnosed with cardiomyopathy at the age of 15 and later developed a slowly progressing weakness of all proximal muscles. Genetical investigation of the family proofed that only the combination of both mutation lead to a phenotype. Except the already described changes in striated muscle weight and structure, they also suffered from a general loss of subcutaneous fatty tissue, rigidity of the spine, scapular winging and dyspnea. Though it is important to keep in mind, that depending on sex myopathies can develop differently and only one male patient was described here (Brambatti et al., 2019; Fanin et al., 2014; Skilving et al., 2016). In Danon disease, a vacuolar myopathy caused by mutations in the Lysosomal-Associated Membrane Protein 2 (*LAMP2*) gene, females developed HCM and DCM, while males usually only developed HCM. However, symptoms in women were almost only of cardiac nature, while in men they were more multisystemic, with cognitive impairment and skeletal myopathy (Brambatti et al., 2019). Myopathies caused by statin treatment, an β-Hydroxy β-methylglutaryl-CoA (HMG Co-A) reductase inhibitor used for cardiovascular disease prevention, were observed to be more severe in females (Skilving et al., 2016). Muscle fiber atrophy in Limb girdle muscular dystrophies (LGMD), a myopathy defined by the progressive wasting of limb girdle muscles caused by different autosomal mutations, on the other hand was more severe in males than in females (Fanin et al., 2014). Those differences between sexes are possibly caused by the regulatory effects of sex hormones on gene transcription (Cavalcanti-de-Albuquerque et al., 2014; White et al., 2013). Testosterone was proven to regulate Akt/mTORC1/FoxO3a signaling in C2C12 cells, linking low levels of the hormone to muscle wasting (White et al., 2013). Ovariectomized rats displayed a reduction in muscle mitochondria and PGC1-α, which could be reversed by estrogen replacement, highlighting the positive effect estrogen has on the striated muscle energy metabolism (Cavalcanti-de-Albuquerque et al., 2014).

5. Aim of thesis

The aim of this thesis was to investigate if MuRF1 and MuRF3 are involved in the metabolism of striated muscles. Previous research mainly focused on their role in skeletal muscle atrophy and muscle wasting via targeting structural proteins like Titin, Myozenin 1 and 2, as well as FHL2 for degradation by the UPS. This study focused on the mitochondrial energy metabolism since previous work with *Trim63/Trim55* and *Trim55/Trim54 DKO* mice revealed a decrease in proteins belonging to the respiratory chain complexes of the ETC in mitochondria. However, if and how MuRFs are connected to mitochondrial energy metabolism was not known. Because patients suffering from mutations in *TRIM63* and *TRIM54* develop a similar phenotype the mechanisms and consequences of the myosin storage myopathy of *Trim63/Trim54* DKO mice are of particular importance. It was also already shown in other protein storage diseases like Alzheimer's or Parkinson that mitochondrial dysfunction is a major factor in disease progression. Therefore, understanding the mechanism behind how the deletion of MuRFs leads to a disturbed synthesis of mitochondrial proteins could be important to understand disease development, which could only be properly investigated *in vivo*.

We aimed to further describe the MuRF1/MuRF3 DKO phenotype with focus on mitochondrial proteins (I) and mitochondrial function (II) in TA and heart muscle, and the possible mechanism in which MuRF1 and/or MuRF3 regulate mitochondrial activity (III). To compare muscle function between control and DKO mice we performed grip strength measurements and muscle force assays with EDL muscle ex vivo. Mass spectrometry, Immunoblot and qRT-PCR were used to assess changes in the amount mitochondrial proteins and their gene expressions. We also measured the activity of ECT complexes I, III and IV via spectrophotometry in lysates from TA and heart tissue. All results were analyzed separated by gender, to reveal any sex specific effects of the DKO.

6. Material and Methods

6.1. Material

6.1.1. Animals

MuRF1 KO mice (Bodine et al., 2001), MuRF3 KO (Fielitz, van Rooij, et al., 2007) and MuRF1/MuRF3 DKO (Fielitz, Kim, et al., 2007) mice were recently published. MuRF1 KO and heterozygous MuRF3 mice were interbred to generate MuRF1/MuRF3 DKO mice. *Trim63* (MuRF1) knockout and *Trim54* (MuRF3) heterozygous mice were breed to generate *Trim63*/*Trim54* (MuRF1/MuRF3) double knockout (DKO) mice. All investigations were performed according to the Guide for the Care and Use of Laboratory Animals published by the US National Institutes of Health (NIH Publication No. 85-23, revised 1985) and the German Law on the Protection of Animals. Our studies were also approved beforehand by the Landesamt für Landwirtschaft, Lebensmittelsicherheit und Fischerei (LALLF, Mecklenburg-Vorpommern, Germany). Adult mice (weeks 5-11) were sacrificed by cervical-dislocation, after being sedated with Isofluran CP® (CP Pharma, Burgdorf, Germany). We harvested heart, liver and the skeletal muscles TA, SOL, EDL, which were weighted and shock frozen in liquid nitrogen. Samples were than stored at -80 °C. All weights were normalized to tibia length. Mice of both sexes were used for the analyses. The number of animals per analysis, their sex as well as their age is provided with the respective experiment.

6.1.2. Cells

Table 2. Eukaryotic cells

Cell line	Organism	Tissue	Cell type	Supplier
C2C12	*Mus musculus*	Muscle	Myoblast	ATCC, Manassas, VA, USA, CRL1772
COS7	*Cercopithecus aethiops*	Kidney	Fibroblast	ATCC, Manassas, VA, USA, CRL1651
PLAT-E	*Homo sapiens*	Kidney	Fibroblast	Cell Biolabs, San Diego, CA, USA, RV-101

6.1.3. Plasmids

Table 3. Overexpression plasmids.

Plasmid with insert	Tag	Resistance	Origin
pcDNA™3.1(+)/FLAG_HDAC5	N-terminal	Ampicillin	AG Fielitz
pcDNA™3.1(+)/FLAG_MuRF1	N-terminal	Ampicillin	AG Fielitz
pcDNA™3.1(+)/FLAG_MuRF3	N-terminal	Ampicillin	AG Fielitz

pcDNA™3.1/myc-His(-)_HDAC5	C-terminal	Ampicillin	AG EN Olson UTSW
pcDNA™3.1/myc-His(-)_HDAC5 100-C	C-terminal	Ampicillin	AG EN Olson UTSW
pcDNA™3.1/myc-His(-)_HDAC5 1-664	C-terminal	Ampicillin	AG EN Olson UTSW
pcDNA™3.1/myc-His(-)_HDAC5 51-C	C-terminal	Ampicillin	AG EN Olson UTSW
pcDNA™3.1/myc-His(-)_HDAC5 540-C	C-terminal	Ampicillin	AG EN Olson UTSW
pcDNA™3.1/myc-His(-)_HDAC5 601-C	C-terminal	Ampicillin	AG EN Olson UTSW
pcDNA™3.1/myc-His(-)_MuRF1	C-terminal	Ampicillin	AG Fielitz
pcDNA™3.1/myc-His(-)_MuRF1Cys39/47Ser	C-terminal	Ampicillin	AG Fielitz
pcDNA™3.1/myc-His(-)_MuRF2	C-terminal	Ampicillin	AG Fielitz
pcDNA™3.1/myc-His(-)_MuRF3	C-terminal	Ampicillin	AG Fielitz
pcDNA™3.1/myc-His(-)_MuRF3Cys42/50Ser	C-terminal	Ampicillin	AG Fielitz
pEGFP-N3-HA-Ubi	N-terminal	Kanamycin	AG Seifert
pMP71_IRES_GFP/6xHis_MuRF1	C-terminal	Ampicillin	AG Fielitz
pMP71_IRES_GFP/6xHis_MuRF3	C-terminal	Ampicillin	AG Fielitz

6.1.4. Antibodies

Table 4. Antibodies.

Antibody	Host/Clonality	Supplier	Dilution
Primary			
Anti-GAPDH	Mouse, monoclonal	Merck, Darmstadt, DE, MAB374	1/50000 (1% BSA)
Anti-MuRF1	Mouse, monoclonal	Abcam, Cambridge, UK, ab57865	1/1000 (1% BSA)
Anti-MuRF3	Rabbit	Self-generated with help of Biogenes Inc., isolated from Rabbit Serum	1/1000 (2% BSA)
Anti-Myc Tag Antibody	Rabbit, polyclonal	Sigma-Aldich, St. Louis, Mo, USA, 06-549-100UG	1/1000 (1% BSA)
DYKDDDDK Tag Antibody (Anti-FLAG®M2)	Rabbit, polyclonal	Cell Signaling, Danvers, MA, USA, 2368S	1/1000 (1% BSA)

HDAC5 (D1J7V) Rabbit mAb	Rabbit, monoclonal	Cell Signaling, Danvers, MA, USA, 20458S	1/1000 (1% Milk powder)
OxPhos Rodent WB Antibody Cocktail (22 kDa: NDUFB8, 28 kDa: SDHB, 48 kDa: UQCRC2, 40 kDa: MTCO1, 55 kDa: ATP5)	Mouse, monoclonal	Life Technologies, Carlsbad, CA, USA, 45-8099	1/1000 (1% BSA)
Secondary			
Anti-mouse IgG, HRP-linked Antibody	Horse	Cell Signaling, Danvers, MA, USA, 7076S	1/10000
Anti-rabbit IgG, HRP-linked Antibody	Goat	Cell Signaling, Danvers, MA, USA, 7074S	1/10000

Antibodies are separated in primary and secondary antibodies. Besides host, clonality and supplier the working dilution in TBST of the antibody with the used blocking reagent is listed here.

6.1.5. Primer

Table 5. Primers. Primers used for genotyping and qRT-PCR.

Primer	Sequence (5' → 3')	Ratio
Genotyping		
GT_MuRF3_rev2	GACAGAAGCAGTGTTGTCTGAG	1:1
GT_Teg_neo_3611F	GCCTTCTAGTTGCCAGCCATCTGTTG	
MURF1_geno_3`	CTCCTGGGGCTCATGTGACAGAGG	1:1:1
MURF1_geno_5`	GATGTCGTTGGCACACTTCCGGCA	
MURF1_LacZ	TAGATGGGCGCATCGTAACCGTGC	
MuRF3_eEx5_rev	GCTTTGAGGAGCCCTCCAAGTGGT	1:1
MuRF3_Ex4_for1	CTCAATGCTCTGGCACACCT	
qRT-PCR		
Mm_ATP5A1_Sybr_for	CGGGCTGAGGAATGTTCA	1:1
Mm_ATP5A1_Sybr_rev	CCAAGTTCAGGGACATACCC	
Mm_Gapdh_Sybr_fwd	ATGGTGAAGGTCGGTGTGA	1:1
Mm_Gapdh_Sybr_rev	AATCTCCACTTTGCCACTGC	

Mm_MTCO1_Sybr_frev	AGTAGTATAGTAATGCCTGCGGCTA	1:1
Mm_MTCO1_Sybr_fwd	TCCACTATTTGTCTGATCCGTACT	
Mm_NDUFB8_Sybr_fwd	TCCCTTCCTACCAGCCTGT	1:1
Mm_NDUFB8_Sybr_rev	GAGCAGGAAAACAGGAATGC	
Mm_PGC1alpha_SYBR_for	TGAAAGGGCCAAACAGAGAG	1:1
Mm_PGC1alpha_SYBR_rev	GTAAATCACACGGCGCTCTT	
Mm_SDHB_Sybr_for	ACTGGTGGAACGGAGACAAG	1:1
Mm_SDHB_Sybr_rev	CCTCTGTGAAGTCGTCTCTGG	
Mm_UQCRC2_Sybr_fwd	TGGGCTCTTTGGAATTTACAC	1:1
Mm_UQCRC2_Sybr_rev	TTGGTTGTAGGCAGCATTGA	

Primers are separated in the ones used for genotyping and qPCR. Besides the sequence, the ratio in which the primers are used with each other is also listed here.

6.1.6. Reagents, Kits, consumables and devices

Table 6. Reagents.

Reagent	Supplier
5,5'-dithiobis (2-nitrobezoic acid) (DTNB)	Sigma-Aldich, St. Louis, Mo, USA
Acetic acid	Sigma-Aldrich, St. Louis, MO, USA
Acetone	Sigma-Aldich, St. Louis, Mo, USA
Acetonitrile (ACN)	J.T. Baker, Deventer, NL
Agarose	Serva, Heidelberg, DE
Ammonium persulfate (APS)	Bio-Rad Laboratories, Hercules, CA, USA
anti-FLAG M2 affinity gel	Sigma-Aldrich, St. Louis, MO, USA
Antimycin A	Sigma-Aldrich, St. Louis, MO, USA
Bovine serum albumin (BSA)	Sigma-Aldich, St. Louis, Mo, USA Carl Roth, Karlsruhe, DE
Bradford Reagent	Bio-Rad Laboratories, Hercules, CA, USA
CaCl$_2$	Merck, Darmstadt, DE
Chloroform	Carl Roth, Karlsruhe, DE
Coenzym Q	Sigma-Aldich, St. Louis, Mo, USA
Coenzyme A (Ac-CoA)	Merck, Darmstadt, DE
cOmplete™	Roche, Basel, CH
Cycloheximide (CHX)	Sigma-Aldrich, St. Louis, MO, USA

Cytochrome C	Sigma-Aldich, St. Louis, Mo, USA
Decylubichinone	Sigma-Aldrich, St. Louis, MO, USA
DMSO	PAN-Biotech, Aidenbach, DE
DTT	ThermoFisher, Waltham, MA, USA
Dulbecco's Modified Eagle Medium (DMEM)	ThermoFisher, Waltham, MA, USA PAN-Biotech, Aidenbach, DE
ethylene glycol-bis(β-aminoethyl ether)-N,N,N',N'-tetraacetic acid (EGTA)	Sigma-Aldrich, St. Louis, MO, USA
Eosin	Carl Roth, Karlsruhe, DE
Ethanol	Carl Roth, Karlsruhe, DE
Ethylenediaminetetraacetic acid (EDTA)	Carl Roth, Karlsruhe, DE
fetal bovine serum	ThermoFisher, Waltham, MA, USA
Fugene®6	Promega Corporation, Madison, WI, USA
Glucose	Carl Roth, Karlsruhe, DE
Gum tragacanth	Sigma-Aldrich, St. Louis, MO, USA
HCL	Carl Roth, Karlsruhe, DE
Hematoxylin	Carl Roth, Karlsruhe, DE
Iodacetamide	Sigma-Aldrich, St. Louis, MO, USA
Isofluran CP®	CP-Pharma, Burgdorf, DE
Isopropanol	Carl Roth, Karlsruhe, DE
KCl	Carl Roth, Karlsruhe, DE
KCN	Sigma-Aldich, St. Louis, Mo, USA
Laemmli sample buffer (2x/4x)	Bio-Rad Laboratories, Hercules, CA, USA
Lipofectamine™ 3000	ThermoFisher, Waltham, MA, USA
MG132	Merck, Darmstadt, DE
$MgSO_4$	Sigma-Aldrich, St. Louis, MO, USA
Milk powder	Carl Roth, Karlsruhe, DE
Na_3VO_4	Sigma-Aldich, St. Louis, Mo, USA
NaCl	Carl Roth, Karlsruhe, DE
Na-Deoxycholate	Merck, Darmstadt, DE
NaF	Merck, Darmstadt, DE
NaH_2PO_4	Merck, Darmstadt, DE
$NaHCO_3$	Merck, Darmstadt, DE
NEM	Sigma-Aldrich, St. Louis, MO, USA

N-Ethylmaleimide	Sigma-Aldich, St. Louis, Mo, USA
Nicotinamide adenine dinucleotide (NADH)	Sigma-Aldich, St. Louis, Mo, USA
NP-40/IGEPAL	ICN biomedicals inc., Costa Mesa, CA, USA
Oxalacetate	Sigma-Aldich, St. Louis, Mo, USA
Penicillin-Streptomycin	Sigma-Aldrich, St. Louis, MO, USA
Phosphate-buffered saline (PBS)	ThermoFisher, Waltham, MA, USA
PhosStop™	Roche, Basel, CH
Polybrene	Santa Cruz, Dallas, TX, USA
RNase free water	Qiagen, Venlo, NL
Rotenon	Sigma-Aldrich, St. Louis, MO, USA
Sodium dodecyl sulfate (SDS)	Carl Roth, Karlsruhe, DE
Sucrose	Sigma-Aldich, St. Louis, Mo, USA
SuperSignal™ West Femto Maximum Sensitivity Substrate	ThermoFisher, Waltham, MA, USA
Tetramethylethylenediamine (TEMED)	Sigma-Aldrich, St. Louis, MO, USA
Thiourea	Sigma-Aldrich, St. Louis, MO, USA
Tris(hydroxymethyl)aminomethan (Tris)	Carl Roth, Karlsruhe, DE
Triton X® 100	Carl Roth, Karlsruhe, DE
TRIzol© reagent	Invitrogen, Waltham, MA, USA
Tween 20	Carl Roth, Karlsruhe, DE
Ubichinone	Sigma-Aldrich, St. Louis, MO, USA
Urea	Sigma-Aldrich, St. Louis, MO, USA
VectaMount® Permanent Mounting Medium	Vector Laboratories, Inc., Burlingame, CA, USA
Xylol	Carl Roth, Karlsruhe, DE
β-Mercaptoethanol	Carl Roth, Karlsruhe, DE

Table 7. Consumables.

Consumables	Supplier
Adhesion slides (SuperFrost®)	R. Langenbrinck, Emmendingen, DE
Amersham™ Hybond™ 0.45 polyvinylidenfluoride (PVDF) membrane	GE Healthcare, Chicago, IL, USA

Cell scraper S	Sarstedt, Nümbrecht, DE
Cover slips	R. Langenbrinck, Emmendingen, DE
Disinfection wipes (Mikrozid® sensitive wipe premium)	Schülke & Mayr, Norderstedt, DE
Falcon tubes (15 ml)	Sarstedt, Nümbrecht, DE
Falcon tubes (50 ml)	Corning Life Science, Corning, NY, USA
Gloves, nitrile (Peha-Soft®)	Paul Hartmann, Heidenheim, DE
Injekt®-F (1 ml)	B. Braun, Melsung, DE
Microlance 21gx1 ½ Nr2 (0,8x40 mm)	BD, Becton, NJ, USA
MS pipette tips (200 µl StackPack)	Sarstedt, Nümbrecht, DE
MS pipette tips (epT.I.P.S. 10 µl, 1000 µl)	Eppendorf, Hamburg, DE
Pipette tips (10 µl)	Carl Roth, Karlsruhe, DE Greiner Bio-One, Frickenhausen, DE
Pipette tips (200 µl, 1000 µl)	Greiner Bio-One, Frickenhausen, DE Sarstedt, Nümbrecht, DE
Pipette tips with filter (SurPhob SafeSeal® LOW BINDING, RNase free)	Biozym Scientific, Hessisch Oldendorf, DE
Reaction vessels (0.25 ml, 0.5 ml, 1.5 ml, 2 ml)	Sarstedt, Nümbrecht, DE
Reaction vessels (2 ml)	Eppendorf, Hamburg, DE
Screw vials	Schott, Mainz, DE
TC Flask T75 vent cap	Sarstedt, Nümbrecht, DE
TC Plate, standard, F (12 and 6 Well)	Sarstedt, Nümbrecht, DE
Weighing dishes	Carl Roth, Karlsruhe, DE
ZipTip® tips (µ-C18)	Merck Millipore, Darmstadt, DE

Table 8. Kits and Enzymes.

Kits/Enzymes	Supplier
FAST START SYBR Green PCR Master Mix	Roche, Basel, CH
Lysine-sensitive aspartokinase 3 (LysC, Lysobacter enzymogenes)	Promega Corporation, Madison, WI, USA
Perfekt 100-1000BP DNA Ladder	Roboklon, Berlin, DE
Pierce™ BCA Protein Assay Kit	ThermoFisher, USA
Proteinase K	Merck Millipore, Darmstadt, DE

Seq. grade Modified Trypsin, porcine	Promega Corporation, Madison, WI, USA
SuperScript® II Reverse Transcriptase	Invitrogen, Waltham, MA, USA
Taq DNA Polymerase 5000 u / Kit (+ dNTPs)	Roboklon, Berlin, DE
TGX Stain-Free™ FastCast™ Acrylamide Kits (7,5%, 10%, 12%)	Bio-Rad Laboratories, Hercules, CA, USA

Table 9. Devices.

Device	Supplier
Accessories for 1D-PAGE	Bio-Rad Laboratories, Hercules, CA, USA
Acclaim™ PepMap™ 100 C18 HPLC Column (75 μm diameter, 3 μm particle size)	Thermo Fisher Scientific, Waltham, MA, USA
Accucore™ C18 HPLC Columns (75 μm diameter, 2.6 μm particle size, 25 cm)	Thermo Fisher Scientific, Waltham, MA, USA
Beadblaster™24	Benchmark Scientific, Edison, NJ, USA
BIO-GS3	Bioseb, Vitrolles, FR
Bio-Rad TGX system	BioRad, Hercules, CA, USA
ChemiDoc™ XRS+ Imaging System	Bio-Rad Laboratories, Hercules, CA, USA
Compact Fluorescence Microscope (BZ-X810)	Keyence, Osaka, JP
Epredia™ CryoStar™ NX50 crytome	Thermo Fisher Scientific, Waltham, MA, USA
Heraeus™ Fresco™ 17/21 centrifuge	Thermo Fisher Scientific, Waltham, MA, USA
Heraeus™ incubator	Thermo Fisher Scientific, Waltham, MA, USA
HeraSafe™ sterile workbench	Thermo Fisher Scientific, Waltham, MA, USA
Magnetic stir bars	VWR International, Darmstadt, DE
Microscope (Mantis Compact)	Vision Engineering, Surrey, UK
MiniStar Microcentrifuge	VWR International, Darmstadt, DE
MR2000, MR3000 magnetic stirrers	Heidolph Instruments, Schwabach, DE
Nanodrop 2000	Thermo Fisher Scientific, Waltham, MA, USA
Orbitrap Exploris™ 480 Mass Spectrometer	Thermo Fisher Scientific, Waltham, MA, USA
pH meter MP230	Mettler-Toledo, Columbus, OH, USA
Pipettes (PIPATMAN® Classic)	Gilson, Middleton, WI, USA
Pipettes (Research® plus)	Eppendorf, Hamburg, DE
PowerPac 200/300 (HC, Basic)	Bio-Rad Laboratories, Hercules, CA, USA
Precision balance (CPA324S)	Sartorius, Göttingen, DE

Precision balance Acculab Atilon	Sartorius, Göttingen, DE
Proflex PCR System	Thermo Fisher Scientific, Waltham, MA, USA
Q Exactive™ Plus Hybrid Quadrupole-Orbitrap™ Mass Spectrometer	Thermo Fisher Scientific, Waltham, MA, USA
QuantStudio™ 3 Real-Time PCR	Thermo Fisher Scientific, Waltham, MA, USA
Rocker shaker Duomax 1030	Heidolph Instruments, Schwabach, DE
Synergy H1 Hybrid plate reader	BioTek, Winooski, VT, USA
Thermomixer comfort	Eppendorf, Hamburg, DE
ThermoMixer®F1.5	Eppendorf, Hamburg, DE
Tissue Homogenizer	Glas-Col, Terre Haute, IN, USA
Trans-Blot® SD Semi-Dry Transfer Cell	Bio-Rad Laboratories, Hercules, CA, USA
UltiMate 3000 UPLC	Thermo Fisher Scientific, Waltham, MA, USA
UV-16000PC spectrophotometer	VWR International, Darmstadt, DE
Vortexer Reax 2000	Heidolph Instruments, Schwabach, DE

6.1.7. Software

Table 10. Software.

Software	Supplier	
ASI 611A Dynamic Muscle Analysis DMA v5.010	Aurora Scientific Inc., Aurora, CA	v5.010
ASI Dynamic Muscle Control DMC v5.300	Aurora Scientific Inc., Aurora, CA	v5.300
BZ-X800 Analyzer	Keyence, Osaka, JP	1.0.0.0
GraphPad Prism 8.30	GraphPad Software, La Jolla, CA, USA	8.30
ImageLab™ 6.0.1	Bio-Rad Laboratories, Hercules, CA, USA	6.0.1
M.Wave Professional 1.0	Mrc lab, Holon, IL	1.0
Microsoft® Office 2016	Microsoft Corporation, Redmond, WA, USA	2016
Procreate®	Savage Interactive Pty Ltd., Hobart, Australia	5.3.3

QuantStudio™ Design & Analysis Software	Thermo Fisher Scientific, Waltham, MA, USA	v.1.5.2
Spectronaut software v14.3.	Biognosys, Schlieren, CH	v14.3.

6.2. Methods

6.2.1. Genotyping of MuRF1/MuRF3 DKO mice

For genotyping the tail tip was dissolved in 51 µl DNA isolation buffer (100 mM Tris pH8.5, 5 mM EDTA pH8.0, 200 mM NaCl, 0.2 % SDS, Proteinase K 10 mg/ml) and digested at 55 °C, while shaking at 800 rpm, overnight. The reaction was stopped on the next day by adding 450 µl aqua des. Samples were centrifuged at 15.000 rpm at room temperature (RT) and the supernatant transferred to a fresh tube. The isolated DNA was used in for PCR analysis, using the Taq DNA Polymerase Kit from Roboklon (Berlin, Germany). Sample preparation as well as the PCR protocol can be inferred from tables 11 to 12. Genotyping was performed with the Proflex PCR System from Thermo Fisher Scientific (Waltham, MA, USA).

Table 11. Sample preparation for genotyping PCR

Chemicals	Volume in [µl]		
	MuRF1 WT and KO	MuRF3 WT	MuRF3 KO
H_2O	19.95	20.05	19,85
10x Puffer C	2.5	2.5	2.5
dNTP´s	0.5	0.5	0.5
MgCl2	0.5	0.5	0.5
Forward primer	0.1	0.1	0.2
Reverse primer	0.1	0.1	0.2
Second forward primer	0.1	-	-
Roboklon Taq Pol	0.25	0.25	0.25
DNA	1	1	0.5

Table 12. Temperature set-up for genotyping PCR

Steps	Temperature		Time		Number of cycles
	MuRF1	MuRF3	MuRF1	MuRF3	
1. Denaturation	95°C	95°C	5 min	5 min	1 x
2. Denaturation	94°C	94°C	30 sec	30 sec	40x
3. Primer	62°C	60 °C	30 sec	1 min	
4. Elongation	72°C	72°C	30 sec	30 sec	
5. Final Elongation	72°C	72°C	10 min	10 min	1 x
6. Infinite hold	4°C	4°C	∞	∞	

PCR products were separated via a 1 % agarose gel. Products with a length of 300 bp (MuRF1) or 350 bp (MuRF3) were expect for WT genes, while KO genes had a length of 450 bp (MuRF1) and 500 bp (MuRF3), respectively.

6.2.2. Grip strength measurement

For grip strength measurement the BIO-GS3 (Bioseb, Vitrolles, France) was used. Mice were held by their tail and brought close to the grit attached to the machine. Due to their natural grip reflex mice held on to the grit with their front legs, and were then pulled away. The strength brought up to hold on was measured in [g]. This was repeated per mouse for at least 3 times, with 10 min breaks intervals. The strength data was normalized to tibia length.

6.2.3. Specific muscle force measurement

We mounted the EDL on a force transducer and bathed it in oxygenized Krebs-Henseleit-buffer (122 mM NaCl, 4.5 mM KCL, 1.2 mM NaH2PO4, 1.2 mM $MgSO_4$, 26 mM $NaHCO_3$, 11 mM Glucose, 2.5 mM $CaCl_2$, 95 % O2, 5% CO_2) at 25 °C. Following a 15 min equilibration, it was adjusted to optimal length. To measure performance the EDL was stimulated in sets of 2 Hz, 10 Hz, 20 Hz, 40 Hz, 60 Hz, 80 Hz, 100 Hz, 125 Hz and 150 Hz. A set contained 3 trains (pulses), with a break of 1000 ms between each of them. There was a break of 3 s between sets. Via the ASI Dynamic Muscle Control DMC v5.300 (Aurora Scientific Inc., Aurora, Canada) and ASI 611A Dynamic Muscle Analysis DMA v5.010 (Aurora Scientific Inc., Aurora, Canada) software we measured muscle contraction and performed analysis. We calculated the muscle cross-sectional area (CSA), by dividing muscle mass in [mg] by optimal length L0 in [mm], the density of skeletal muscle (1.06 g/cm³) and the ratio of myofibre length to muscle length, which is 0.45 for EDL. The CSA was then used to normalize the measured force development. Measurements were performed by Brita Püschel.

6.2.4. Hematoxylin and eosin staining

TA was embedded in gum tragacanth (Sigma-Aldrich, St. Louis, MO, USA), bathed in liquid nitrogen cooled isopentane, shock frozen in liquid nitrogen and cut in 8 μm thick sections with the Epredia™ CryoStar™ NX50 crytome (Thermo Fisher Scientific, Waltham, MA, USA) and placed on Adhesion slides (SuperFrost®, R. Langenbrinck, Emmendingen, Germany), after being stored at −80 °C. The sections were then rehydrated using a descending ethanol row (2x 100%, 96%, 80%, 70%, diluted in aqua des). They were stained with hematoxylin (Carl Roth, Karlsruhe, Germany) for 10 min, followed by a washing step with

aqua des. After staining with eosin (Carl Roth, Karlsruhe, Germany) for 5 min the slides were washed with aqua dest again. Sections were dehydrated with 95% and 100% ethanol followed by two 5 min xylol steps (Carl Roth, Karlsruhe, Germany), after a final washing step. VectaMount® Permanent Mounting Medium (Vector Laboratories, Inc., Burlingame, USA) was used to fixate the tissue and seal it with a cover slip. Preparation of sections and staining was performed by Kirsten Bartels.

6.2.5. RNA isolation from tissue, cDNA production and qRT-PCR

TA and heart tissue was homogenized in TRIzol© reagent (Invitrogen, Waltham, MA, USA) using the Beadblaster™24 (Benchmark Scientific, Edison, NJ, USA). Samples were than incubated on ice for 5 min and afterwards 200 µl of Chloroform was added. They were vortexed and centrifuged at 14.000 g for 10 min at 4 °C. The upper clear supernatant layer was transferred into a new Eppendorf tube, while the rest was discarded. 500 µl of Isopropanol were added to the sample, the they were incubated again on ice for 10 min. Following a centrifugation at 14 000 g for 30 min at 4 °C, the supernatant was discarded. The pallet was washed with 1000µl 80% Ethanol 2x times, air dried and resuspended in 20- 50 µl RNase free water, depending on pallet size. RNA concentration was estimated via Nanodrop (Thermo Fisher Scientific, Waltham, MA, USA). 1000 ng of RNA template were used for cDNA synthesis with the SuperScript® II Reverse Transcriptase kit from Invitrogen (Waltham, MA, USA) and the Proflex PCR System (Thermo Fisher Scientific, Waltham, MA, USA), following manufacturer's instructions. For measuring RNA expression, we used quantitative real-time polymerase chain reaction (qRT-PCR) performed with the QuantStudio®3 thermocycler (Thermo Fisher Scientific, Waltham, MA, USA). The FAST START SYBR Green PCR Master Mix from Roche (Roche, Basel, Switzerland) was used for this method. Details about sample preparation and qRT-PCR set-up can be found in Table 13 and 14.

Table 13. Sample preparation for qRT-PCR.

Chemicals	Volume in [µl]
Nuclease free water	6
Forward Primer	1
Reverse Primer	1
FAST START SYBR Green PCR Master Mix	10
cDNA	2

Table 14. Temperature set-up for qRT-PCR

Stages	Temperature	Time	Number of cycles
1. Hold stage	50 °C	2 min	1 x
	95 °C	10 min	1 x
2. PCR stage	95 °C	15 s	40 x
	60 °C	1 min	
3. Melt curve stage	95 °C	15 s	1 x
	60 °C	1 min	1x
	95 °C	15 s	1x
4. Infinite stage	4 °C	∞	

cDNA amount was calculated via a standard curve. We normalized our results to the expression levels of the housekeeping gene glyceraldehyde-3-phosphate dehydrogenase (*Gapdh*).

6.2.6. Protein Isolation and Western-Blot

The Beadblaster™24 (Benchmark Scientific, Edison, NJ, USA) was used to homogenize heart and TA tissue in Radioimmunoprecipitation assay (RIPA) buffer (50 mM Tris-HCL (pH 7.4), 150 mM NaCl, 1% NP-40, 1 mM EDTA, 0.25% Na-Deoxycholate, 1x cOmplete™ (Roche, Basel, Switzerland), 1x PhosStop™ (Roche, Basel, Switzerland), 0.1 mM Na_3VO_4, 1 mM NaF, 0.01 % SDS) to isolate proteins. To get rid of debris we centrifuged the samples at 10.000 g for 10 min at 4 °C. The supernatant was then transferred into a new Eppendorf tube, the pellet was discarded. With the Pierce™ BCA Protein Assay Kit (Thermo Fisher Scientific, Waltham, MA, USA) and the Synergy H1 Hybrid plate reader (BioTek, Winooski, VT, USA) we determined the Protein concentration following manufacturer's manual. Laemmli buffer (Bio-Rad Laboratories, Hercules, CA, USA) was then added to the samples and they were boiled at 95 °C for 5 min. We used the semi dry Bio-Rad TGX system from BioRad (Hercules, CA, USA) for Sodium dodecylsulfate polyacrylamide gel electrophoresis (SDS-PAGE) with the TGX Stain-Free™ FastCast™ Acrylamide Kits (7,5%, 10%, 12%), also following manufacturer's manual. Proteins were blotted with the Trans-Blot® SD

Semi-Dry Transfer Cell onto Amersham™ Hybond™ 0.45 Polyvinylidenfluoride (PVDF) membrane (GE Healthcare, Chicago, IL, USA) and then blocked for 1 h at room temperature. The blocking reagent, 5% milk powder or 3% BSA in TBS-T, depended on the primary antibody. A list of all primary antibodies with the used blocking reagent and dilution, as well as the same data for the corresponding secondary antibody can be found in Table 6.

Incubation with primary antibody took place over night at 4° C. Secondary antibody incubation was for 1 h at room temperature, after washing the membrane 3x times with 1x TBS-T (2.42 g/l Tris, 8 g/l NaCl, 1% Tween 20, pH 7.6) for 5 min. After a final washing step, again 3x times 1x TBS-T for 5 min, proteins were detected with the ChemiDoc™ MP Imaging System (Bio-Rad Laboratories, Hercules, CA, USA) and SuperSignal™ West Femto Maximum Sensitivity Substrate (Thermo Fisher Scientific, Waltham, MA, USA) or the Clarity™ Western ECL Substrate (Bio-Rad Laboratories, Hercules, CA, USA), depending on signal intensity. We used the the ImageLab™ 6.0.1 software (Bio-Rad Laboratories, Hercules, CA, USA) to analyze western blot pictures.

6.2.7. Photospectrometric measurement of Complex I, III, IV and citrate synthase activity

For measurement of Complex I, III, IV and citrate synthase activity we followed the protocol of Spinazzi et al., 2012. In short, we used the tissue Homogenizer from Glas-Col (Terre Haute, IN, USA) to extract intact mitochondria from heart and TA tissue in sucrose buffer (250 mM) (0,242 g/l Tris, 0,30 g/l KCL, 0,076 g/l EGTA, pH 7.4; add 0,854 g sucrose to 10 ml buffer on day of usage). Protein concentration was determined with the Pierce™ BCA Protein Assay Kit (Thermo Fisher Scientific, Waltham, MA, USA) and samples were diluted to a concentration of 0.5 µg/µl. We than measured activity as followed with the UV-16000PC spectrophotometer (VWR International, Darmstadt, DE):

Citrate synthase activity: The assay buffer was prepared as followed in a 1 ml cuvette: 500µl Tris (stock solution: 200 mM, pH 8.0) with Triton™ X-100 (Sigma-Aldrich, St. Louis, MO, USA) (stock solution: 0.2%), 100 µl 5,5'-dithiobis (2-nitrobezoic acid) (DTNB) (stock solution: 1 mM), 30 µl Coenzyme A (Ac-CoA) (stock solution: 10 mM) and 5 µg of isolated protein (TA or heart). Volume was adjusted to 950 µl by adding aqua des. Light absorption of the sample at 412 nm was measured for 3 min, as a baseline. We than added 50 µl oxaloacetic acid (stock solution: 10 mM), a substrate of citrate synthase, to start the reaction and absorption was measured again at 412 nm for 3 min.

Complex I: The assay buffer was prepared as followed in a 1 ml cuvette: 100 µl Potassium-Phosphate buffer (stock solution: 500 mM, pH 7.5), 60 µl Bovine serum albumin (BSA) (stock solution: 50 mg/ml), 30 µl Potassium cyanide (KCN) (stock solution: 10 mM), 10 µl Nicotinamide adenine dinucleotide (NADH) (stock solution: 10 mM) and 10 µg of isolated protein (TA or heart). Volume was adjusted to 994 µl by

adding aqua des. A second sample was prepared containing 10 µl the complex I inhibitor rotenone (stock solution: 1 mM), to correct for none complex I specific activity. The absorption of each sample was measured at 340 nm for 2 min, as a baseline. We than added 6 µl ubiquinone (stock solution: 10 mM), the electron acceptor of complex I, to start the reaction and measured the absorption again at 340 nm for 2 min. The activity was corrected by subtracting the absorption of the sample with rotenone from the sample without the inhibitor.

Complex III: The assay buffer was prepared as followed in a 1 ml cuvette: 50 µl Potassium-Phosphate buffer (stock solution: 500 mM, pH 7.5), 75 µl oxidized Cytochrome c (stock solution: 1 mM), 50 µl KCN (stock solution: 10 mM), 20 µl Ethylenediaminetetraacetic acid (EDTA) (stock solution: 5 mM, pH 7.5), 10 µl Tween-20 (stock solution: 2.5%) and 2.5 µg of isolated protein (TA or heart). Volume was adjusted to 990 µl by adding aqua des. A second sample was prepared containing 10 µl of the complex III inhibitor Antimycine A (stock solution: 1 mg/ml), to correct for none complex III specific activity. The absorption of each sample was measured at 550 nm for 3 min min, as a baseline. We than added 10 µl decylubiquinone (stock solution: 10 mM), the substrate of complex III, to start the reaction and measured the absorption again at 550 nm for 3 min. The Activity was corrected by subtracting the absorption of the sample with Antimycine A from the sample without inhibitor.

Complex IV: The assay buffer was prepared as followed in a 1 ml cuvette: 500 µl Potassium-Phosphate buffer (stock solution: 100 mM, pH 7.0) and 60 µl reduced Cytochrome c (stock solution: 1 mM) into one plastic cuvette. Volume was adjusted to 995 µl by adding aqua des. A second sample was prepared containing 30 µl of the complex IV inhibitor KCN (stock solution: 10 mM), to correct for none complex IV specific activity. The absorption of each sample was measured at 550 nm for 3 min min, as a baseline. We than added 2 µg of isolated protein, from TA or heart, to start the reaction and measured the absorption again at 550 nm for 3 min. The Activity was corrected by subtracting the absorption of the sample with KCN from the sample without inhibitor.

6.2.8. Culturing of COS7 cells

We cultivated COS7 Cells in Dulbecco's Modified Eagle Medium (DMEM; 4.5 g/L D-Glucose, L-Glutamine, Pyruvate (gibco, Thermo Fisher Scientific, Waltham, MA, USA), 10% Fetal Bovine Serum (Sigma-Aldrich, St. Louis, MO, USA), 1% Penicillin-Streptomycin (Sigma-Aldrich, St. Louis, MO, USA)), which was changed every second day. When cells reached a confluence of 70 %, they were passage into a new bottle. For this they were washed with 5 ml PBS (gibco, Thermo Fisher Scientific, Waltham, MA, USA), before 1 ml of Trypsin (Sigma-Aldrich, St. Louis, MO, USA) was added. After a 5 min incubation step at 37 °C, cells were suspended in 9 ml fresh medium and transferred into a falcon tube. They were than centrifuged for 5 min

at 500 g. The supernatant was discarded and the cell pallet diluted in new growth medium, which was placed into new cell culture flaks.

6.2.9. Transfection of COS7 cells with Fugene®6

Fugene®6 (Promega Corporation, Madison, WI, USA) was used according to manufacturer's protocol. 91 µl of serum free DMEM (4.5 g/L D-Glucose, L-Glutamine, Pyruvate (gibco, Thermo Fisher Scientific, Waltham, MA, USA)) was mixed with 9 µl Fugene®6. This master mix was then split into Eppendorf tubes and plasmid DNA was added as indicated (2 µg/µl – 4 µg/µl). The Plasmid-Fugene®6 mix was than incubated for 30 min at room temperature. COS7 cells seeded a day before on 6 Well plates (150 000 cells per well) were washed with PBS and fresh DMEM added to them. After the incubation step the Plasmid-Fugene®6 mix was transferred to the wells. After 48 h of overexpression COS7 cells were harvested or treated for further assays as indicated.

6.2.10. Culturing of C2C12 cells

C2C12 myoblasts were cultivated in growth medium (GM)(DMEM (1 g/L Glucose, L-Glutamine, Sodium Pyruvate, 3.7 g/L NaHCO3 (PAN-Biotech, Aidenbach, Germany), 10% Fetal Bovine Serum (Sigma-Aldrich, St. Louis, MO, USA), 1% Penicillin-Streptomycin (Sigma-Aldrich, St. Louis, MO, USA)). The medium was changed every second day and when cells reached a confluence of 70%, we passaged them into new cell culture flask as described for COS7 cells (6.2.8). To differentiate myoblast into myotubes growth medium was changed to differentiation medium (DM) (DMEM (1 g/L Glucose, L-Glutamine, Sodium Pyruvate, 3.7 g/L NaHCO3 (PAN-Biotech, Aidenbach, Germany), 2% Fetal Bovine Serum (Sigma-Aldrich, St. Louis, MO, USA), 1% Penicillin-Streptomycin (Sigma-Aldrich, St. Louis, MO, USA)), which was changed daily. After 3 days of differentiation cells were treated and harvested as indicated.

6.2.11. Transduction of C2C12 cells via Retrovirus containing pMP71 Plasmid

Retrovirus were created by transfecting Platinum-E (PLAT-E, Cell Biolabs, San Diego, CA, USA) retroviral packaging cells with retroviral expressing constructs of pMP71-IRES-GFP, pMP71-IRES-MuRF1-Flag and pMP71-IRES-MuRF3-Flag with Lipofectamine™ 3000, following manufacturer's instructions. After 48 h the supernatant was harvested. For transduction, C2C12 cells were seeded on 12 Well plates (33.000 cells per well). A day after seeding the medium was changed to DMEM, without Serum and Penicillin-Streptomycin, with 4 µg/ml polybrene. To each well 80 µl (pMP71-IRES-GFP control and pMP71-IRES-MuRF3) or 100 µl (pMP71-IRES-MuRF1) of retrovirus was added. The plates were than centrifuged at 800x

g for 90 min at 32 °C. After 4 - 5 h incubation at 37 °C the medium was changed to GM for 24 h. 48 h after transduction differentiation was started by adding DM to the cells.

6.2.12. Coimmunoprecipitation

Transfected COS7 cells were harvest after 48 h of overexpression in 200 µl of lysis buffer (1x PBS (gibco, Thermo Fisher Scientific, Waltham, MA, USA), 1x cOmplete™ (Roche, Basel, Switzerland), 0,5 % Triton™ X-100 (Sigma-Aldrich, St. Louis, MO, USA)). Cells were lysed via rotating at 15 rpm at 4 °C for 30 min. To get rid of debris samples were then centrifuged for 10 min at 10 000x g at 4 °C. The supernatant was transferred into a new tube. 20 µl of sample (10%) were removed as an input control and prepared for western blot by adding 2x Laemmli buffer and heating them up to 95 °C for 5 min. They were then stored over night at -20 °C. The volume of the remaining sample was increased to 1 ml by adding appropriate amounts of lysis buffer. Anti-FLAG M2 Affinity gel (Sigma-Aldrich, St. Louis, MO, USA) was 3x times washed with PBS and then diluted 1:2 with PBS. 30 µl of washed Anti-FLAG M2 Affinity gel was added to the samples, before incubating them at 4 °C overnight, while rotating at 15 rpm. Afterwards this mixture was centrifuged, the supernatant was discarded and the Anti-FLAG M2 Affinity gel was washed 3x times with PBS. To release the proteins attached to the affinity gel, 40 µl of 2x Laemmli buffer (Bio-Rad Laboratories, Hercules, CA, USA) were added and then boiled at 95 °C for 3 min. After transferring the supernatant into a new tube 1 µl of β-mercaptoethanol (Carl Roth, Karlsruhe, Germany) was added to the sample. They were then boiled again 95 °C for 3 min. Following this last step, Input and IP samples were used for immunoblot analysis.

6.2.13. Cycloheximide assay

pMP71-IRES-MuRF1, pMP71-IRES-MuRF3, pMP71-IRES-MuRF1 and pMP71-IRES-MuRF3 and pMP71-IRES-GFP control transduced C2C12 myoblast were differentiated for 3 days on 12-well plates. Afterwards the medium was changed, and they were treated with 50 µg/ml Cycloheximide for 6 h, to inhibit protein synthesis. Samples were taken during that time at 0 h, 3 h and 6 h. Samples were harvested in 200 µl of RIPA buffer. After shock freezing the samples in liquid nitrogen and letting them thaw at room temperature, they were stored on ice for 15 min, followed by a centrifugation step (15.000 rpm, 4 °C, 10 min). The supernatant was transferred into a new tube. The BCA kit from Thermo Fisher was used to estimate the protein concentration of the samples. 25 µg of protein per sample was then used for an immunoblot assay.

6.2.14. Ubiquitination assay

Transfected COS7 cells, overexpressing pcDNA™3.1(+)/FLAG_HDAC5, pEGFP-N3-HA-Ubi, pcDNA™3.1/myc-His(-)_MuRF1 and/or pcDNA™3.1/myc-His(-)_MuRF3 (Table 15), were cultivated for 48 h on 6-well plates (150.000 cells per well) and then treated with MG132, to inhibit proteasomal protein degradation, or DMSO (25 μM) as a control (solvent for MG132) for 6 h.

Table 15. 6 Well plate set-up for ubiquitin assay

Well	1	2	3
A	HDAC5-Flag + pcDNA3.1-myc-his	HDAC5-Flag + MuRF1-Myc and/or MuRF3-Myc + pcDNA3.1-myc-his	HDAC5-Flag + MuRF1Cys39/47-Myc and/or MuRF3Cys42/50-Myc + pcDNA3.1-myc-his
B	HDAC5-Flag + Ubiquitin-HA	HDAC5-Flag + MuRF1-Myc and/or MuRF3-Myc + Ubiquitin-HA	HDAC5-Flag + MuRF1Cys39/47-Myc and/or MuRF3Cys42/50-Myc + Ubiquitin-HA

pcDNA™3.1/myc-His(-)_MuRF1Cys39/47 and pcDNA™3.1/myc-His(-)_MuRF3Cys42/50-Myc are inactive mutants, with a non-functioning RING domain, created by side-directed mutagenesis (AG Fielitz). After the 6 h treatment the cells were harvested in 200 μl CO-IP lysis buffer with 15 mM N-Ethylmaleimide (NEM) to prohibit deubiquitination of proteins. IP, like CO-IP lysis buffer preparation, was then performed as described in Coimmunoprecipitation.

6.2.15. Mass spectrometry of protein lysates from heart and skeletal muscle

Proteins were isolated from TA and heart tissue in 200 μl 1xUT buffer (8 M Urea, 2 M Thiourea, in aqua des) with a bead mill (Retsch, Haan, Germany) at 2.600 rpm for 2 min. Afterwards the samples were centrifuged at 16.000 x g for 60 min at 20 °C, the supernatant was transferred into a new Eppendorf tube. Nucleic acids were digested with benzonase (0.125 U/μg protein), before estimating protein concertation via Bradford assay (Bio-Rad Laboratories, Hercules, CA, USA). Samples were prepared by reducing them with DTT (2.5 mM, in 20 mM Ammonium bicarbonate (ABC)) for 30 min at 37°C and alkylating them with iodacetamide (10 mM, in 20 mM ABC) for 15 min at 37°C them. They were then digested with LysC (enzyme to protein ratio 1:100, Promega, Germany) for 3h at 37 °C as well as trypsin (1:25, Promega) for 16 h at 37°C, which was stopped by adding acetic acid (1 %), to increase the amount of peptides from the

protein lysate. Peptide mixtures were purified from contaminations with C-18 reverse phase material (ZipTip μ-C18, Millipore Corporation, USA) packet tips. We then eluted the samples in 50 and 80 % acetonitrile (CAN) in 1% acetic acid. Pooled eluates were concentrated by lyophilization and resuspended in 2% ACN in 0.1 % acetic acid. LC-MS/MS analysis was performed with an UltiMate 3000 UPLC system coupled to a Q Exactive™ Plus (Heart) (Thermo Fisher Scientific, Waltham, MA, USA) or Orbitrap Exploris™ 480 (TA) instrument (Thermo Fisher Scientific, Waltham, MA, USA), set in the data-independent acquisition (DIA) mode. For peptide separation we used a 25 cm Accucore column (75 μm inner diameter, 2.6 μm, 150 A, C18). Further information can be found in supplement table 16 and 17.

Raw mass spectrometric data was analyzed with the Spectronaut software (v14.3., Biognosys, Switzerland). For peptide and protein identification the Direct DIA approach, based on UniProt database limited to Mus musculus entries (version 04_2020), was used. We defined carbamidomethylation at cysteine as a static modification, while oxidation at methionine and protein N-terminal acetylation were considered a variable one. We also allowed up to two missed cleavages. Both of these steps were done to adjust the databank search parameters as optimal as possible. More details on the quantitation algorithms can be found in supplement table 18 and 19.

Our data will be publicly available after publication. Statistical data analysis were performed by an in-house developed R-tool, based on median-normalized MS2 total peak area intensities (EG.TotalQuantity). We removed Methionine oxidized peptides before quantification. Differential abundant proteins, (p ≤ 0.05) applied on peptide level, were identified via the ROPECA algorithm (Suomi & Elo, 2017). For further analyses, we only used proteins for which at least two peptides were identified. Sample preparation was performed by Ulrike Lissner and data analysis by Elke Hammer at the interfaculty Institute of Genetics and Functional Genomics (FunGene).

6.2.16. Statistical analysis

All experiments were performed independently with at least three biological triplicates. The fold change was calculated in Excel 2010 (Microsoft, USA). A One-way ANOVA or welch's t test, for western blot data because of the small sample size, was then performed with Prism 8.3.0 (Graphpad Software, Inc., USA). One-way ANOVA results were correct p-values, here referred to as q-values. Violin plots were used to visualize data. Every dot presents one single data point. Specific force measurement results were visualized with points connected via lines. The error bar in those graphs is the standard deviation. Quantification of plots was performed with the ChemiDoc™ MP Imaging System (Bio-Rad, USA) and Image Lab™ Software (Biorad, USA). P (welch's t test) and q values (One-way ANOVA) of < 0.05 were considered statistically significant.

7. Results

7.1. Phenotype of MuRF1/MuRF3 DKO mice

7.1.1. Breeding of MuRF1/MuRF3 DKO mice

Trim63 (MuRF1) knockout (KO) and *Trim54* (MuRF3) heterozygous mice were interbred to obtain MuRF1/MuRF3 double knockout (DKO) mice in the F1 generation. We will refer to DKO mice as MuRF1/MuRF3 DKO, to minimize confusion. MuRF3 WT/WT and MuRF3 WT/KO littermates were used as controls, to ensure same age and conditions for DKO and control mice (Figure 8).
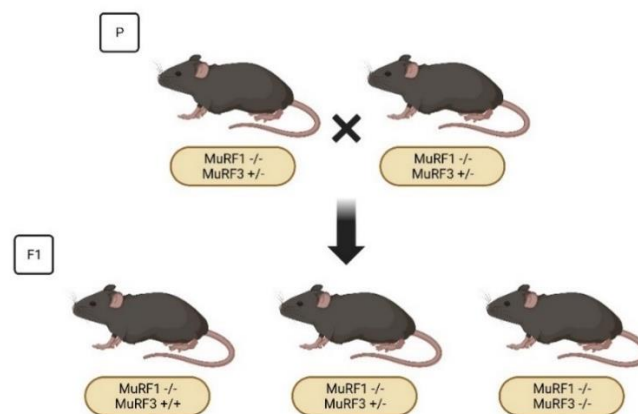

Figure 8. MuRF1/MuRF3 DKO breeding scheme. The breeding of MuRF1 DKO and MuRF3 heterozygous mice (parental generation, P), generated MuRF1 DKO mice with a wild type, heterozygous or DKO MuRF3 allele in the first filial generation (F1), according to the mendelian rules. Created with BioRender.com.

The genotype was determined by using 3 different PCR setups (MuRF1 WT/KO, MuRF3 WT, MuRF3 KO) with specific primer pairs and PCR conditions, followed by separation of the PCR products via gel electrophoresis as details in *Methods* (Figure 9).
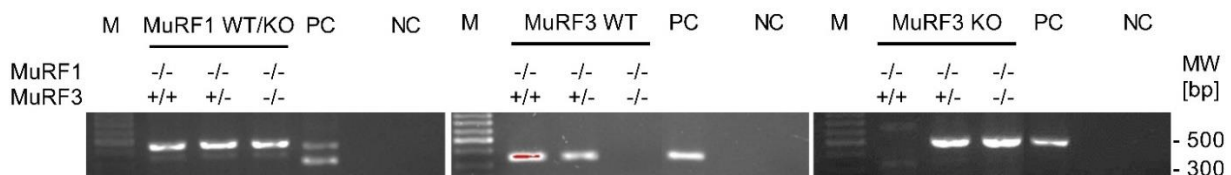

Figure 9. Agarose gel electrophoresis of PCR products for genotyping. PCR setups MuRF1 T/KO, MuRF3 WT and MuRF3 DKO were analyzed to determine the genotype. As an example, Figure 8 shows the results of MuRF1 DKO (450 bp) animals with heterozygous, WT (300 bp) and KO (500 bp) MuRF3 alleles, which are the expected genotypes. The Perfect DNA™ 100 bp Ladder (M) was used to estimated product length. Positive (PC) and negative controls (NC) proofed that PCR was performed correctly.

MuRF3 heterozygous mice would show a product in both, MuRF3 WT (300 bp) and KO (500 bp), while mice with only KO or WT alleles would only display a product in the corresponding PCR. Products of MuRF1 KO mice had a length of 450 bp, while WT alleles would lead to a product of 300 bp. Two products in the same sample would be a sign for heterozygous MuRF1 mice. Western blot analyses of proteins isolated from TA muscle of the different genotypes were performed to confirm absence of MuRF1 and MuRF3 in DKO mice, with wildtype FVB mice (Janvier) as a control. The reason we chose those mice was that our control animals were MuRF1 KO littermates and were therefore lacking MuRF1 (Figure 10).
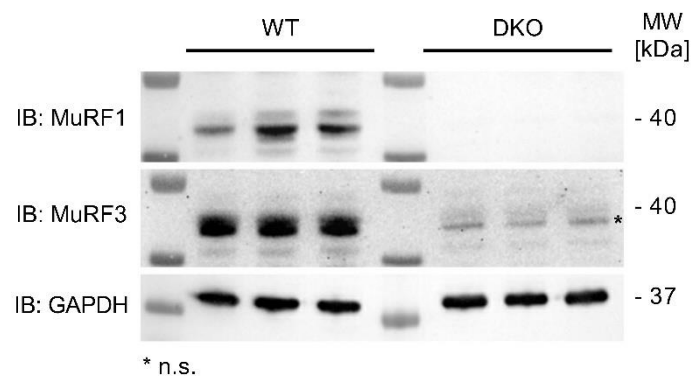

Figure 10. Proof of MuRF1 and 3 deletions in DKO mice. MuRF1 and MuRF3 immunoblot of TA from DKO and control MuRF1 and MuRF3. The non-specific (n.s.) band in the MuRF3 immunoblot is highlighted with a star. We used Wildtype (WT) FVB animals as a positive control. Animals were 9 to 10 weeks old.

7.1.2. Muscle weight and function

We measured the grip strength to assess if muscle function is affected in vivo. In all samples (q<0.0001) as well as after separation by sex (male q<0.0001; female q<0.0006) we saw a significant decrease in strength of DKO mice compared to controls, with no significant difference between males and females (Figure 11 a). Specific muscle force measurements of EDL also revealed a significant decrease in muscle function in all samples, as well as in females and males, compared to their corresponding controls (Figure 11 b - d).
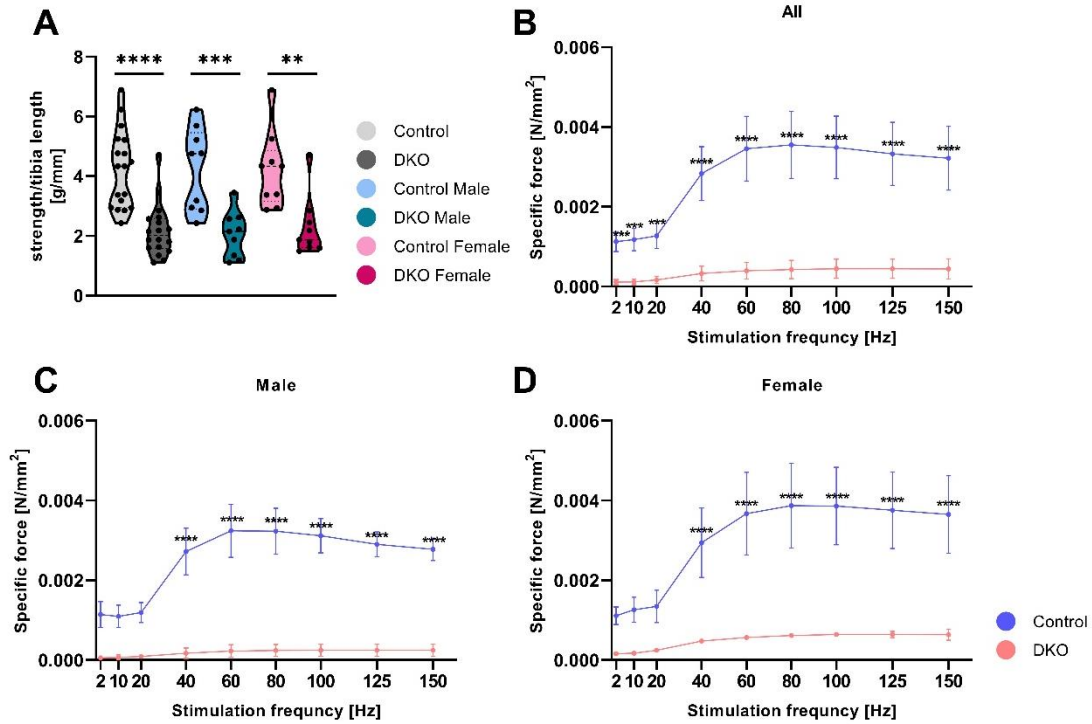
Figure 11. Impaired muscle function in DKO mice. (a) grip strength (g) normalized to tibia length (mm) of control and DKO mice; (male/female: control, n=18, DKO, n =18; male: control, n=9, DKO, n=9; female: control, n=9, DKO, n=9; animals were 7 to 11 weeks old). (b), (c) and (d) specific muscle force of EDL in (N/mm^2) of DKO and control mice; (male/female: control, n=6, DKO, n= 6; male: control, n=3, DKO, n=3; female: control, n=3, DKO, n=3; animals were 7 to 9)   One-way ANOVA and Two-way ANOVA was used to analyze data. *q<0.05, **q<0.01, ***q<0.005, ****q<0.001.

Compared to control littermates DKO mice displayed a significant increase in the normalized weights of all three muscles investigated (heart: +31%, q<0.0001; TA: +16.2%, q<0.0001; SOL: +40%, q<0.0001 all vs control mice). When separated by sex a trend towards a higher increase of heart and SOL weights was observed in female DKO mice (control vs DKO female: heart +36.6%, q<0.0001; SOL +50%, q<0.0001) compared to controls, than in male DKO compared to controls (control vs DKO male: heart +15.9%, q<0.0049; SOL +24.4%, q<0.0012), which however did not reach statistical significance (DKO male vs DKO female: heart q<0.8069; SOL q<0.9949). No sex specific difference was observed in TA (control vs DKO male +15.2%, q<0.0029; control vs DKO female +18.1%, q<0.0024) weight (Figure 12 a-c).
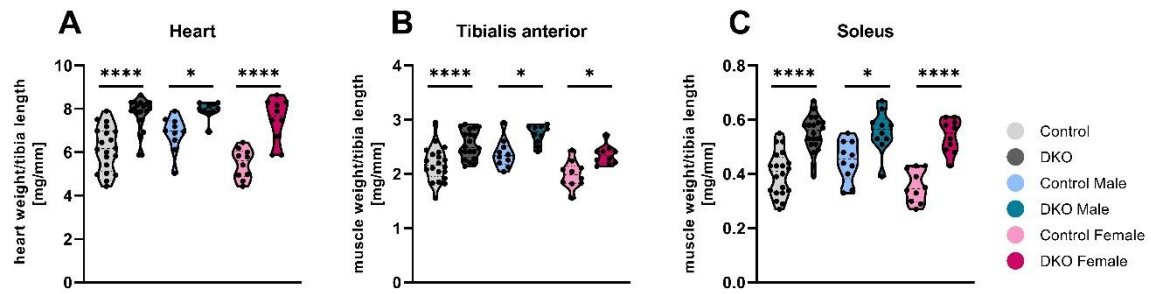
Figure 12. Increase of muscle weight of heart, TA and SOL in DKO mice. To tibia (mm) normalized muscle weight (mg) for (a) heart, (b) TA and (c) SOL, (male/female: control, n=20, DKO, n =20; male: control, n=10, DKO, n=10; female: control, n=10, DKO, n=10; animals were 5 to 9 weeks old); One-way ANOVA was used to analyze data. *$q<0.05$, **$q<0.01$, ***$q<0.005$, ****$q<0.001$.

H&E staining of histological cross sections from TA muscle of control and DKO mice displayed subsarcolemmal protein aggregates surrounding a central myofiber core, highlighted in white, in both male and female DKO mice (Figure 13).
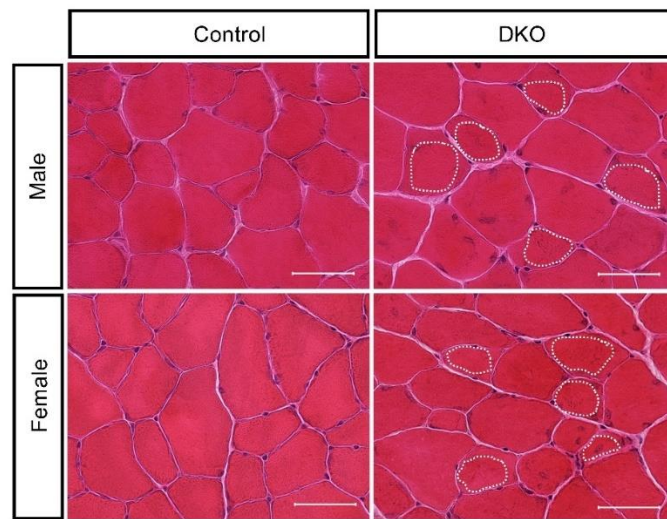

Figure 13. Protein accumulations in TA of DKO mice. Hematoxylin and eosin-stained tissue sections from male and female TA, control and DKO mice (10 weeks old), bar = 50 µm, accumulations are highlighted in white

All of the described results are in line with the previous publication from Fielitz et al. 2007. They also observed a decrease in muscle function.

7.2. Reduction of mitochondrial proteins and function

7.2.1. Mass spectrometric analysis of proteins isolated from TA and heart

To further characterize the phenotype of DKO mice, we performed proteome analysis of heart and TA muscle. TA displayed a significant difference between control and DKO animals. 368 proteins were upregulated, while 334 were significantly reduced in DKO mice compared to controls (q<0.05, log2-fold difference (FD)>|1.3|). Separated by sex 372 proteins were upregulated in males and 258 in females DKO mice compared to their corresponding controls. We observed a reduction of 267 proteins in male and 312 in female DKO mice compared to controls (Figure 14 a-c).
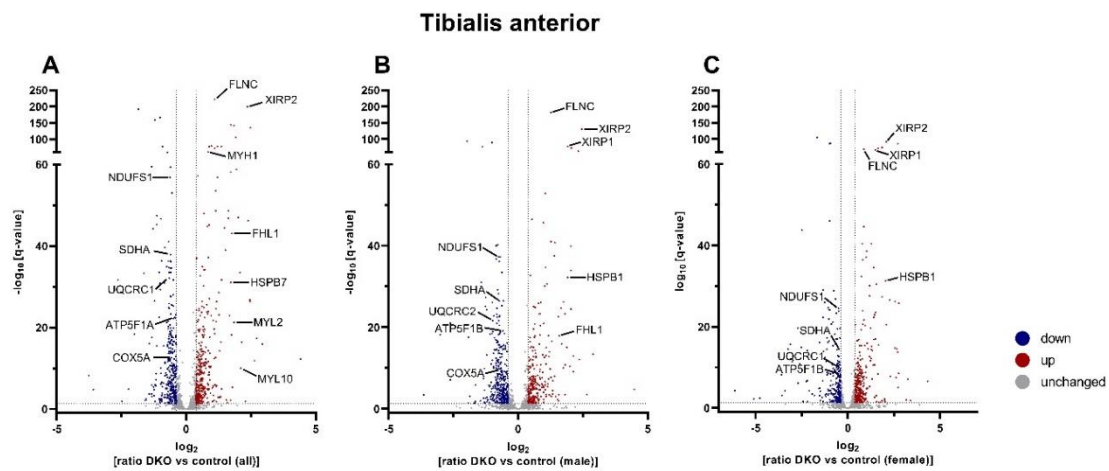

Figure 14. Dysregulation of proteins in TA of DKO mice. Volcano plot of MuRF1/MuRF3 DKO proteom data from TA. Data is shown as all animals (a); and separated by males (b) and females (c). Y axis displays the -Log$_{10}$ of q-value, while X axis displays the magnitude of the difference in log$_2$ ratio. Grey dots indicate a q>0.05 and a log2-fold difference (FD)<|1.3|, while colored dots indicate a q<0.05 and a log2-FD>|1.3|, highlighted proteins are ETC complex subunits and stress markers, (male/female: control, n=12, DKO, n =12; male: control, n=6, DKO, n=6; female: control, n=6, DKO, n=6; animals were 5 to 11 weeks old)

The 30 most upregulated proteins were further analyzed and their functional categorization revealed an increase of proteins of cytoskeleton organization, muscle fiber, I-band, Z-band and muscle stress markers for myopathy (FHL1, filamin C (FLNC)), oxidative stress (Heat Shock Protein Family B (Small) Member 1 (HSPB1)) and muscle damage (Myosin light chain 2 (MYL2), MyHC7, Xin Actin Binding Repeat Containing 1 (XIRP1, XIRP2). All of the mentioned stress markers were gathered in Figure 15 a.

Among the 30 most down regulated proteins were mainly proteins involved in Respirasome, tricarboxylic acid cycle (TCA) cycle, and oxidative phosphorylation. Subunits of electron chain complex I (NADH dehydrogenase [ubiquinone] iron-sulfur protein 8, mitochondrial (NDUFS8), NADH dehydrogenase [ubiquinone] iron-sulfur protein 4, mitochondrial (NDUFS4)), complex II (Succinate dehydrogenase

[ubiquinone] iron-sulfur subunit, mitochondrial (SDHB)), complex III (Cytochrome b-c1 complex subunit 7 (UQCRB)) and complex IV (Cytochrome c oxidase subunit 7A2, mitochondrial (COX7A2)) were reduced. Glutaryl-CoA dehydrogenase (GCDH), a protein important for L-lysine, L-hydroxylysine, and L-tryptophan metabolism, was also downregulated. MuRF1/MuRF3 DKO mice showed a reduction in pyruvate dehydrogenase E1 subunit beta (PHDB), a subunit of the pyruvate dehydrogenase complex, the link between glycolysis and the TCA cycle. All of the mentioned proteins were gathered in Figure 15 b.

We also analyzed our data for possible MuRF1, MuRF2 and MuRF3 interaction partners, detected by Nowak et al. 2019 and Witt et al. 2008 via YTH screening. From 78 possible partners 24 were detected in TA (all: up 11, down 5, unchanged 8; male: up 8, down 5, unchanged 11; female: up 11, down 1, unchanged 12; q<0.05) (Supplement Table 20). The 7 most accumulated in DKO compared to control were gathered in Figure 15 c. Proteins in this list were part of the cytoskeleton (DES), the ribosomes (Ribosomal Protein S26 (RPS26), Ribosomal Protein S4 X-Linked (RS4X)) and are connected to cardiac hypertrophy (LIM And Cysteine Rich Domains 1 (LMCD1)), autophagy (Sequestosome-1 (SQSTM1)) as well as transcription (Protein arginine N-methyltransferase 5 (PRMT5)).
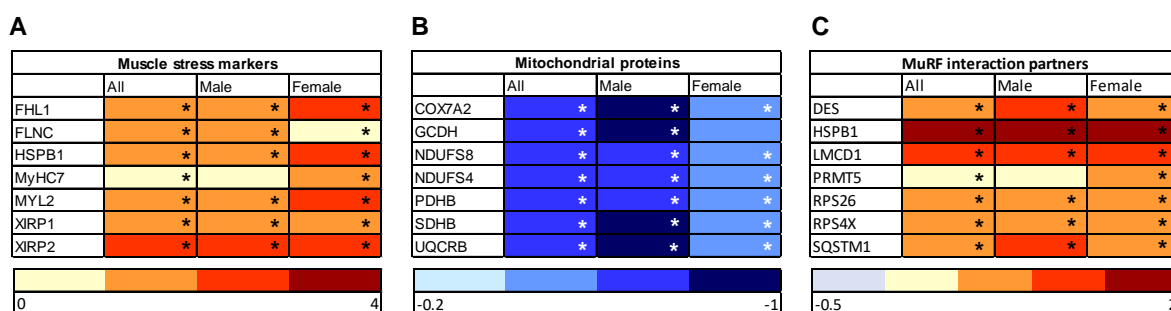

A

Muscle stress markers			
	All	Male	Female
FHL1	*	*	*
FLNC	*	*	*
HSPB1	*	*	*
MyHC7	*		*
MYL2	*	*	*
XIRP1	*	*	*
XIRP2	*	*	*

0 — 4

B

Mitochondrial proteins			
	All	Male	Female
COX7A2	*	*	*
GCDH	*	*	
NDUFS8	*	*	*
NDUFS4	*	*	*
PDHB	*	*	*
SDHB	*	*	*
UQCRB	*	*	*

-0.2 — -1

C

MuRF interaction partners			
	All	Male	Female
DES	*	*	*
HSPB1	*	*	*
LMCD1	*	*	*
PRMT5	*		*
RPS26	*	*	*
RPS4X	*	*	*
SQSTM1	*	*	*

-0.5 — 2

Figure 15. Dysregulation of muscle stress markers, mitochondrial proteins and MuRF interaction partners in TA of DKO mice. Heat maps of muscle stress markers (a), mitochondrial proteins (b) and possible MuRF1, MuRF2 and MuRF3 interaction partners (c) in the proteome data set of MuRF1/MuRF3 DKO mice from TA tissue. Displayed here in color code is the $\log_2$ ratio. Significant values (q<0.05) are highlighted with a star.

Compared to TA, there were less significant changes in the heart of DKOs compared to controls. We detected 702 dysregulated proteins in DKO TA compared to controls, while only 289 dysregulated proteins in DKO hearts compared to controls (q<0.05, log2-FD>|1.3|). 211 proteins were increase, while 78 were reduced in DKO mice compared to controls. In DKO males we detected an increase of 30 proteins and a decrease of 21 compared to controls. DKO Females displayed an increase of 200 proteins and a decrease of 89 compared to controls (Figure 16 a-c).
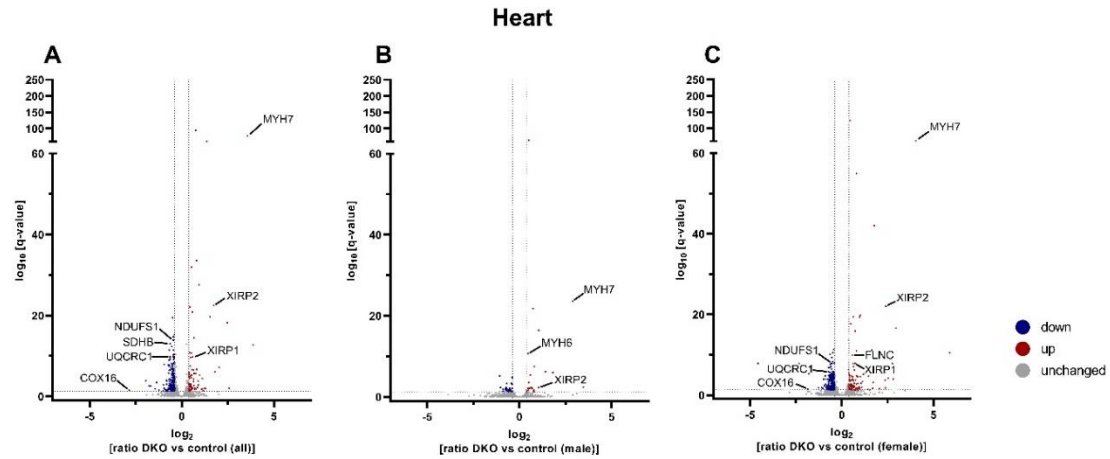
Figure 16. Dysregulation of proteins in heart of DKO mice. Volcano plot of heart proteome data. Data is shown as complete data set (a); and separated by males (b) and females (c). Y axis displays the -$\log_{10}$ of q-value, while X axis displays the magnitude of the difference in $\log_2$ ratio. Grey dots indicate a q>0.05 and log2-FD<|1.3|, while colored dots indicate a q<0.05 and a $\log_2$-FD>|1.3|, highlighted proteins are ETC complex subunits and stress markers, (male/female: control, n=12, DKO, n =12; male: control, n=6, DKO, n=6; female: control, n=6, DKO, n=6; animals were 5 to 11 weeks old)

Proteins for cytoskeleton organization, muscle fiber, I-band, Z-band and muscle stress markers were increased (FHL1, FLNC, HSPB1, MYL2, MyHC7, XIRP1, XIRP2), while proteins involved in respirasome, TCA cycle, and oxidative phosphorylation decreased (NDUFS8, NDUFS4, SDHB, UQCRB, COX7A2, GCDH, PHDB) in DKO compared to controls, but the changes were less significant. Though interestingly, females displayed more significantly dysregulated proteins than males compared to their controls, seen in Figure 17 a and b by the higher number of significant proteins in the female samples. Only 3 stress markers were significantly increased in male DKO mice compared to controls (HSPB1, MyHC7, XIRP2), while all 7 were significantly increased in female DKO mice compared to controls. In female DKO mice we observed a significant reduction of 5 mitochondrial proteins compared to controls (GCDH, NDUFS4, PDHB, SDHB, UQCRB), while only UQCRB was significantly reduced in male DKO mice compared to controls. Of 78 possible MuRF interaction partners 27 were detected in heart (all: up 3, down 5, unchanged 19; male: up 1, down 1, unchanged 25; female: up 3, down 6, unchanged 18; q<0.05) (Supplement Table 20). We checked the same possible MuRF interaction partners as in TA, with similar results, except for PRMT5 that could not be detected. They were still upregulated, but the changes in TA were more pronounced than in DKO hearts compared to controls, indicating that TA is more affected by the MuRF1/MuRF3 DKO than the heart (Figure 17 c).
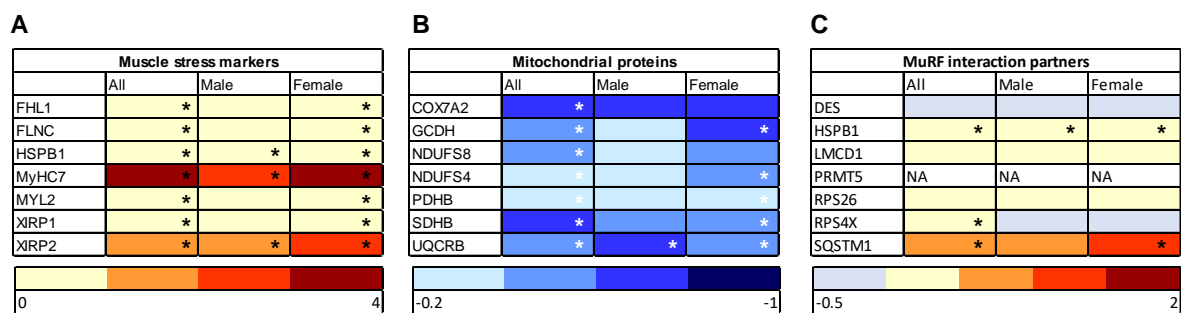
A

Muscle stress markers			
	All	Male	Female
FHL1	*		*
FLNC	*		*
HSPB1	*	*	*
MyHC7	*	*	*
MYL2	*		*
XIRP1	*		*
XIRP2	*	*	*

0 — 4

B

Mitochondrial proteins			
	All	Male	Female
COX7A2	*		
GCDH	*		*
NDUFS8	*		
NDUFS4			*
PDHB			
SDHB	*		*
UQCRB	*	*	*

-0.2 — -1

C

MuRF interaction partners			
	All	Male	Female
DES			
HSPB1	*	*	*
LMCD1			
PRMT5	NA	NA	NA
RPS26			
RPS4X	*		
SQSTM1	*		*

-0.5 — 2

Figure 17. Dysregulation of muscle stress markers, mitochondrial proteins and MuRF interaction partners in heart of DKO mice. Heat maps of muscle stress markers (a), mitochondrial proteins (b) and possible MuRF1, MuRF2 and MuRF3 interaction partners (c) in the proteome data set of MuRF1/MuRF3 DKO mice from heart tissue. Displayed here in color code is the $\log_2$ ratio. Significant values (q<0.05) are highlighted with a star.

7.2.2. Western blot and qRT-PCR of electron transport chain subunits

Since previous work with *Trim63*/*Trim55* DKO and *Trim55*/*Trim54* DKO mice revealed a connection between MuRF proteins and the mitochondrial energy metabolism, further analyses focused on mitochondrial proteins and ETC subunits, (Lodka et al., 2016; C. C. Witt et al., 2008). To support our proteome data, we performed western blot analysis of TA and heart tissue with the OxPhos antibody Cocktail that detects one subunit of every ETC complex, NDUFB8 (Complex I), SDHB (Complex II), UQCRC2 (Complex III), MTCO1 (Complex IV) and ATP5 (Complex V) and allows an estimation on the amount of mitochondrial complexes. Like our proteome data NDUFB8 (Complex I) (p<0.0044, fold change: 0.67), SDHB (Complex II) (p<0.0244, fold change: 0.67), UQCRC2 (Complex III) (p<0.0041, fold change: 0.71) and ATP5 (Complex V) (p<0.0457, fold change: 0.85) were reduced in the TA of DKO mice compared to controls. Interestingly, there was a sex-specific difference between males and females. NDUFB8 (p<0.0031, fold change: 0.65), SDHB (p<0.0121, fold change: 0.64), UQCRC2 (p<0.0033, fold change: 0.77), MTCO1 (Complex IV) (p<0.0114, fold change: 0.71) and ATP5 (p<0.0195, fold change: 0.86) were all significantly reduced in female mice, while only UQCRC2 (p<0.0087, fold change: 0.63) and ATP5 (p<0.0124, fold change: 0.84) were decreased in males (Figure 18 a).

In heart we only saw a significant reduction of NDUFB8 (p<0.0055, fold change: 0.66) in DKO mice compared to controls. Divided by sex UQCRC2 (p<0.0033, fold change: 0.80), MTCO1 (p<0.0079, fold change: 0.75), and ATP5 (p<0.0091, fold change: 0.69) were significantly decreased in female DKOs compared to controls. In males NDUFB8 (p<0.0152, fold change: 0.65) was reduced, while there was an increase of UQCRC2 (p<0.0352, fold change: 1.11) and ATP5 (p<0.0206, fold change: 1.23) (Figure 18 b)

in DKO compared to controls. These data support our proteomic analysis, were we also detected a reduction of ETC subunits, which was more pronounced in TA compared to heart.
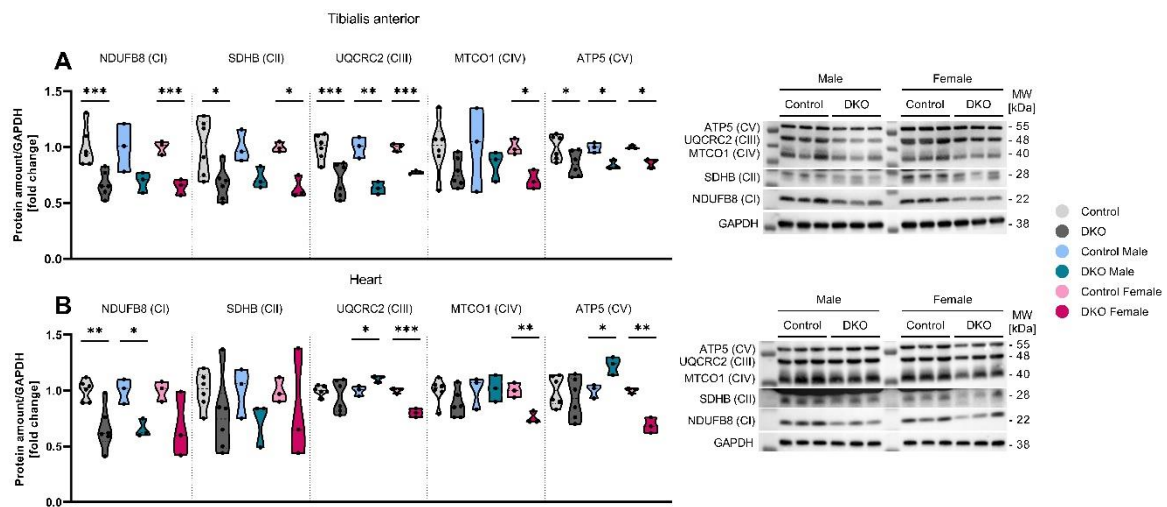

Figure 18. Reduction of ECT subunits in TA and heart of DKO mice. TA (a) and heart (b) OxPhos western blot analysis. Results are presented as complete data set, and separated by males and females. All subunits were normalized by GAPDH. We calculated the fold change by dividing through the corresponding control. (male/female: control, n=6, DKO, n =6; male: control, n=3, DKO, n=3; female: control, n=3, DKO, n=3; animals were 7 to 10 weeks old); Welch's t-test was used to analyze the data. *p<0.05, **p<0.01, ***p<0.005, ****p<0.001.

We performed qRT-PCR of the same subunits as detected by the OxPhos antibody, to investigate if the reduction of ETC subunits at protein level, is caused by a reduction in their gene expression. The expression of *Ndufb8* (q<0.0001, fold change: 0.61), *Sdhb* (q<0.0001, fold change, fold change: 0.65), *Mtco1* (q<0.0027, fold change: 0.41) and *Atp5* (q<0.0001, fold change: 0.57) was significantly reduced in TA of DKO mice compared to controls. More significant changes were found in females than in males. *Ndufb8* (q<0.0049, fold change: 0.66), *Sdhb* (q<0.0019, fold change: 0.70), *Mtco1* (q<0.0477, fold change: 0.41) and *Atp5* (q<0.0015, fold change: 0.57) gene expression was significantly decreased in females compared to controls, while in males only *Ndufb8* (q<0.0003, fold change: 0.54), *Sdhb* (q<0.0001, fold change: 0.58) and *Atp5* (q<0.0034, fold change: 0.57) were affected (Figure 19 a).

Fewer changes in ETC gene expression were found in heart of DKO compared to controls. In all DKO mice, as well as in female DKO mice, *Sdhb* (all q<0.0077, fold change: 0.84; female q<0.0150, fold change: 0.80) and *Mtco1* (all q<0.0001, fold change: 0.60; female q<0.0017, fold change: 0.56) were reduced compared to their controls. In males we only saw a significant decrease in *Mtco1* (q<0.0348, fold change: 0.64) gene expression compared to controls (Figure 19 b).
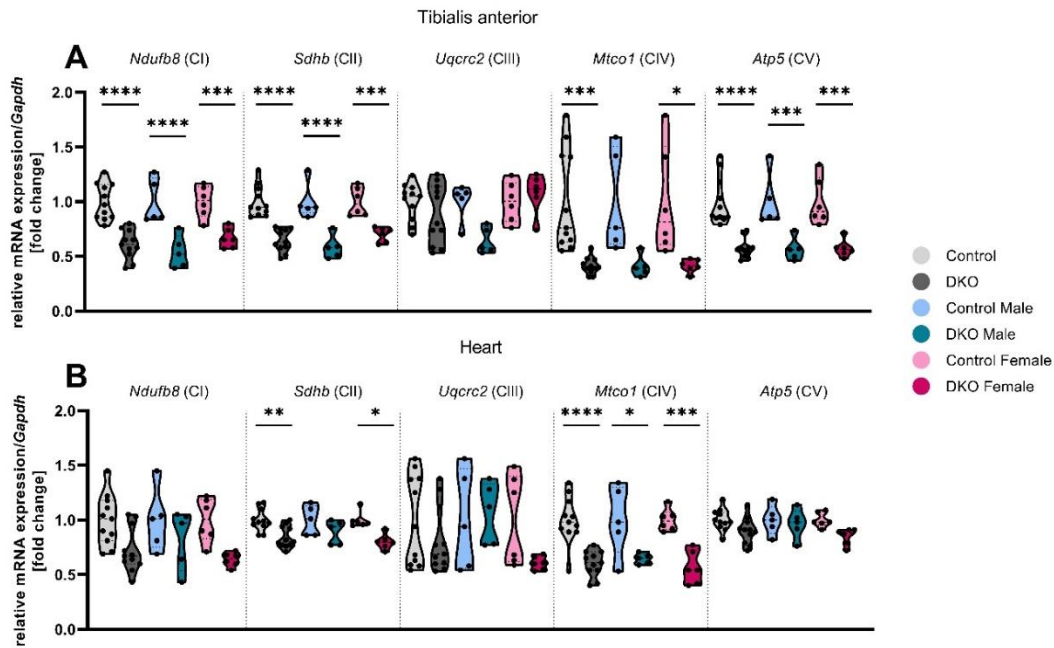
Figure 19. Reduction of ETC subunit gene expression in TA and heart of DKO mice. TA (a) and heart (b) qRT-PCR analysis. Results are presented as complete data set, and separated by sex into males and females. All subunits were normalized by the stably expressed *Gapdh.* We calculated the fold change by dividing through the corresponding control. (male/female: control, n=11, DKO, n =11; male: control, n=5, DKO, n=5; female: control, n=6, DKO, n=6; animals were 5 to 11 weeks old); One-way ANOVA was used to analyze data. *q<0.05, **q<0.01, ***q<0.005, ****q<0.001.

In summary, both protein and gene expression data show that the heart is less affected by the MuRF1/MuRF3 DKO than TA. We were also able to detect a sex specific difference, in which females showed a higher number of significantly regulated ETC genes and proteins than males.

7.2.3. Citrate synthase, Complex I, III and IV activities in TA and heart of DKO mice

By measuring ETC complex I, complex III, complex IV and citrate synthase activity (CS), we determined mitochondrial function. CS activity was measured as biomarker for the number of intact mitochondria in a sample, and therefore used to normalize the overall muscular activity data, which we will refer to as relative data. In TA we observed a significant reduction of complex I (q<0.0056, fold change: 0.56) and complex III (q<0.0045, fold change: 0.45) overall muscular activity in DKO mice compared to controls. The same results were detected in the overall muscular activity of female DKO mice (complex I: q<0.0078, fold change: 0.40; complex III: q<0.0218, fold change: 0.34) compared to controls, with negative trends in CS (q<0.2450, fold change: 0.76) and complex IV activity (q<0.9131, fold change: 0.80), compared to

controls. The negative trend in CS activity could indicate that female DKO mice have a reduced mitochondrial content. While we observed a negative trend for complex I (q<0.5445, fold change: 0.73) and complex III (q<0.2701, fold change: 0.57) activity in the overall muscular activity of male DKO mice compared to controls, none of the results were significant (Figure 20 a). After normalizing by CS activity, we observed the same results in our relative data (Figure 20 b). Relative complex I and complex III activity was reduced in TA of all DKO mice (complex I: q<0.0017, fold change: 0.60; complex III: q<0.0049, fold change: 0.50) and in females (complex I: q<0.0089, fold change: 0.51; complex III: q<0.0400, fold change: 0.44), compared to their controls, while males only displayed a trend (complex I: q<0.9999, fold change: 0.69; complex III: q<0.1888, fold change: 0.57)
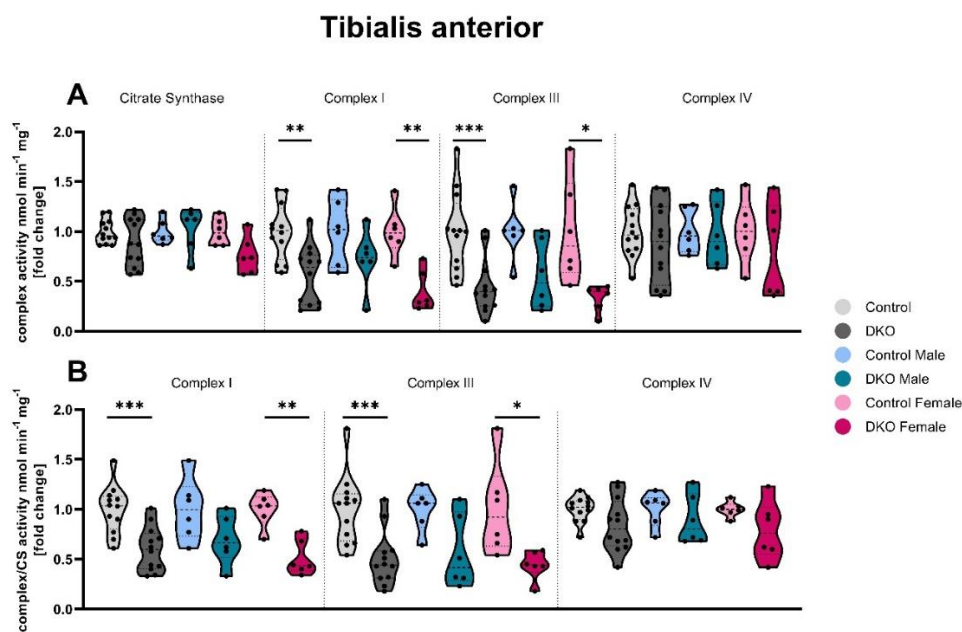

Figure 20. Impaired mitochondrial function in TA of DKO mice. Overall muscular (a) and relative (b) mitochondrial activity data of TA. Results are presented as complete data set, and separated by males and females. Complex I, III and IV activities were normalized by CS activity (relative data). We calculated the fold change by dividing through the corresponding control. (male/female: control, n=12, DKO, n =12; male: control, n=6, DKO, n=6; female: control, n=6, DKO, n=6; animals were 5 to 11 weeks old); One-way ANOVA was used to analyze data. *q<0.05, **q<0.01, ***q<0.005, ****q<0.001.

We observed no changes in complex or CS activity in the heart of DKO mice compared to controls, neither in the overall muscular (CS: q<0.7879, fold change: 0.91; complex I: q<0.7194, fold change: 0.91; complex III: q<0.0619, fold change: 0.76; complex IV: q<0.9999, fold change: 0.98) nor the relative data (complex I: q<0.9999, fold change: 0.99; complex III: q<0.4469, fold change: 0.82; complex IV: q<0.9989, fold change: 1.06) (Figure 21 a and b). After dividing in male (overall muscular CS: q<0.9451, fold change: 0.91;

overall muscular complex I: q<0.8867, fold change: 0.90; overall muscular complex III: q<0.3834 , fold change: 0.76; overall muscular complex IV: q<0.9914, fold change: 0.88; relative complex I: q<0.9999, fold change: 0.98; relative complex III: q<0.8393, fold change: 0.84; relative complex IV: q<0.9999, fold change:0.95) and female (overall muscular CS: q<0.9366, fold change: 0.91; overall muscular complex I: q<0.9398, fold change: 0.92; overall muscular complex III: q<0.2885, fold change: 0.75; overall muscular complex IV: q<0.9986, fold change: 1.08; relative complex I: q<0.9999, fold change: 1.0; relative complex III: q<0.7119, fold change: 0.81; relative complex IV: q<0.9685, fold change: 1.16) mice, we did not detect changes in CS or complex activities between DKO and control mice in raw or normalized data.
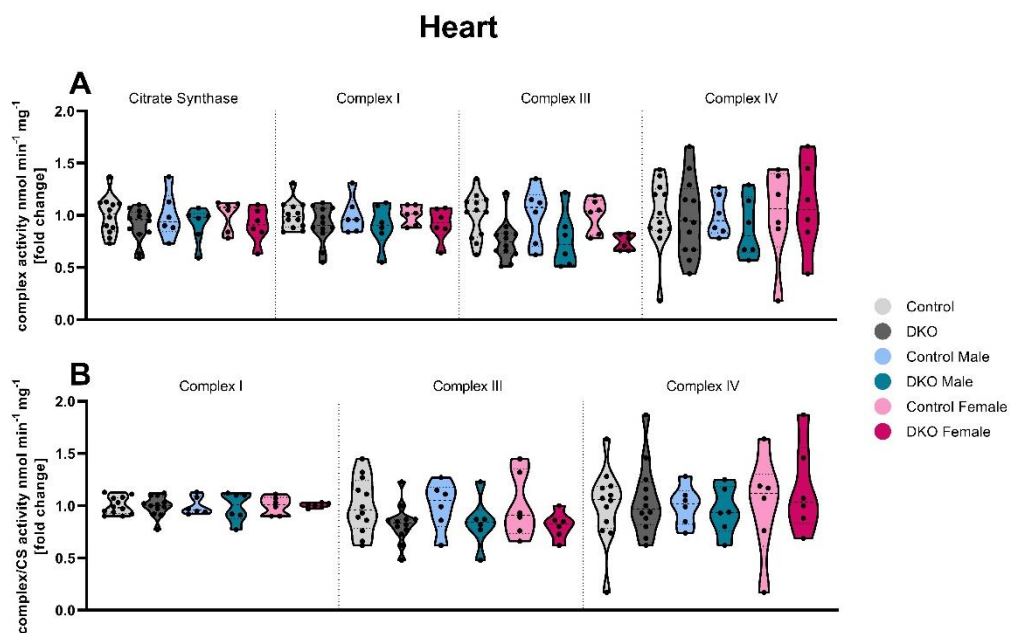

Figure 21. Mitochondrial function in heart of DKO mice. Overall muscular (a) and relative (b) mitochondrial activity data of the heart. Results are presented as complete data set, and separated by males and females. Complex I, III and IV activities were normalized by CS activity (relative data). We calculated the fold change by dividing through the corresponding control. (male/female: control, n=12, DKO, n =12; male: control, n=6, DKO, n=6; female: control, n=6, DKO, n=6; animals were 8 to 9 weeks old); One-way ANOVA was used to analyze data. *q<0.05, **q<0.01, ***q<0.005, ****q<0.001.

The enzymatic activity data strengthen our hypothesis that the heart is less effected than TA, and males less than females. While complex I and complex III activity was significantly reduced in TA, we detected no changes in DKO hearts compared to controls. The same applies for the heart of female and male DKO mice.

7.3. Targeting of HDAC5 by MuRF1

7.3.1. qRT-PCR of *Ppargc1a* and Western blot of its repressor HDAC5

The gene *Ppargc1a* encodes the Protein PGC1-α. It is the master regulator of mitochondrial biogenesis and protein synthesis, via upregulating NRF1 and NRF2, which leads to an increase of mitochondrial proteins like ETC subunits (Athale et al., 2012; Pandit et al., 2009). We observed a reduced gene expression of ETC subunits in TA and heart of DKO mice, therefore we hypothesized that changes in PGC1-α may be responsible for this phenotype. We first investigated the gene expression of *Ppargc1a* and observed a significant reduction of *Ppargc1a* gene expression (q<0.0001, fold change: 0.57) in TA of DKO mice compared to controls. After dividing the mice by sex, the decrease in *Ppargc1a* gene expression could be detected in male (q<0.0035, fold change: 0.57) and female (q<0.0014, fold change: 0.57) DKO mice compared to their controls, without a sex specific difference. We observed no significant changes in *Ppargc1a* gene expression (q<0.2870, fold change: 0.68) in heart of DKO mice compared to controls, neither in female (q<0.5270, fold change: 0.65) nor male DKO mice (q<0.7853, fold change: 0.71) (Figure 22 a). This result is in line with our previous results, were we also detected less changes in ETC gene expression in heart, compared to TA. Western blot analysis of HDAC5, a known PGC1-α inhibitor, was performed with samples from TA. We observed a significant increase of HDAC5 in DKO compared to controls (p<0.0285, fold change: 1.81), as well as in female DKO mice (p<0.0321, fold change: 2.10) compared to controls, but not in males (p<0.3115, fold change: 1.61) (Figure 22 b and c).
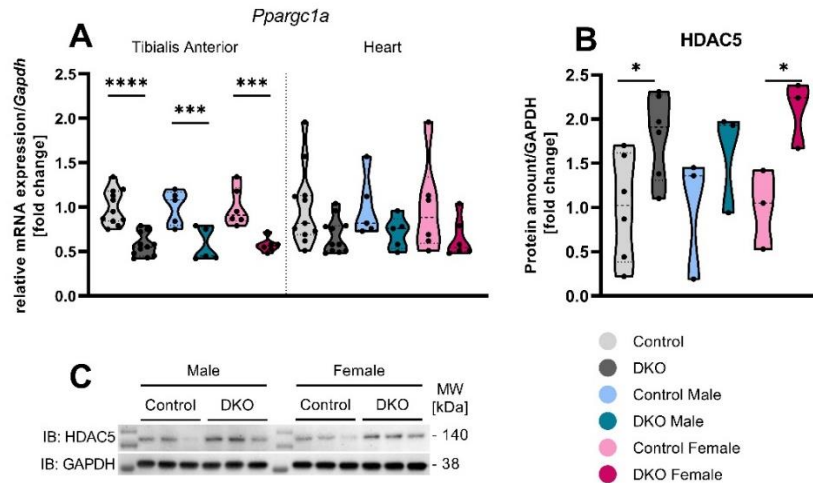
Figure 22. Decrease of *Ppargc1a* gene expression is accompanied with an increase of HDAC5 in TA of DKO mice. (a) TA and heart qRT-PCR analysis of *Ppargc1a*. Results are presented as complete data set, and separated by sex into male and female mice. *Ppargc1a* gene expression was normalized to stably expressed *Gapdh*. We calculated the fold change by dividing through the corresponding control. (male/female: control, n=11, DKO, n =11; male: control, n=5, DKO, n=5; female: control, n=6, DKO, n=6; animals were 5 to 11 weeks old); (b) HDAC5 western blot analysis in TA. Results are presented as complete data set, and separated by sex into male and female mice. HDAC5 was normalized by GAPDH. We calculated the fold change of HDAC5/GAPDH by dividing through the corresponding control. (male/female: control, n=6, DKO, n =6; male: control, n=3, DKO, n=3; female: control, n=3, DKO, n=3; animals were 6 to 11 weeks old); (c) HDAC5 immunoblot of male and female TA samples; one-way ANOVA and Welch's t-test were used to analyze the data. $*q<0.05$, $**q<0.01$, $***q<0.005$, $****q<0.001$ (one-way ANOVA) or $*p<0.05$, $**p<0.01$, $***p<0.005$, $****p<0.001$ (Welch's t-test).

7.3.2. MuRF1 interacts with HDAC5

The increase in HDAC5 in muscle of MuRF1/MuRF3 DKO mice let to the hypothesis that HDAC5 is targeted by MuRF1 and or MuRF3 for UPS dependent degradation. To test this hypothesis, we first used CO-IP analysis to test if HDAC5 and MuRF1, MuRF2 and MuRF3 physically interact with each other. For this we overexpressed pcDNA™3.1/myc-His(-)_MuRF1, pcDNA™3.1/myc-His(-)_MuRF2 and pcDNA™3.1/myc-His(-)_MuRF3 separately and together with pcDNA™3.1(+)/FLAG_HDAC5 in COS7 cells and performed immunoprecipitation followed by Western blot analysis. Only MuRF1 but not MuRF2 or MuRF3 interacted with HDAC5 (Figure 23 a). We used the HDAC5 deletion mutants pcDNA™3.1/myc-His(-)_HDAC5 1-664, pcDNA™3.1/myc-His(-)_HDAC5 51-C, pcDNA™3.1/myc-His(-)_HDAC5 100-C, pcDNA™3.1/myc-His(-)_HDAC5 540-C and pcDNA™3.1/myc-His(-)_HDAC5 601-C-Myc to investigate if there is a specific binding region within HDAC5 that is responsible for its interaction with MuRF1. With

this experiment we identified a region between amino acids 540 to 601 within HDAC5 that is essential for its interaction with MuRF1 (Figure 23 b and c).
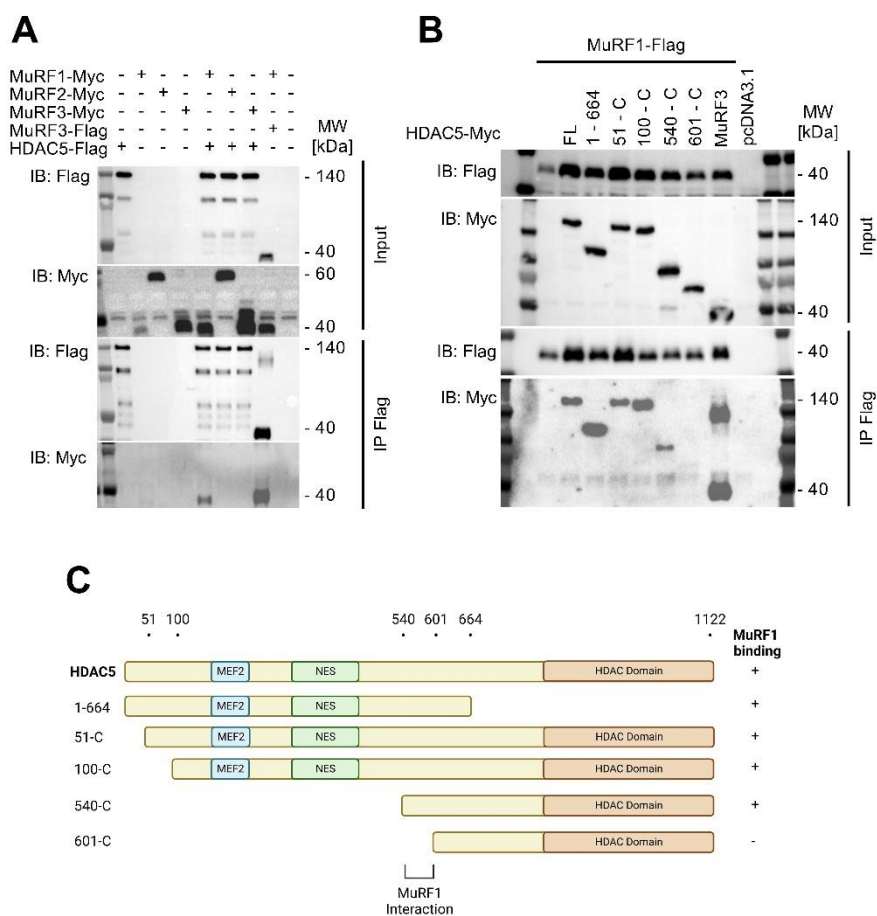

Figure 23. MuRF1 interacts directly with HDAC5. (a) Co-IP of pcDNA™3.1/myc-His(-)_MuRF1, pcDNA™3.1/myc-His(-)_MuRF2 and pcDNA™3.1/myc-His(-)_MuRF3 with pcDNA™3.1(+)/FLAG_HDAC5. Shown here are the immuno blots of the Input controls with Flag and Myc antibody, as the results after IP. pCDNA3.1 treated cells were used as a negative control, while MuRF1/MuRF3 was a positive control; (b) Co-IP of pcDNA™3.1/myc-His(-)_HDAC5, pcDNA™3.1/myc-His(-)_HDAC5 1-664, pcDNA™3.1/myc-His(-)_HDAC5 51-C, pcDNA™3.1/myc-His(-)_HDAC5 100-C, pcDNA™3.1/myc-His(-)_HDAC5 540-C and pcDNA™3.1/myc-His(-)_HDAC5 601-C-Myc with pcDNA™3.1(+)/FLAG_MuRF1. Shown here are the immuno blots of the Input controls with Flag and Myc antibody, as the results after IP. pcDNA™3.1 treated cells were used as a negative control, while pcDNA™3.1/myc-His(-)_MuRF1/ pcDNA™3.1(+)/FLAG_MuRF3 was a positive control. (c) Graphic of HDAC5 and HDAC5 deletion mutants. Mutants who were able to interact with MuRF1 are marked with a + and the interaction region with MuRF1 between 540 to 601 was highlighted. Created with BioRender.com

7.3.3. MuRF1 mediates ubiquitination of HDAC5

To test if MuRF1 or MuRF3 mediate ubiquitination of HDAC5, we performed a ubiquitination assay, respectively. COS7 cells were transfected with pcDNA™3.1(+)/FLAG_HDAC5 and either pcDNA™3.1, pcDNA™3.1/myc-His(-)_MuRF1 or pcDNA™3.1/myc-His(-)_MuRF1Cys39/47Ser. In these RING-finger mutants of MuRF1 we replaced the conserved cysteine residues Cys39 and Cys47, which are required for zinc ion binding, by serine residues that inactivates the function of the RING-finger. HA-tagged ubiquitin (pEGFP-N3-HA-Ubi) or a control vector were co-expressed. Inhibition with MG132 for 6 h was used to inhibit proteasomal protein degradation, and DMSO served as a. To investigate the effects of MuRF3, we used the same approach using pcDNA™3.1/myc-His(-)_MuRF3 and the RING-finger mutant pcDNA™3.1/myc-His(-)_MuRF3Cys42/50Ser. Using the same assay employing pcDNA™3.1/myc-His(-)_MuRF1 or pcDNA™3.1/myc-His(-)_MuRF1Cys39/47Ser together with pcDNA™3.1/myc-His(-)_MuRF3 or pcDNA™3.1/myc-His(-)_MuRF3Cys42/50Ser, as indicated, was performed to uncover any combined effects of MuRF1 and MuRF3 on HDAC5 (Figure 24 a-c).
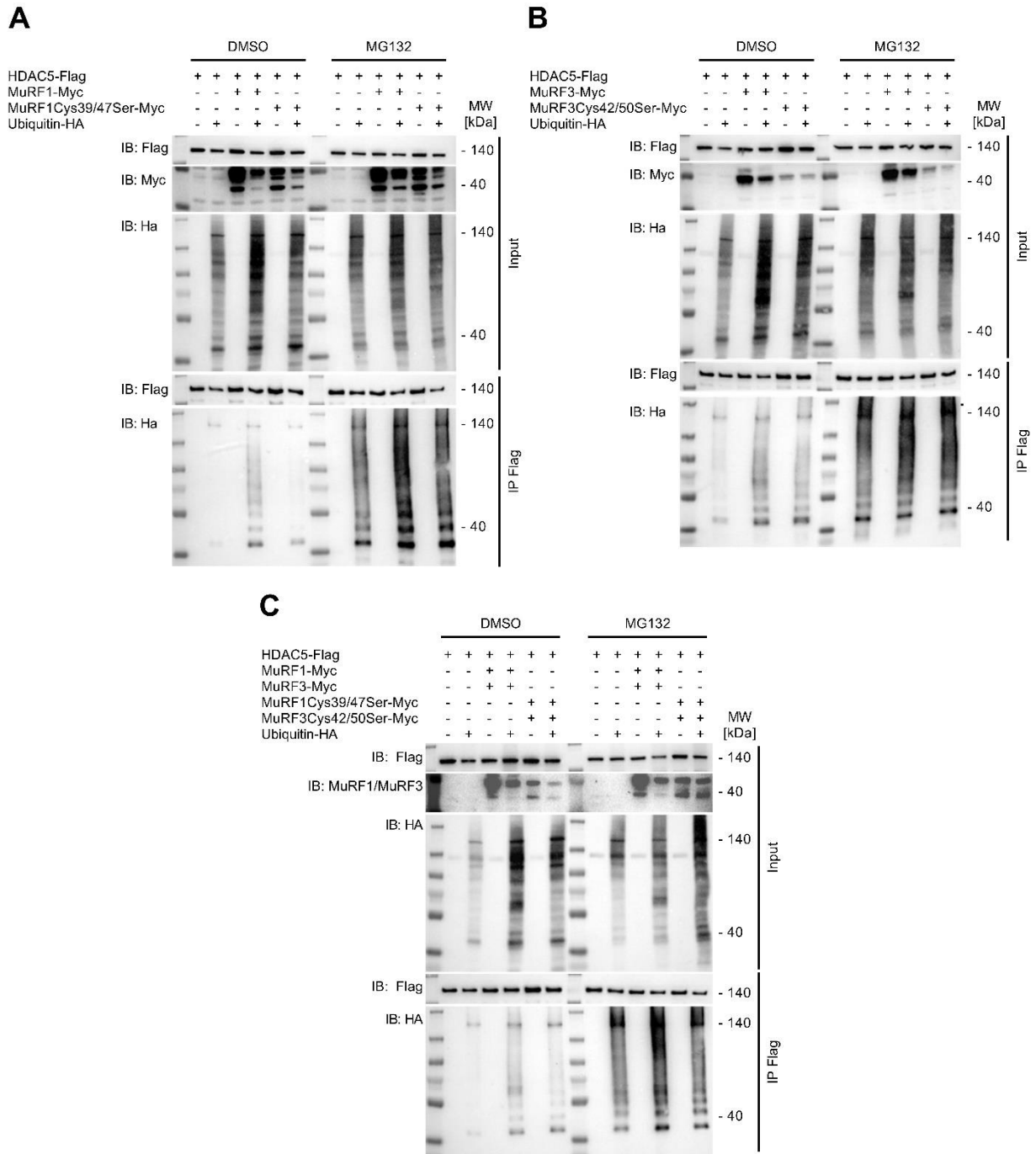
Figure 24. MuRF proteins increase ubiquitination of HDAC5. Input and IP Flag immuno blots of HDAC5 ubiquitin assays with pcDNA™3.1/myc-His(-)_MuRF1 (a), pcDNA™3.1/myc-His(-)_MuRF3 (b) and pcDNA™3.1/myc-His(-)_MuRF1/ pcDNA™3.1/myc-His(-)_MuRF3 (b). Cells were treated with MG132 or DMSO for 6h. pcDNA™3.1/myc-His(-)_MuRF1Cys39/47Ser and pcDNA™3.1/myc-His(-)_MuRF3Cys42/50Ser are nonfunctioning mutants, who served as an additional negative control here, together with pcDNA™3.1(+)/FLAG_HDAC5/pcDNA™3.1 treated cells.

An increase in HDAC5-ubiquination was found in MuRF1 as well as MuRF1/MuRF3, but not MuRF3 transfected cells. This is in line with our CO-IP data, where we observed a direct interaction between MuRF1 and HDAC5, but not MuRF3. Samples with the nonfunctional MuRF1Cys39/47Ser and MuRF3Cys42/50Ser mutants displayed results comparable to the control (pcDNA™3.1(+)/FLAG_HDAC5, pEGFP-N3-HA-Ubi), therefore we can also conclude that a functioning RING domain is necessary for this interaction.

7.3.4. MuRF1 decreases stability of native HDAC5

To test if MuRF1 and/or MuRF3 influences the stability of endogenous HDAC5, we performed a cycloheximide (CHX) chase assay in C2C12 cells transfected with pMP71_IRES_GFP/6xHis_MuRF1 and/or pMP71_IRES_GFP/6xHis_MuRF3. Treatment with CHX that inhibits protein synthesis took place over 0h, 3h and 6h as indicated (Figure 25 a-c).
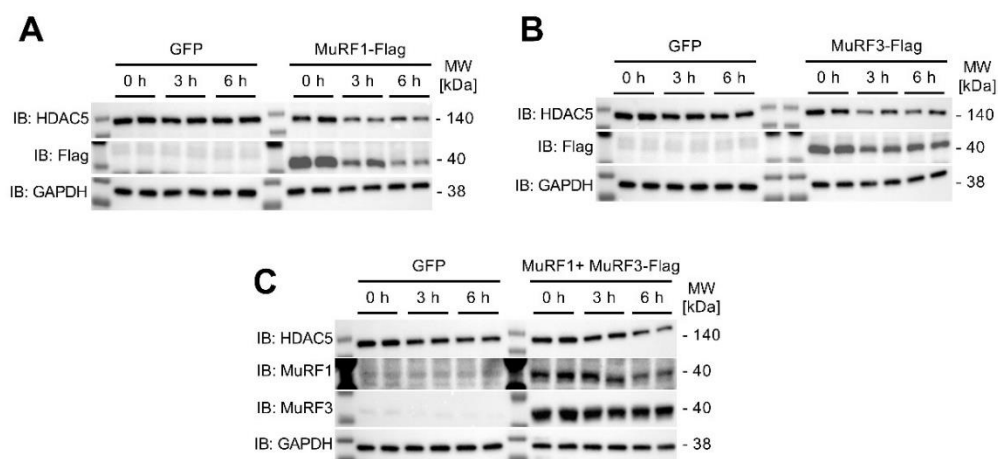
Figure 25. MuRF proteins decrease stability of HDAC5. Immunoblots of HDAC5 CHX assays with pMP71_IRES_GFP/6xHis_MuRF1 (a), pMP71_IRES_GFP/6xHis_MuRF3 (b) and pMP71_IRES_GFP/6xHis_MuRF1/ pMP71_IRES_GFP/6xHis_MuRF3 (c). Cells were treated with CHX for 6 h. Samples were taken at 0 h, 3 h and 6h. GFP overexpressing cells were used as a negative control.

Overexpression of MuRF1, MuRF3 and MuRF1/MuRF3 lead to decreased stability of native HDAC5, compared to controls. Regarding our CO-IP, ubiquitin assay and CHX assay data, we therefore propose that MuRF1, either as a homodimer or heterodimer with MuRF3, targets HDAC5 for degradation via the UPS.

8. Discussion

8.1. Physiological changes and function of heart and skeletal muscles

8.1.1. Increase of heart, TA and SOL weight

We measured heart, TA and SOL weight of DKO and control mice. In all DKO mice, as well as after separation by sex, we detected an increase in weight of all three muscles compared to controls. While increase in TA did not seem to differ between sexes, increase of SOL and heart weight was more enhanced in females compared to controls, than in males. This increase in muscle weight was already observed by Fielitz et al., 2007, who first described the MuRF1/MuRF3 DKO phenotype, as well as in a patient suffering from a homozygous null mutation of MuRF1 and a heterozygous deleterious missense mutation of MuRF3, leading to a hypertrophic cardiomyopathy (Olivé et al., 2015). Therefore, the DKO of MuRF1/MuRF3 leads to a similar phenotype in mice and in human, indicating a high transferability of data collected in either organism. Interestingly though, MuRF2/MuRF3 DKO mice did not show a hypertrophy of the skeletal muscles, while in MuRF1/MuRF2 mice hypertrophy could only be observed in the heart (Lodka et al., 2016; C. C. Witt et al., 2008). While MuRFs are known to work redundantly (Willis et al., 2014; S. H. Witt et al., 2005), those results highlight that depending on muscle type, skeletal or heart, different MuRFs or combinations of MuRFs are important to upkeep the integrity of the organ.

8.1.2. Subsarcolemmal protein aggregates and muscle strength

Grip strength measurements revealed a significant decrease of muscle strength in DKO mice, independent of sex, comparted to controls. Similar results could be observed in the specific muscle force measurements of the EDL of DKO mice. All DKO, as well female and male mice displayed a significant reduction compared to their controls. This loss of muscle function was also described by Fielitz et al., 2007 and in the patient by Olivé et al., 2015 manifesting in a waddling gait and the inability to lift heavy objects or to stand up without support. The increased muscle weight and loss of function could be caused by subsarcolemmal accumulation of proteins around a myofiber core, which we observed in H&E-stained TA muscle tissue. DKO muscle fibers also had numerous, often centralized, nuclei. Those results are again in line with the publication of Fielitz et al., 2007 who identified MyHCs as the main component of the accumulations, and Olivé et al., 2015. Both methods used to measure muscular function here only measure a short amount of time, which could explain why we see no sex specific difference. Our mice display a decrease in mitochondrial function, besides protein aggregates, and therefore likely develop a lack of energy production. Long time exercise by e.g. forced running could identify sex specific differences. Heart and skeletal muscle dysfunction, caused by protein accumulations, is a common symptom in myosin storage myopathies (MSM), that so far have been mainly connected to *MyHC7* mutations (Laing et al.,

2005; Tajsharghi et al., 2003). Though our results emphasize, that the MuRF1/MuRF3 DKO mice are a suitable model to study mechanisms and consequences of MSM.

8.2. Proteom analysis of TA and heart tissue

We performed mass spectrometric analysis of MuRF1/MuRF3 DKO mice to further illustrate the phenotype. Because MuRF1 and MuRF3 are specific for striated muscles, we decided to focus on heart and TA. In TA we saw a significant difference between DKO and control animals, with no obvious sex specific differences. Those changes were less pronounced in heart, indicated by the lower number in dysregulated proteins, though females were more effected than males.

8.2.1. Increase of structural proteins and muscle stress markers

The 30 most upregulated proteins in TA were proteins of the cytoskeleton organization, muscle fiber, I-band and Z-band. There was also a significant increase of muscle stress markers for myopathy, oxidative stress and muscle damage. FHL1 was shown to promote muscle hypertrophy or atrophy, depending on the presence of myostatin (J. Y. Lee et al., 2015). An increase of FLNC, caused by a conditional knockout (CKO) of *Hspb7* in mice, lead to a progressive myopathy in skeletal muscles via aggregate accumulations in muscle cells (Juo et al., 2016). HSPB1 plays an important role in the defense against oxidative stress and in the response to oxidative stress injury of cardiomyocytes (X. Liu et al., 2021; Terra et al., 2019). Myosin light and heavy chains, like MYL2 and MHC7 (Noguchi et al., 2003; Wang et al., 2015), are commonly upregulated in muscle regeneration, and are therefore together with XIRP1 and XIRP2, which are increased during injury, markers for muscle damage (Nilsson et al., 2013). The same proteins were upregulated in heart, but the changes were less severe compared to TA.

8.2.2. Decrease of mitochondrial proteins

Proteins involved in Respirasome, TCA cycle, and oxidative phosphorylation were most common in the 30 most down regulated proteins in TA. We focused here on mitochondrial proteins (GCDH, PHDB), especially ETC complex I (NDUFS8, NDUFS4), complex II (SDHB), complex III (UQCRB) and complex IV (COX7A2) subunits. NDUFS8 and NDUFS4 are essential for complex I assembly and activity (Haack et al., 2012; Petruzzella et al., 2001). Likewise, SDHB is needed for complex II function (Ardissone et al., 2015). Angiogenesis was shown to be regulated by UQCRB via the generation of reactive oxygen species, possibly connecting it to mitochondria-mediated metabolic disorders (Chang et al., 2014). In humans lack of GCDH is the cause of Glutaric acidemia type 1 (GA1), a severe neurological disease (Strauss et al., 2020).

MuRF1/MuRF3 DKO mice also displayed a lack of PHDB, a subunit of the pyruvate dehydrogenase complex, the link between glycolysis and the TCA cycle. Similar to GCDH, this has severe neurological consequences of different magnitudes in patients (Barnerias et al., 2010). All of this pointed at a potential mitochondrial dysfunction, as well as possible neurological limitations of the MuRF1/MURF3 DKO mice. Again, heart was less affected than TA, as seen by the lower number of reduced proteins.

8.2.3. MuRF interaction partners

We compared our findings with data from YTH screenings that were performed to identify novel interaction partners of MuRF1, MuRF2 and MuRF3 and proteins that are degraded by the proteasome, published by Witt et al., 2008 and Nowak et al., 2019. From 78 possible MuRF interaction partners 27 were detected in Heart and 24 in TA. 60 of these Proteins were possible MuRF1 and MuRF2 interaction partners. Proteins that are regulated by MuRF2 or MuRF2 and MuRF1 are less likely to accumulate in our DKO, since MuRF2 is still active, and therefore more difficult to detected making our list incomplete. It could also explain why the amount of some interaction partners was unchanged. A comparison of detected MuRF interaction partners between MuRF1/MuRF3 and MuRF1/MuRF2 DKO mice could be interesting, to complete the list. Another reason why this list could be incomplete, besides a small protein amount, could be the protein size. Smaller proteins like transcription factors are less likely to be detected by mass spectrometry, compared to large structural proteins. MuRFs are known to stabilize structures like microtubules in cells, which could explain the down regulation of some interaction partners (McElhinny et al., 2004; Pizon et al., 2002). The seven most upregulated MuRF interaction partners in TA were DES, HSPB1, RPS26, RPS4X, LMCD1, SQSTM1 and PRMT5. DES is a part of the cytoskeleton and plays an important role in maintain sarcomere structure. Mutations in this protein can cause restrictive cardiomyopathy (Brodehl et al., 2013; Herrmann et al., 2020). As transcriptional cofactor LIM domain proteins regulate cell differentiation and remodeling of the cell cytoskeleton. LMCD1 in particular was brought into correlation with cardiac hypertrophy via calcineurin (Bian et al., 2010). Both RPS26 and RPS4X are subunits of the ribosomes (Filipenko et al., 1998; Zinn et al., 1994), while PRMT5 was shown to regulate transcription (Fabbrizio et al., 2002; Zhao et al., 2015), linking MuRFs to protein synthesis. SQSTM1 plays an important role in autophagy (Turco et al., 2021). These points at a dysregulation of protein synthesis, degradation and hypertrophy, which we could observe in skeletal and heart muscle, in the absence of MuRF1 and MuRF3.

8.3. Mitochondrial function in TA and heart

8.3.1. Reduction of ETC subunits on protein and gene expression level

We decided to focus on the reduction of ETC subunits. To support our mass spectrometry data, we performed immunoblots of TA and heart tissue with the OxPhos antibody. In TA of DKO mice we saw a significant reduction of all ETC subunits compared to controls. Female mice were more affected, since all ETC subunits were significantly down regulated compared to controls, while in male mice we only detected a decrease of UQCRC2 and ATP5 in DKOs. Smaller changes were observed in heart tissue, which is in line with our mass spectrometry data. NDUFB8 was significantly reduced in DKO and male DKO compared to controls, while in DKO females a decrease of UQCRC2, MTCO1, and ATP5 was found. ETC subunits were already brought into correlation with MuRFs in the past. YTH screens of MuRF1 and MuRF2 revealed a possible interaction with the mitochondrial proteins enoyl CO-A hydratase I, ATPMB, NDUFA1 (complex I) and UQCRC1 (complex III) (C. C. Witt et al., 2008). Furthermore, proteom analysis of SOL from MuRF2/MuRF3 DKO mice revealed a decrease in proteins needed for mitochondrial function and cellular energy supply (Lodka et al., 2016). Dysregulation of proteins involved in oxidative phosphorylation was also described in protein storage disease like Alzheimer's (Manczak et al., 2004). To verify if this dysregulation of ETC subunits is caused by changes on the protein or gene expression level, we performed qRT-PCR of the same subunits. *Ndufb8*, *Sdhb*, *Mtco1* and *Atp5* were decreased in DKO mice compared to controls in the TA. DKOs female mice displayed more significant down regulated subunits compared to controls than male DKOs, comparable to the western blot analysis. In heart *Sdhb* and *Mtco1* were decreased in DKO mice compared to controls and in female DKO mice, while in male mice only *Mtco1* remained significant. Sex specific differences were already described in different myopathies (Brambatti et al., 2019; Skilving et al., 2016).

8.3.2. Impaired function of ETC complexes I and III in TA

Spectrophotometric measurement revealed an impaired function of complex I and III in TA, in overall muscular and relative data, for possible differenced in mitochondria content. this result only remained significant in females, in overall muscular and relative data. No changes in complex activity, neither in overall muscular or relative data, could be observed in heart. Mitochondrial dysfunction was also described in patients suffering from MFM, which belongs to the PAMs like MSM. Compared to aged matched controls, they showed a more prominent decrease in complex I and IV activity (Vincent, Grady, et al., 2016). MFM causing DES mutations, aggregate-prone and non-aggregate-prone, were also proven to reduce mitochondrial function (Smolina et al., 2020). It is also commonly described in other protein storage diseases like Alzheimer's, Parkinson and Huntington (Aliev et al., 2003; Blin et al., 1994; Costa et al., 2010; Manczak et al., 2011; She et al., 2011). The activity data results support our proteome data,

who pointed at a possible mitochondrial dysfunction, and highlight that TA is more effected in the MuRF1/MURF3 DKO than heart, and females more than males.

8.4. Degradation of HDAC5 by MuRF1 and MuRF3 via the UPS

8.4.1. Impaired *Ppargc1a* gene expression and increase of HDAC5

We performed qRT-PCR of *Ppargc1a* (PGC1-α), the master regulator for mitochondrial protein synthesis and biogenesis, in TA and heart, since gene expression of ETC subunits was impaired, hinting at the possibility of a disturbed *Ppargc1a* expression. While we observed a significant decrease in TA of DKO mice compared to controls, in both female and DKO male mice, we detected no changes in heart. This is in line with our previous data, regarding ETC subunits protein amount and gene expression as well as complex activity. Muscle specific *Ppargc1a* KO mice developed a myopathy of the skeletal muscles, via a fiber type shift from type-I and type typ-IIA to type-IIB and type-IIX fibers in correlation with fiber damage, which leads to a reduced endurance capacity. They also display an increase of inflammation markers after exercise (Handschin et al., 2007). An impaired PGC1-α function was also described in muscle tissue from patients suffering from Huntington disease (Chaturvedi et al., 2009). Interestingly, differences in heart and skeletal muscle regarding *Ppargc1a* gene expression were described in patient suffering from statin-induced myopathy. While statin had a positive effect on *Ppargc1a* in heart, it decreased gene expression in plantaris muscle (Bouitbir et al., 2012). This highlights that the same stimuli can have different effects depending on the type of muscle, which we also see in our DKO mice. Immuno blot of HDAC5, a known repressor of *Ppargc1a*, with TA samples, revealed a significant increase in DKO mice compared to controls, as well as in female mice DKO mice, but not in males. The increase of HDAC5 could indicate that it is a target of MuRF1 and/or MuRF3 and the cause of loss of mitochondrial function observed in the DKO mice.

8.4.2. Interaction of HDAC5 with MuRF1 and MuRF3

This accumulation of HDAC5 could be explained, if it is a target of MuRF1/MuRF3 for degradation via the UPS. To test this hypothesis, we performed a CO-IP assay with HDAC5 and all three MuRF proteins, which proofed that MuRF1 directly interacts with HDAC5, but not MuRF2 or MuRF3. We narrowed down the minimal interaction region within HDAC5 to AA 540-601. To proof that HDAC5 was tagged for degradation via the UPS, ubiquitination assays were performed, overexpressing HDAC5, MuRF1 and/or MuRF3, RING-finger inactive mutants of MuRF1 and or MuRF3 as well as ubiquitin. An increase of ubiquitinated HDAC5 in samples overexpressing MuRF1 and MuRF1/MuRF3 could be observed, but not in the samples who only overexpressed MuRF3. To test if the ubiquitination of HDAC5 by MuRF1 and or MuRF3 does also lead to a reduced stability of HDAC5, we performed an CHX assay in C2C12 cells. This assay showed that the

stability of endogenous HDAC5 was reduced when MuRF1, MuRF3 or both were overexpressed. The differences in effectivity of MuRF3 could be explained by the fact, that C2C12 cells also contain native MuRF1, while COS7 do not. MuRF1 and MuRF3 are known to form homo- and heterodimers (Centner et al., 2001; Spencer et al., 2000). It is therefore possible that overexpressed MuRF3 can form a hetero-dimer with endogenous MuRF1 that could allow MuRF3 to indirectly interact with HDAC5. Both results, the increase of ubiquitination and the reduction of stability of HDAC5, support our thesis that HDAC5 is a target of MuRF1 and/or MuRF3 for degradation by the UPS.

8.4.3. MuRF1 and MuRF3 regulate mitochondrial function in the striated muscle by targeting HDAC5 for degradation by the UPS

We propose the following mechanism. MuRF1 regulates mitochondrial function, as a homo- or hetero-dimer with MuRF3, by targeting HDAC5 for degradation via the UPS, which represses PGC1-α gene expression by inhibiting MEF2 and ERα. (Figure 26)
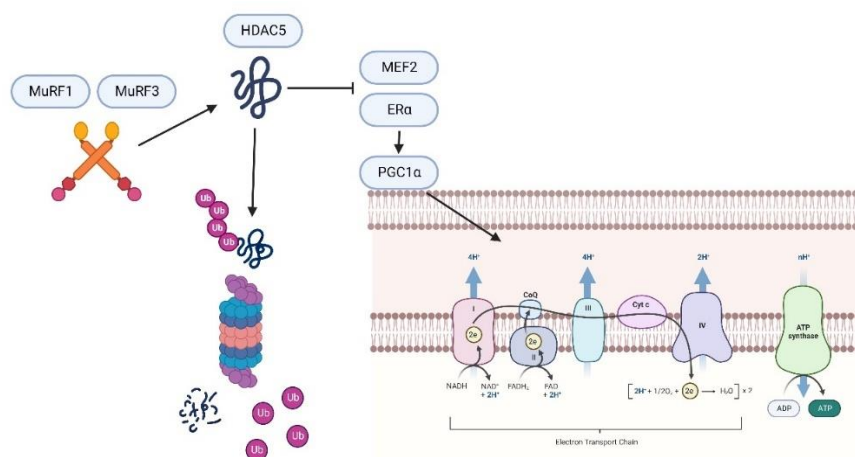

Figure 26. Regulation of mitochondrial activity by MuRF1 and MuRF3 via HDAC5. MuRF1, as a homo or heterodimer with MuRF3, targets HDAC5 for degradation via the UPS. HDAC5 represses the gene expression of PGC1α, the master regulator of mitochondrial protein synthesis, by inhibiting MEF2 and ERα activity. Therefore, by controlling the amount of HDAC5, MuRF1 and MuRF3 regulate mitochondrial activity.

Czubryt et al., established that HDAC5 regulates PGC1-α by inhibiting MEF2 (Czubryt et al., 2003). This is further supported by the fact that MEF2 activity maintains mitochondrial adaptation in cardiac pressure overload and that HDAC inhibitors induce mitochondrial biogenesis (el Azzouzi et al., 2010; Galmozzi et al., 2013; Yang et al., 2019). ETC complex I, specific its ND6 subunit, seems to be especially targeted here, which is in line with the reduction of complex I activity we see in TA of our DKO mice (el Azzouzi et al., 2010; She et al., 2011). Van Rooij et al. reported that HDAC5 and HDAC9 directly inhibit ERα (Van Rooij et al., 2010). It was also shown in breast cancer models that HDAC inhibitors restore ERα activity and that

ERα has a positive effect on mitochondrial function, for example increasing PGC1-α expression (Hamilton et al., 2016; Sabnis et al., 2011; Torres et al., 2018). Complex I activity seems to be of especially influenced here (Torres et al., 2018). The DKO of MuRF1/MuRF3 leads to an increase of HDAC5 and therefore to a disturbed PGC1-α gene expression, as seen in TA. Mitochondrial protein synthesis, like ETC subunits, is then downregulated, causing mitochondrial dysfunction. Heart could be less affected than TA, because of protective measurements to upkeep a proper function, to keep the organism alive. Adding a second stressor like TAC could give a better insight here. Another reason could be the intact MuRF2. Witt et al. described in 2008 that their MuRF1/MuRF2 DKO has a stronger effect on heart than on skeletal muscle, which could imply that especially MuRF2, or the combination of MuRF1 and MuRF2, is important for the maintenance of heart function.

The ERα pathway could be the reason why DKO females were more affected than males in our study. As mentioned before regulates HDAC5 PGC1-α by inhibiting MEF2 (Czubryt et al., 2003). MEF2 was also shown to regulate ERα gene expression, by van Rooij et al (Van Rooij et al., 2010). Therefore, HDAC5 regulates ERα not only directly by inhibiting its activity, but also by repressing its gene expression. Interestingly, Czubryt et al., 2003 observed a 100% mortality of male cardiac *HDAC5* overexpressing mice 7-10 days after induction of gene expression, via doxycycline (DOX) withdrawal, while females survived up to day 30. While female mice developed collagen accumulations and a dilated cardiomyopathy, there was no change in heart-to-body weight ratio in males. Signs of necrosis, inflammation and deformed mitochondria were specific for male mice. Those results contrast with our data, where females were more effected than males, thought this could be explained by the different type of muscle, TA instead of heart, as well as our phenotype. While the MuRF1/MuRF2 DKO phenotype had a strong effect on the heart, our mice displayed more changes in TA (C. C. Witt et al., 2008). The importance of ERα and female sex hormones in regulating mitochondrial function in the striated muscle of females is well known. For example, after ovariectomy female rats suffer from a lower muscle mitochondria content, a trend we also observed in female DKO mice with a slightly reduced CS activity, and a decrease of PGC1-α expression, which we could also detect our female DKO mice, that could be reverted by estrogen replacement (Cavalcanti-de-Albuquerque et al., 2014). Female muscle-specific ERα KO mice displayed an impaired glucose homeostasis and muscle oxidative metabolism, as well as deformed mitochondria, highlighting its importance for maintaining mitochondrial function (Ribas et al., 2016). An impaired oxidative metabolism was also observed in female MuRF1/MuRF3 DKO mice via the reduced function of ETC complex I and III. Compared to males, elderly females are more often affected by sarcopenia (Janssen et al., 2002), age related muscle wasting, while estradiol treatment in early-postmenopausal women reduced markers for muscle wasting (Y. M. Park et al., 2019). Proteome analysis of muscle tissue from postmenopausal woman also revealed a dysregulation of mitochondrial proteins, similar to our findings (Laakkonen et al., 2017). Interestingly dysfunctions of the UPS and the mitochondria are pathways

discussed in the development of statin induced myopathies (Sahebkar et al., 2020; Schirris et al., 2015; Stringer et al., 2013), which are more pronounced in females compared to males (Skilving et al., 2016). Especially complex III activity, like in our female DKO mice, seems to be affected here (Schirris et al., 2015). Statin was also proven to interact with ERα, having either a positive or negative effect on its gene expression depending on the organ (X. Li et al., 2011; J. B. Park et al., 2012), creating another link between our female DKO mice and statin induced myopathy. The inhibition of both, ERα activity and gene expression, could therefore enhance the DKO effect in our female mice as seen by the more pronounced reduction of ETC subunits and complex activity compared to males. Further research in the MuRF1/MuRF3 DKO model, for example measurement of ERα activity in correlation with HDAC inhibitor treatment, needs to be performed in the future to illustrate this pathway more.

8.5. Conclusion

In this thesis we further characterized the MuRF1/MuRF3 DKO phenotype, focusing on its effect on the striated muscle energy metabolism. In line with previously published work, DKO mice suffered from heart and skeletal muscle hypertrophy, caused by subsarcolemmal protein aggregates, which lead to impaired skeletal muscle function. Here we demonstrate that TA is more affected by the DKO than the heart, and that females are more affected than males. We also show that MuRF1/MuRF3 DKO mice suffer from mitochondrial dysfunction, more specifically a decrease in ETC complex I and complex III activity, as a consequence of an impaired *Ppargc1a* gene expression, which leads to a decrease in ETC subunits. Our proposed mechanism here is that MuRF1 and/or MuRF3 directly regulate mitochondrial function by targeting HDAC5, a *Ppargc1a* gene repressor, for degradation via the UPS. Their DKO leads to an accumulation of HDAC5, as observed in TA of DKO mice, which causes the described dysfunction. Females are likely more effected, since HDAC5 represses *Ppargc1a* gene expression by inhibiting MEF2 and ERα, and the ERα pathway plays an important role in female mic, but not in males. Therefore, we were able to link MuRF1 and MuRF3 directly to the striated muscle energy metabolism by regulating mitochondrial function via HDAC5. This could give further inside in the development of PAMs, where mitochondrial dysfunction has already been described as a symptom, as well as for other protein storage diseases like Alzheimer's, Parkinson and Huntington. It also validates the MuRF1/MuRF3 phenotype as a model organism for PAMs, especially MSM.

9. Bibliography

Abe, T., Ohga, Y., Tabayashi, N., Kobayashi, S., Sakata, S., Misawa, H., Tsuji, T., Kohzuki, H., Suga, H., Taniguchi, S., & Takaki, M. (2002). Left ventricular diastolic dysfunction in type 2 diabetes mellitus model rats. *American Journal of Physiology-Heart and Circulatory Physiology*, *282*(1), H138–H148. https://doi.org/10.1152/ajpheart.2002.282.1.H138

Acín-Pérez, R., Fernández-Silva, P., Peleato, M. L., Pérez-Martos, A., & Enriquez, J. A. (2008). Respiratory Active Mitochondrial Supercomplexes. *Molecular Cell*, *32*(4), 529–539. https://doi.org/10.1016/j.molcel.2008.10.021

Ahuja, A. S. (2018). Understanding mitochondrial myopathies: A review. *PeerJ*, *2018*(5). https://doi.org/10.7717/peerj.4790

Akutsu, M., Dikic, I., & Bremm, A. (2016). Ubiquitin chain diversity at a glance. *Journal of Cell Science*, *129*(5), 875–880. https://doi.org/10.1242/jcs.183954

Aliev, G., Smith, M. A., Obrenovich, M. E., De, J. C., Torre, L. A., & Perry, G. (2003). Role of Vascular Hypoperfusion-induced Oxidative Stress and Mitochondria Failure in the Pathogenesis of Alzheimer Disease. *Neurotoxicity Research*, *5*(7), 491–504. www.fpgrahamco.com

Amm, I., Sommer, T., & Wolf, D. H. (2014). Protein quality control and elimination of protein waste: The role of the ubiquitin-proteasome system. In *Biochimica et Biophysica Acta - Molecular Cell Research* (Vol. 1843, Issue 1, pp. 182–196). https://doi.org/10.1016/j.bbamcr.2013.06.031

Ardissone, A., Invernizzi, F., Nasca, A., Moroni, I., Farina, L., & Ghezzi, D. (2015). Mitochondrial leukoencephalopathy and complex II deficiency associated with a recessive SDHB mutation with reduced penetrance. *Molecular Genetics and Metabolism Reports*, *5*, 51–54. https://doi.org/10.1016/j.ymgmr.2015.10.006

Artham, S. M., Lavie, C. J., Milani, R. v., Patel, D. A., Verma, A., & Ventura, H. O. (2009). Clinical Impact of Left Ventricular Hypertrophy and Implications for Regression. *Progress in Cardiovascular Diseases*, *52*(2), 153–167. https://doi.org/10.1016/j.pcad.2009.05.002

Asmussen, G., Schmalbruch, I., Soukup, T., & Pette, D. (2003). Contractile properties, fiber types, and myosin isoforms in fast and slow muscles of hyperactive Japanese waltzing mice. *Experimental Neurology*, *184*(2), 758–766. https://doi.org/10.1016/S0014-4886(03)00294-2

Athale, J., Ulrich, A., Chou MacGarvey, N., Bartz, R. R., Welty-Wolf, K. E., Suliman, H. B., & Piantadosi, C. A. (2012). Nrf2 promotes alveolar mitochondrial biogenesis and resolution of lung injury in Staphylococcus aureus pneumonia in mice. *Free Radical Biology and Medicine*, *53*(8), 1584–1594. https://doi.org/10.1016/j.freeradbiomed.2012.08.009

Augusto, V., Padovani, C. R., & Rocha Campos, G. E. (2004). Skeletal muscle fiber types in C57Bl6J mice. In *Braz. J. morphol. Sci* (Vol. 21, Issue 2).

Bahrudin, U., Morisaki, H., Morisaki, T., Ninomiya, H., Higaki, K., Nanba, E., Igawa, O., Takashima, S., Mizuta, E., Miake, J., Yamamoto, Y., Shirayoshi, Y., Kitakaze, M., Carrier, L., & Hisatome, I. (2008). Ubiquitin-Proteasome System Impairment Caused by a Missense Cardiac Myosin-binding Protein C Mutation and

Associated with Cardiac Dysfunction in Hypertrophic Cardiomyopathy. *Journal of Molecular Biology*, *384*(4), 896–907. https://doi.org/10.1016/j.jmb.2008.09.070

Banerjee, R., He, J., Spaniel, C., Quintana, M. T., Wang, Z., Bain, J. R., Newgard, C. B., Muehlbauer, M. J., & Willis, M. S. (2015). Non-targeted metabolomics analysis of cardiac Muscle Ring Finger-1 (MuRF1), MuRF2, and MuRF3 in vivo reveals novel and redundant metabolic changes. *Metabolomics*, *11*(2), 312–322. https://doi.org/10.1007/s11306-014-0695-1

Barclay, C. J. (2017). Energy demand and supply in human skeletal muscle. In *Journal of Muscle Research and Cell Motility* (Vol. 38, Issue 2, pp. 143–155). Springer International Publishing. https://doi.org/10.1007/s10974-017-9467-7

Barnerias, C., Saudubray, J. M., Touati, G., de Lonlay, P., Dulac, O., Ponsot, G., Marsac, C., Brivet, M., & Desguerre, I. (2010). Pyruvate dehydrogenase complex deficiency: Four neurological phenotypes with differing pathogenesis. *Developmental Medicine and Child Neurology*, *52*(2). https://doi.org/10.1111/j.1469-8749.2009.03541.x

Baumgarten, G., Knuefermann, P., Kalra, D., Gao, F., Taffet, G. E., Michael, L., Blackshear, P. J., Carballo, E., Sivasubramanian, N., & Mann, D. L. (2002). Load-dependent and -independent regulation of proinflammatory cytokine and cytokine receptor gene expression in the adult mammalian heart. *Circulation*, *105*(18), 2192–2197. https://doi.org/10.1161/01.CIR.0000015608.37608.18

Berg, J. M., Tymoczko, J. L., Gatto, G. J., & Stryer, L. (2013a). *Biochemie* (7th ed.). Springer Verlag. Oxidative Phosphorylierung: 528-564 https://doi.org/10.1007/978-3-662-54620-8

Berg, J. M., Tymoczko, J. L., Gatto, G. J., & Stryer, L. (2013b). *Biochemie* (7th ed.). Springer Verlag. Proteinumsatz und Aminosäurekatabolismus: 683-689 https://doi.org/10.1007/978-3-662-54620-8

Betts, J. G., College, T. J., Desaix, P., Johnson, J. E., Wise, J. A., Womble, M., & Young, K. A. (2017a). *Anatomy & Physiology*. OpenStax. 4.4. Muscle Tissue and Motion: 160-162

Betts, J. G., College, T. J., Desaix, P., Johnson, J. E., Wise, J. A., Womble, M., & Young, K. A. (2017b). *Anatomy & Physiology*. OpenStax. 10. Muscle Tissue: 406-432

Betts, J. G., College, T. J., Desaix, P., Johnson, J. E., Wise, J. A., Womble, M., & Young, K. A. (2017c). *Anatomy & Physiology*. OpenStax. The Cardio Vascular System: The Heart: 823-846

Bian, Z. Y., Huang, H., Jiang, H., Shen, D. F., Yan, L., Zhu, L. H., Wang, L., Cao, F., Liu, C., Tang, Q. Z., & Li, H. (2010). LIM and cysteine-rich domains 1 regulates cardiac hypertrophy by targeting calcineurin/nuclear factor of activated T cells signaling. *Hypertension*, *55*(2), 257–263. https://doi.org/10.1161/HYPERTENSIONAHA.109.135665

Bierbrauer, J., Koch, S., Olbricht, C., Hamati, J., Lodka, D., Schneider, J., Luther-Schröder, A., Kleber, C., Faust, K., Wiesener, S., Spies, C. D., Spranger, J., Spuler, S., Fielitz, J., & Weber-Carstens, S. (2012). Early type II fiber atrophy in intensive care unit patients with nonexcitable muscle membrane. *Critical Care Medicine*, *40*(2), 647–650. https://doi.org/10.1097/CCM.0b013e31823295e6

Blanchi, C., Genova, M. L., Castelli, G. P., & Lenaz, G. (2004). The mitochondrial respiratory chain is partially organized in a supercomplex assembly: Kinetic evidence using flux control analysis. *Journal of Biological Chemistry*, *279*(35), 36562–36569. https://doi.org/10.1074/jbc.M405135200

Blin, O., Desnuelle, C., Rascol, O., Borg, M., Peyro, H., Azulay, P., Bill6, F., Figarella, D., Coulom, F., Pellissier, J. F., Montastruc, J. L., Chatel, M., & Serratrice, G. (1994). Mitochondrial respiratory failure in skeletal muscle from patients with Parkinson's disease and multiple system atrophy. In *Journal of the Neurological Sciences* (Vol. 125).

Bodine, S. C., Latres, E., Baumhueter, S., K-M Lai, V., Nunez, L., Clarke, B. A., Poueymirou, W. T., Panaro, F. J., Na, E., Dharmarajan, K., Pan, Z.-Q., Valenzuela, D. M., DeChiara, T. M., Stitt, T. N., Yancopoulos, G. D., & Glass, D. J. (2001). Identification of Ubiquitin Ligases Required for Skeletal Muscle Atrophy. *Trends Ecol. Evol*, *294*(5547), 1706–1708. www.sciencemag.org/cgi/content/full/294/5547/1702/

Bouitbir, J., Charles, A.-L., Echaniz-Laguna, A., Kindo, M., Daussin, F., Auwerx, J., Piquard, F., Geny, B., & Zoll, J. (2012). Opposite effects of statins on mitochondria of cardiac and skeletal muscles: a 'mitohormesis' mechanism involving reactive oxygen species and PGC-1. *European Heart Journal*, *33*(11), 1397–1407. https://doi.org/10.1093/eurheartj/ehr224

Brambatti, M., Caspi, O., Maolo, A., Koshi, E., Greenberg, B., Taylor, M. R. G., & Adler, E. D. (2019). Danon disease: Gender differences in presentation and outcomes. *International Journal of Cardiology*, *286*, 92–98. https://doi.org/10.1016/j.ijcard.2019.01.020

Brodehl, A., Dieding, M., Klauke, B., Dec, E., Madaan, S., Huang, T., Gargus, J., Fatima, A., Šaric, T., Cakar, H., Walhorn, V., Tönsing, K., Skrzipczyk, T., Cebulla, R., Gerdes, D., Schulz, U., Gummert, J., Svendsen, J. H., Olesen, M. S., … Milting, H. (2013). The novel desmin mutant p.A120D impairs filament formation, prevents intercalated disk localization, and causes sudden cardiac death. *Circulation: Cardiovascular Genetics*, *6*(6), 615–623. https://doi.org/10.1161/CIRCGENETICS.113.000103

Bua, E., Johnson, J., Herbst, A., Delong, B., Mckenzie, D., Salamat, S., & Aiken, J. M. (2006). ARTICLE Mitochondrial DNA-Deletion Mutations Accumulate Intracellularly to Detrimental Levels in Aged Human Skeletal Muscle Fibers. In *The American Journal of Human Genetics* (Vol. 79). www.ajhg.org

Campbell, G., Krishnan, K. J., Deschauer, M., Taylor, R. W., & Turnbull, D. M. (2014). Dissecting the mechanisms underlying the accumulation of mitochondrial DNA deletions in human skeletal muscle. *Human Molecular Genetics*, *23*(17), 4612–4620. https://doi.org/10.1093/hmg/ddu176

Cavalcanti-de-Albuquerque, J. P. A., Salvador, I. C., Martins, E. L., Jardim-Messeder, D., Werneck-de-Castro, J. P. S., Galina, A., & Carvalho, D. P. (2014). Role of estrogen on skeletal muscle mitochondrial function in ovariectomized rats: a time course study in different fiber types. *Journal of Applied Physiology*, *116*(7), 779–789. https://doi.org/10.1152/japplphysiol.00121.2013

Centner, T., Yano, J., Kimura, E., McElhinny, A. S., Pelin, K., Witt, C. C., Bang, M. L., Trombitas, K., Granzier, H., Gregorio, C. C., Sorimachi, H., & Labeit, S. (2001). Identification of muscle specific ring finger proteins as potential regulators of the titin kinase domain. *Journal of Molecular Biology*, *306*(4), 717–726. https://doi.org/10.1006/jmbi.2001.4448

Chang, J., Jung, H. J., Jeong, S. H., Kim, H. K., Han, J., & Kwon, H. J. (2014). A mutation in the mitochondrial protein UQCRB promotes angiogenesis through the generation of mitochondrial reactive oxygen species. *Biochemical and Biophysical Research Communications*, *455*(3–4), 290–297. https://doi.org/10.1016/j.bbrc.2014.11.005

Chaturvedi, R. K., Adhihetty, P., Shukla, S., Hennessy, T., Calingasan, N., Yang, L., Starkov, A., Kiaei, M., Cannella, M., Sassone, J., Ciammola, A., Squitieri, F., & Beal, M. F. (2009). Impaired PGC-1α function in muscle in Huntington's disease. *Human Molecular Genetics*, *18*(16), 3048–3065. https://doi.org/10.1093/hmg/ddp243

Cipolat, S., de Brito, O. M., Dal Zilio, B., & Scorrano, L. (2004). OPA1 requires mitofusin 1 to promote mitochondrial fusion. *Proceedings of the National Academy of Sciences*, *101*(45), 15927–15932. https://doi.org/10.1073/pnas.0407043101

Cogswell, A. M., Stevens, R. J., & Hood, D. A. (1993). Properties of skeletal muscle mitochondria isolated from subsarcolemmal and intermyofibrillar regions. *American Journal of Physiology-Cell Physiology*, *264*(2), C383–C389. https://doi.org/10.1152/ajpcell.1993.264.2.C383

Costa, V., Giacomello, M., Hudec, R., Lopreiato, R., Ermak, G., Lim, D., Malorni, W., Davies, K. J. A., Carafoli, E., & Scorrano, L. (2010). Mitochondrial fission and cristae disruption increase the response of cell models of Huntington's disease to apoptotic stimuli. *EMBO Molecular Medicine*, *2*(12), 490–503. https://doi.org/10.1002/emmm.201000102

Cox, E. J., & Marsh, S. A. (2014). A Systematic Review of Fetal Genes as Biomarkers of Cardiac Hypertrophy in Rodent Models of Diabetes. *PLoS ONE*, *9*(3), e92903. https://doi.org/10.1371/journal.pone.0092903

Crugnola, V., Lamperti, C., Lucchini, V., Ronchi, D., Peverelli, L., Prelle, A., Sciacco, M., Bordoni, A., Fassone, E., Fortunato, F., Corti, S., Silani, V., Bresolin, N., Di Mauro, S., Comi, G. Pietro, & Moggio, M. (2010). Mitochondrial Respiratory Chain Dysfunction in Muscle From Patients With Amyotrophic Lateral Sclerosis. *Archives of Neurology*, *67*(7). https://doi.org/10.1001/archneurol.2010.128

Czubryt, M. P., McAnally, J., Fishman, G. I., & Olson, E. N. (2003). Regulation of peroxisome proliferator-activated receptor γ coactivator 1α (PGC-1α) and mitochondrial function by MEF2 and HDAC5. *Proceedings of the National Academy of Sciences*, *100*(4), 1711–1716. https://doi.org/10.1073/pnas.0337639100

Dahl, R., Larsen, S., Dohlmann, T. L., Qvortrup, K., Helge, J. W., Dela, F., & Prats, C. (2015). Three-dimensional reconstruction of the human skeletal muscle mitochondrial network as a tool to assess mitochondrial content and structural organization. *Acta Physiologica*, *213*(1), 145–155. https://doi.org/10.1111/apha.12289

de Stefani, D., Raffaello, A., Teardo, E., Szabó, I., & Rizzuto, R. (2011). A forty-kilodalton protein of the inner membrane is the mitochondrial calcium uniporter. *Nature*, *476*(7360), 336–340. https://doi.org/10.1038/nature10230

Dietz, J. R. (2005). Mechanisms of atrial natriuretic peptide secretion from the atrium. In *Cardiovascular Research* (Vol. 68, Issue 1, pp. 8–17). https://doi.org/10.1016/j.cardiores.2005.06.008

DiMauro, S., & Williams, L. (2006). Mitochondrial myopathies. In *Current Opinion in Rheumatology* (Vol. 18).

Dou, H., Buetow, L., Sibbet, G. J., Cameron, K., & Huang, D. T. (2012). BIRC7-E2 ubiquitin conjugate structure reveals the mechanism of ubiquitin transfer by a RING dimer. *Nature Structural and Molecular Biology*, *19*(9), 876–883. https://doi.org/10.1038/nsmb.2379

Driesen, R. B., Verheyen, F. K., Debie, W., Blaauw, E., Babiker, F. A., Cornelussen, R. N. M., Ausma, J., Lenders, M. H., Borgers, M., Chaponnier, C., & Ramaekers, F. C. S. (2009). Re-expression of alpha skeletal actin as a marker for dedifferentiation in cardiac pathologies. *Journal of Cellular and Molecular Medicine*, *13*(5), 896–908. https://doi.org/10.1111/j.1582-4934.2008.00523.x

Duda, D. M., Olszewski, J. L., Schuermann, J. P., Kurinov, I., Miller, D. J., Nourse, A., Alpi, A. F., & Schulman, B. A. (2013). Structure of HHARI, a RING-IBR-RING ubiquitin ligase: Autoinhibition of an Ariadne-family E3 and insights into ligation mechanism. *Structure*, *21*(6), 1030–1041. https://doi.org/10.1016/j.str.2013.04.019

Eason, J. M., Schwartz, G. A., Pavlath, G. K., & English, A. W. (2000). Sexually dimorphic expression of myosin heavy chains in the adult mouse masseter. *Journal of Applied Physiology*, *89*(1), 251–258. https://doi.org/10.1152/jappl.2000.89.1.251

Eisner, V., Lenaers, G., & Hajnóczky, G. (2014). Mitochondrial fusion is frequent in skeletal muscle and supports excitation-contraction coupling. *Journal of Cell Biology*, *205*(2), 179–195. https://doi.org/10.1083/jcb.201312066

el Azzouzi, H., van Oort, R. J., van der Nagel, R., Sluiter, W., Bergmann, M. W., & de Windt, L. J. (2010). MEF2 transcriptional activity maintains mitochondrial adaptation in cardiac pressure overload. *European Journal of Heart Failure*, *12*(1), 4–12. https://doi.org/10.1093/eurjhf/hfp165

Elsasser, S., Chandler-Mitilello, D., Müller, B., Hanna, J., & Finley, D. (2004). Rad23 and Rpn10 serve as alternate ubiquitin receptors for the proteasome. *Journal of Biological Chemistry*, *279*(26), 26817–26822. https://doi.org/10.1074/jbc.M404020200

Fabbrizio, E., el Messaoudi, S., Polanowska, J., Paul, C., Cook, J. R., Lee, J. H., Nère, V., Rousset, M., Pestka, S., le Cam, A., & Sardet, C. (2002). Negative regulation of transcription by the type II arginine methyltransferase PRMT5. *EMBO Reports*, *3*(7), 641–645. https://doi.org/10.1093/embo-reports/kvf136

Falzarano, M. S., Scotton, C., Passarelli, C., & Ferlini, A. (2015). Duchenne muscular dystrophy: From diagnosis to therapy. *Molecules*, *20*(10), 18168–18184. https://doi.org/10.3390/molecules201018168

Fanin, M., Nascimbeni, A. C., & Angelini, C. (2014). Gender difference in limb-girdle muscular dystrophy: A muscle fiber morphometric study in 101 patients. *Clinical Neuropathology*, *33*(3), 179–185. https://doi.org/10.5414/NP300728

Ferreira, R., Vitorino, R., Alves, R. M. P., Appell, H. J., Powers, S. K., Duarte, J. A., & Amado, F. (2010). Subsarcolemmal and intermyofibrillar mitochondria proteome differences disclose functional specializations in skeletal muscle. *Proteomics*, *10*(17), 3142–3154. https://doi.org/10.1002/pmic.201000173

Ferrington, D. A., Husom, A. D., & Thompson, L. v. (2005). Altered proteasome structure, function, and oxidation in aged muscle. *The FASEB Journal*, *19*(6), 1–24. https://doi.org/10.1096/fj.04-2578fje

Fielitz, J., Kim, M. S., Shelton, J. M., Latif, S., Spencer, J. A., Glass, D. J., Richardson, J. A., Bassel-Duby, R., & Olson, E. N. (2007). Myosin accumulation and striated muscle myopathy result from the loss of muscle RING finger 1 and 3. *Journal of Clinical Investigation*, *117*(9), 2486–2495. https://doi.org/10.1172/JCI32827

Fielitz, J., van Rooij, E., Spencer, J. A., Shelton, J. M., Latif, S., van der Nagel, R., Bezprozvannaya, S., de Windt, L., Richardson, J. A., Bassel-Duby, R., & Olson, E. N. (2007). Loss of muscle-specific RING-finger 3 predisposes the heart to cardiac rupture after myocardial infarction. *Proceedings of the National Academy of Sciences*, *104*(11), 4377–4382. https://doi.org/10.1073/pnas.0611726104

Filipenko, M. L., Vinichenko, N. A., Karpova, G. G., Mertvetsov, N. P., & Amaldi, F. (1998). Isolation, structural analysis and mapping of the functional gene of human ribosomal protein S261. In *Gene* (Vol. 211).

Freemont, P. S., Hanson, I. M., & Trowsdale, J. (1991). A novel gysteine-rich sequence motif. *Cell*, *64*(3), 483–484. https://doi.org/10.1016/0092-8674(91)90229-R

Frey, T. G., & Mannella, C. A. (2000). The internal structure of mitochondria. *Trends in Biochemical Sciences*, *25*(7), 319–324. https://doi.org/10.1016/S0968-0004(00)01609-1

Galmozzi, A., Mitro, N., Ferrari, A., Gers, E., Gilardi, F., Godio, C., Cermenati, G., Gualerzi, A., Donetti, E., Rotili, D., Valente, S., Guerrini, U., Caruso, D., Mai, A., Saez, E., de Fabiani, E., & Crestani, M. (2013). Inhibition of class i histone deacetylases unveils a mitochondrial signature and enhances oxidative metabolism in skeletal muscle and adipose tissue. *Diabetes*, *62*(3), 732–742. https://doi.org/10.2337/db12-0548

Garnett, M. J., Mansfeld, J., Godwin, C., Matsusaka, T., Wu, J., Russell, P., Pines, J., & Venkitaraman, A. R. (2009). UBE2S elongates ubiquitin chains on APC/C substrates to promote mitotic exit. *Nature Cell Biology*, *11*(11), 1363–1369. https://doi.org/10.1038/ncb1983

Gaur, V., Connor, T., Sanigorski, A., Martin, S. D., Bruce, C. R., Henstridge, D. C., Bond, S. T., McEwen, K. A., Kerr-Bayles, L., Ashton, T. D., Fleming, C., Wu, M., Pike Winer, L. S., Chen, D., Hudson, G. M., Schwabe, J. W. R., Baar, K., Febbraio, M. A., Gregorevic, P., … McGee, S. L. (2016). Disruption of the Class IIa HDAC Corepressor Complex Increases Energy Expenditure and Lipid Oxidation. *Cell Reports*, *16*(11), 2802–2810. https://doi.org/10.1016/j.celrep.2016.08.005

Giorgio, M., Migliaccio, E., Orsini, F., Paolucci, D., Moroni, M., Contursi, C., Pelliccia, G., Luzi, L., Minucci, S., Marcaccio, M., Pinton, P., Rizzuto, R., Bernardi, P., Paolucci, F., & Pelicci, P. G. (2005). Electron transfer between cytochrome c and p66Shc generates reactive oxygen species that trigger mitochondrial apoptosis. *Cell*, *122*(2), 221–233. https://doi.org/10.1016/j.cell.2005.05.011

Glancy, B., Hartnell, L. M., Combs, C. A., Fenmou, A., Sun, J., Murphy, E., Subramaniam, S., & Balaban, R. S. (2017). Power Grid Protection of the Muscle Mitochondrial Reticulum. *Cell Reports*, *19*(3), 487–496. https://doi.org/10.1016/j.celrep.2017.03.063

Goldberg, L. R., & Jessup, M. (2006). Stage B heart failure: Management of asymptomatic left ventricular systolic dysfunction. In *Circulation* (Vol. 113, Issue 24, pp. 2851–2860). https://doi.org/10.1161/CIRCULATIONAHA.105.600437

Gomes, M. D., Lecker, S. H., Jagoe, R. T., Navon, A., & Goldberg, A. L. (2001). Atrogin-1, a muscle-specific F-box protein highly expressed during muscle atrophy. *Proceedings of the National Academy of Sciences*, *98*(25), 14440–14445. https://doi.org/10.1073/pnas.251541198

González, G. E., Rhaleb, N. E., D'Ambrosio, M. A., Nakagawa, P., Liu, Y., Leung, P., Dai, X., Yang, X. P., Peterson, E. L., & Carretero, O. A. (2015). Deletion of interleukin-6 prevents cardiac inflammation, fibrosis and dysfunctionwithout affecting blood pressure in angiotensin II-high salt-induced hypertension. *Journal of Hypertension*, *33*(1), 144–152. https://doi.org/10.1097/HJH.0000000000000358

Griparic, L., van der Wel, N. N., Orozco, I. J., Peters, P. J., & van der Bliek, A. M. (2004). Loss of the Intermembrane Space Protein Mgm1/OPA1 Induces Swelling and Localized Constrictions along the Lengths of Mitochondria. *Journal of Biological Chemistry*, *279*(18), 18792–18798. https://doi.org/10.1074/jbc.M400920200

Groettrup, M., Pelzer, C., Schmidtke, G., & Hofmann, K. (2008). Activating the ubiquitin family: UBA6 challenges the field. In *Trends in Biochemical Sciences* (Vol. 33, Issue 5, pp. 230–237). https://doi.org/10.1016/j.tibs.2008.01.005

Grossman, W., Jones, D., & McLaurin, L. P. (1975). Wall stress and patterns of hypertrophy in the human left ventricle. *Journal of Clinical Investigation*, *56*(1), 56–64. https://doi.org/10.1172/JCI108079

Gruber, B. L. (2003). Mast Cells in the Pathogenesis of Fibrosis Introduction-Mast Cell Biology. *Current Rheumatology Reports*, *5*, 147–153.

Haack, T. B., Haberberger, B., Frisch, E. M., Wieland, T., Iuso, A., Gorza, M., Strecker, V., Graf, E., Mayr, J. A., Herberg, U., Hennermann, J. B., Klopstock, T., Kuhn, K. A., Ahting, U., Sper, W., Wilichowski, E., Hoffmann, G. F., Tesarova, M., Hansikova, H., … Prokisch, H. (2012). Molecular diagnosis in mitochondrial complex I deficiency using exome sequencing. *Journal of Medical Genetics*, *49*(4), 277–283. https://doi.org/10.1136/jmedgenet-2012-100846

Hamilton, D. J., Minze, L. J., Kumar, T., Cao, T. N., Lyon, C. J., Geiger, P. C., Hsueh, W. A., & Gupte, A. A. (2016). Estrogen receptor alpha activation enhances mitochondrial function and systemic metabolism in high-fat-fed ovariectomized mice. *Physiological Reports*, *4*(17). https://doi.org/10.14814/phy2.12913

Han, X.-R., Sasaki, N., Jackson, S. C., Wang, P., Li, Z., Smith, M. D., Xie, L., Chen, X., Zhang, Y., Marzluff, W. F., & Xiong, Y. (2020). C E L L B I O L O G Y CRL4 DCAF1/VprBP E3 ubiquitin ligase controls ribosome biogenesis, cell proliferation, and development. In *Sci. Adv* (Vol. 6). https://www.science.org

Handschin, C., Chin, S., Li, P., Liu, F., Maratos-Flier, E., LeBrasseur, N. K., Yan, Z., & Spiegelman, B. M. (2007). Skeletal muscle fiber-type switching, exercise intolerance, and myopathy in PGC-1α muscle-specific knock-out animals. *Journal of Biological Chemistry*, *282*(41), 30014–30021. https://doi.org/10.1074/jbc.M704817200

Harrison, B. C., Allen, D. L., & Leinwand, L. A. (2011). IIb or not IIb? Regulation of myosin heavy chain gene expression in mice and men. *Skeletal Muscle, 1*(1). https://doi.org/10.1186/2044-5040-1-5

Herrmann, H., Cabet, E., Chevalier, N. R., Moosmann, J., Schultheis, D., Haas, J., Schowalter, M., Berwanger, C., Weyerer, V., Agaimy, A., Meder, B., Müller, O. J., Katus, H. A., Schlötzer-Schrehardt, U., Vicart, P.,

Ferreiro, A., Dittrich, S., Clemen, C. S., Lilienbaum, A., & Schröder, R. (2020). Dual Functional States of R406W-Desmin Assembly Complexes Cause Cardiomyopathy With Severe Intercalated Disc Derangement in Humans and in Knock-In Mice. *Circulation*, *142*(22), 2155–2171. https://doi.org/10.1161/CIRCULATIONAHA.120.050218

Hershko, A., Ciechanover, A., Heller, H., Haas, A. L., & Rose, I. A. (1980). Proposed role of ATP in protein breakdown: conjugation of protein with multiple chains of the polypeptide of ATP-dependent proteolysis. *Proceedings of the National Academy of Sciences*, *77*(4), 1783–1786. https://doi.org/10.1073/pnas.77.4.1783

Hershko, A., Ciechanover, A., & Rose, I. A. (1979). Resolution of the ATP-dependent proteolytic system from reticulocytes: a component that interacts with ATP. *Proceedings of the National Academy of Sciences*, *76*(7), 3107–3110. https://doi.org/10.1073/pnas.76.7.3107

Hershko, A., Heller, H., Elias, S., & Ciechanover, A. (1983). Components of ubiquitin-protein ligase system. Resolution, affinity purification, and role in protein breakdown. *Journal of Biological Chemistry*, *258*(13), 8206–8214. https://doi.org/10.1016/S0021-9258(20)82050-X

Hirner, S., Krohne, C., Schuster, A., Hoffmann, S., Witt, S., Erber, R., Sticht, C., Gasch, A., Labeit, S., & Labeit, D. (2008). MuRF1-dependent Regulation of Systemic Carbohydrate Metabolism as Revealed from Transgenic Mouse Studies. *Journal of Molecular Biology*, *379*(4), 666–677. https://doi.org/10.1016/j.jmb.2008.03.049

Ho, C. Y., López, B., Coelho-Filho, O. R., Lakdawala, N. K., Cirino, A. L., Jarolim, P., Kwong, R., González, A., Colan, S. D., Seidman, J. G., Díez, J., & Seidman, C. E. (2010). Myocardial Fibrosis as an Early Manifestation of Hypertrophic Cardiomyopathy A bs tr ac t. In *N Engl J Med* (Vol. 363).

Huang, D. T., Ayrault, O., Hunt, H. W., Taherbhoy, A. M., Duda, D. M., Scott, D. C., Borg, L. A., Neale, G., Murray, P. J., Roussel, M. F., & Schulman, B. A. (2009). E2-RING Expansion of the NEDD8 Cascade Confers Specificity to Cullin Modification. *Molecular Cell*, *33*(4), 483–495. https://doi.org/10.1016/j.molcel.2009.01.011

Husnjak, K., Elsasser, S., Zhang, N., Chen, X., Randles, L., Shi, Y., Hofmann, K., Walters, K. J., Finley, D., & Dikic, I. (2008). Proteasome subunit Rpn13 is a novel ubiquitin receptor. *Nature*, *453*(7194), 481–488. https://doi.org/10.1038/nature06926

Iqbal, S., Ostojic, O., Singh, K., Joseph, A. M., & Hood, D. A. (2013). Expression of mitochondrial fission and fusion regulatory proteins in skeletal muscle during chronic use and disuse. *Muscle & Nerve*, *48*(6), 963–970. https://doi.org/10.1002/mus.23838

Jacobs, R. A., Flück, D., Bonne, T. C., Bürgi, S., Christensen, P. M., Toigo, M., & Lundby, C. (2013). Improvements in exercise performance with high-intensity interval training coincide with an increase in skeletal muscle mitochondrial content and function. *J Appl Physiol*, *115*, 785–793. https://doi.org/10.1152/japplphysiol.00445.2013.-Six

Janssen, I., Heymsfield, S. B., & Ross, R. (2002). Low Relative Skeletal Muscle Mass (Sarcopenia) in Older Persons Is Associated with Functional Impairment and Physical Disability. *Journal of the American Geriatrics Society*, *50*(5), 889–896. https://doi.org/10.1046/j.1532-5415.2002.50216.x

Jennings, R. B., & Reimer, K. A. (1991). The Cell Biology of Acute Myocardial Ischemia. *Annual Review of Medicine*, *42*(1), 225–246. https://doi.org/10.1146/annurev.me.42.020191.001301

Jin, X., Nauta, J. F., Hung, C. L., Ouwerkerk, W., Teng, T. H. K., Voors, A. A., Lam, C. S., & van Melle, J. P. (2022). Left atrial structure and function in heart failure with reduced (HFrEF) versus preserved ejection fraction (HFpEF): systematic review and meta-analysis. In *Heart Failure Reviews* (Vol. 27, Issue 5, pp. 1933–1955). Springer. https://doi.org/10.1007/s10741-021-10204-8

Juo, L. Y., Liao, W. C., Shih, Y. L., Yang, B. Y., Liu, A. B., & Yan, Y. T. (2016). HSPB7 interacts with dimerized FLNC and its absence results in progressive myopathy in skeletal muscles. *Journal of Cell Science*, *129*(8), 1661–1670. https://doi.org/10.1242/jcs.179887

Kalia, R., Wang, R. Y. R., Yusuf, A., Thomas, P. v., Agard, D. A., Shaw, J. M., & Frost, A. (2018). Structural basis of mitochondrial receptor binding and constriction by DRP1. *Nature*, *558*(7710), 401–405. https://doi.org/10.1038/s41586-018-0211-2

Kamadurai, H. B., Qiu, Y., Deng, A., Harrison, J. S., MacDonald, C., Actis, M., Rodrigues, P., Miller, D. J., Souphron, J., Lewis, S. M., Kurinov, I., Fujii, N., Hammel, M., Piper, R., Kuhlman, B., & Schulman, B. A. (2013). Mechanism of ubiquitin ligation and lysine prioritization by a HECT E3. *ELife*, *2*. https://doi.org/10.7554/elife.00828

Kammoun, M., Cassar-Malek, I., Meunier, B., & Picard, B. (2014). A simplified immunohistochemical classification of skeletal muscle fibres in mouse. *European Journal of Histochemistry*, *58*(2), 163–168. https://doi.org/10.4081/ejh.2014.2254

Kannel, W. B., Dannenberg, A. L., & Levy, D. (1987). Population implications of electrocardiographic left ventricular hypertrophy. *The American Journal of Cardiology*, *60*(17), 85–93. https://doi.org/10.1016/0002-9149(87)90466-8

Kirby, D. M., Salemi, R., Sugiana, C., Ohtake, A., Parry, L., Bell, K. M., Kirk, E. P., Boneh, A., Taylor, R. W., Dahl, H. H. M., Ryan, M. T., & Thorburn, D. R. (2004). NDUFS6 mutations are a novel cause of lethal neonatal mitochondrial complex I deficiency. *Journal of Clinical Investigation*, *114*(6), 837–845. https://doi.org/10.1172/JCI20683

Kirkwood, S. P., Munn, E. A., & Brooks, G. A. (1986). Mitochondrial reticulum in limb skeletal muscle. *American Journal of Physiology-Cell Physiology*, *251*(3), C395–C402. https://doi.org/10.1152/ajpcell.1986.251.3.C395

Kitajima, Y., Yoshioka, K., & Suzuki, N. (2020). The ubiquitin-proteasome system in regulation of the skeletal muscle homeostasis and atrophy: From basic science to disorders. In *Journal of Physiological Sciences* (Vol. 70, Issue 1). BioMed Central Ltd. https://doi.org/10.1186/s12576-020-00768-9

Kitamura, K., Erlangga, J. S., Tsukamoto, S., Sakamoto, Y., Mabashi-Asazuma, H., & Iida, K. (2020). Daidzein promotes the expression of oxidative phosphorylation- and fatty acid oxidation-related genes via an estrogen-related receptor α pathway to decrease lipid accumulation in muscle cells. *Journal of Nutritional Biochemistry*, *77*. https://doi.org/10.1016/j.jnutbio.2019.108315

Kleiger, G., Hao, B., Mohl, D. A., & Deshales, R. J. (2009). The acidic tail of the Cdc34 ubiquitin-conjugating enzyme functions in both binding to and catalysis with ubiquitin ligase SCFCdc4. *Journal of Biological Chemistry*, *284*(52), 36012–36023. https://doi.org/10.1074/jbc.M109.058529

Kleiger, G., & Mayor, T. (2014). Perilous journey: A tour of the ubiquitin-proteasome system. In *Trends in Cell Biology* (Vol. 24, Issue 6, pp. 352–359). Elsevier Ltd. https://doi.org/10.1016/j.tcb.2013.12.003

Kleinbongard, P., Schulz, R., & Heusch, G. (2011). TNFα in myocardial ischemia/reperfusion, remodeling and heart failure. *Heart Failure Reviews*, *16*(1), 49–69. https://doi.org/10.1007/s10741-010-9180-8

Koyama, S., Hata, S., Witt, C. C., Ono, Y., Lerche, S., Ojima, K., Chiba, T., Doi, N., Kitamura, F., Tanaka, K., Abe, K., Witt, S. H., Rybin, V., Gasch, A., Franz, T., Labeit, S., & Sorimachi, H. (2008). Muscle RING-Finger Protein-1 (MuRF1) as a Connector of Muscle Energy Metabolism and Protein Synthesis. *Journal of Molecular Biology*, *376*(5), 1224–1236. https://doi.org/10.1016/j.jmb.2007.11.049

Kwong, J. Q., & Molkentin, J. D. (2015). Physiological and Pathological Roles of the Mitochondrial Permeability Transition Pore in the Heart. In *Cell Metabolism* (Vol. 21, Issue 2, pp. 206–214). Cell Press. https://doi.org/10.1016/j.cmet.2014.12.001

Laakkonen, E. K., Soliymani, R., Karvinen, S., Kaprio, J., Kujala, U. M., Baumann, M., Sipilä, S., Kovanen, V., & Lalowski, M. (2017). Estrogenic regulation of skeletal muscle proteome: a study of premenopausal women and postmenopausal MZ cotwins discordant for hormonal therapy. *Aging Cell*, *16*(6), 1276–1287. https://doi.org/10.1111/acel.12661

Lafuse, W. P., Wozniak, D. J., & Rajaram, M. V. S. (2021). Role of cardiac macrophages on cardiac inflammation, fibrosis and tissue repair. In *Cells* (Vol. 10, Issue 1, pp. 1–27). MDPI. https://doi.org/10.3390/cells10010051

Laing, N. G., Ceuterick-de Groote, C., Dye, D. E., Liyanage, K., Duff, R. M., Dubois, B., Robberecht, W., Sciot, R., Martin, J.-J., & Goebel, H. H. (2005). Myosin storage myopathy: Slow skeletal myosin (MYH7) mutation in two isolated cases. *Neurology*, *64*(3), 527–529. https://doi.org/10.1212/01.WNL.0000150581.37514.30

Lange, S., Xiang, F., Yakovenko, A., Vihola, A., Hackman, P., Rostkova, E., Kristensen, J., Brandmeier, B., Franzen, G., Hedberg, B., Gunnarsson, L. G., Hughes, S. M., Marchand, S., Sejersen, T., Richard, I., Edström, L., Ehler, E., Udd, B., & Gautel, M. (2005). Cell biology: The kinase domain of titin controls muscle gene expression and protein turnover. *Science*, *308*(5728), 1599–1603. https://doi.org/10.1126/science.1110463

Lee, J. Y., Lori, D., Wells, D. J., & Kemp, P. R. (2015). FHL1 activates myostatin signalling in skeletal muscle and promotes atrophy. *FEBS Open Bio*, *5*, 753–762. https://doi.org/10.1016/j.fob.2015.08.011

Lee, K.-B., Wang, D., Lippard, S. J., & Sharp, P. A. (2002). Transcription-coupled and DNA damage-dependent ubiquitination of RNA polymerase II *in vitro*. *Proceedings of the National Academy of Sciences*, *99*(7), 4239–4244. https://doi.org/10.1073/pnas.072068399

Lekavich, C. L., Barksdale, D. J., Neelon, V., & Wu, J. R. (2015). Heart failure preserved ejection fraction (HFpEF): an integrated and strategic review. *Heart Failure Reviews*, *20*(6), 643–653. https://doi.org/10.1007/s10741-015-9506-7

Letts, J. A., Fiedorczuk, K., & Sazanov, L. A. (2016). The architecture of respiratory supercomplexes. *Nature*, *537*(7622), 644–648. https://doi.org/10.1038/nature19774

Li, W., Bengtson, M. H., Ulbrich, A., Matsuda, A., Reddy, V. A., Orth, A., Chanda, S. K., Batalov, S., & Joazeiro, C. A. P. (2008). Genome-Wide and Functional Annotation of Human E3 Ubiquitin Ligases Identifies MULAN, a Mitochondrial E3 that Regulates the Organelle's Dynamics and Signaling. *PLoS ONE*, *3*(1), e1487. https://doi.org/10.1371/journal.pone.0001487

Li, X., Song, Q. S., Wang, J. Y., Leng, H. J., Chen, Z. Q., Liu, Z. J., Dang, G. T., & Song, C. L. (2011). Simvastatin induces estrogen receptor-alpha expression in bone, restores bone loss, and decreases ERα expression and uterine wet weight in ovariectomized rats. *Journal of Bone and Mineral Metabolism*, *29*(4), 396–403. https://doi.org/10.1007/s00774-010-0231-y

Liao, R., Nascimben, L., Friedrich, J., Gwathmey, J. K., & Ingwall, J. S. (1996). Decreased Energy Reserve in an Animal Model of Dilated Cardiomyopathy. *Circulation Research*, *78*(5), 893–902. https://doi.org/10.1161/01.RES.78.5.893

Liew, C. W., Sun, H., Hunter, T., & Day, C. L. (2010). RING domain dimerization is essential for RNF4 function. *Biochemical Journal*, *431*(1), 23–29. https://doi.org/10.1042/BJ20100957

Linke, K., Mace, P. D., Smith, C. A., Vaux, D. L., Silke, J., & Day, C. L. (2008). Structure of the MDM2/MDMX RING domain heterodimer reveals dimerization is required for their ubiquitylation in trans. *Cell Death and Differentiation*, *15*(5), 841–848. https://doi.org/10.1038/sj.cdd.4402309

Liu, J., Tang, M., Mestril, R., & Wang, X. (2006). Aberrant protein aggregation is essential for a mutant desmin to impair the proteolytic function of the ubiquitin-proteasome system in cardiomyocytes. *Journal of Molecular and Cellular Cardiology*, *40*(4), 451–454. https://doi.org/10.1016/j.yjmcc.2005.12.011

Liu, X., Xiao, W., Jiang, Y., Zou, L., Chen, F., Xiao, W., Zhang, X., Cao, Y., Xu, L., & Zhu, Y. (2021). Bmal1 Regulates the Redox Rhythm of HSPB1, and Homooxidized HSPB1 Attenuates the Oxidative Stress Injury of Cardiomyocytes. *Oxidative Medicine and Cellular Longevity*, *2021*. https://doi.org/10.1155/2021/5542815

Lodka, D., Pahuja, A., Geers-Knörr, C., Scheibe, R. J., Nowak, M., Hamati, J., Köhncke, C., Purfürst, B., Kanashova, T., Schmidt, S., Glass, D. J., Morano, I., Heuser, A., Kraft, T., Bassel-Duby, R., Olson, E. N., Dittmar, G., Sommer, T., & Fielitz, J. (2016). Muscle RING-finger 2 and 3 maintain striated-muscle structure and function. *Journal of Cachexia, Sarcopenia and Muscle*, *7*(2), 165–180. https://doi.org/10.1002/jcsm.12057

Lopez, J., John, S. W., Tenev, T., Rautureau, G. J. P., Hinds, M. G., Francalanci, F., Wilson, R., Broemer, M., Santoro, M. M., Day, C. L., & Meier, P. (2011). CARD-Mediated Autoinhibition of cIAP1's E3 Ligase Activity Suppresses Cell Proliferation and Migration. *Molecular Cell*, *42*(5), 569–583. https://doi.org/10.1016/j.molcel.2011.04.008

Lorick, K. L., Jensen, J. P., Fang, S., Ong, A. M., Hatakeyama, S., & Weissman, A. M. (1999). RING fingers mediate ubiquitin-conjugating enzyme (E2)-dependent ubiquitination. In *National Institutes of Health* (Vol. 96). www.pnas.org.

Manczak, M., Calkins, M. J., & Reddy, P. H. (2011). Impaired mitochondrial dynamics and abnormal interaction of amyloid beta with mitochondrial protein Drp1 in neurons from patients with Alzheimer's disease: Implications for neuronal damage. *Human Molecular Genetics*, *20*(13), 2495–2509. https://doi.org/10.1093/hmg/ddr139

Manczak, M., Park, B. S., Jung, Y., & Reddy, P. H. (2004). Differential Expression of Oxidative Phosphorylation Genes in Patients With Alzheimer's Disease Implications for Early Mitochondrial Dysfunction and Oxidative Damage. *Manczak et al. NeuroMolecular Medicine*, *147*.

Mann, D. L. (2011). The emerging role of innate immunity in the heart and vascular system: For whom the cell tolls. *Circulation Research*, *108*(9), 1133–1145. https://doi.org/10.1161/CIRCRESAHA.110.226936

Marsiglia, J. D. C., Credidio, F. L., de Oliveira, T. G. M., Reis, R. F., Antunes, M. D. O., de Araujo, A. Q., Pedrosa, R. P., Barbosa-Ferreira, J. M. B., Mady, C., Krieger, J. E., Arteaga-Fernandez, E., & Pereira, A. D. C. (2013). Screening of MYH7, MYBPC3, and TNNT2 genes in Brazilian patients with hypertrophic cardiomyopathy. *American Heart Journal*, *166*(4), 775–782. https://doi.org/10.1016/j.ahj.2013.07.029

Martin, M. L., & Blaxall, B. C. (2012). Cardiac intercellular communication: Are myocytes and fibroblasts fair-weather friends? *Journal of Cardiovascular Translational Research*, *5*(6), 768–782. https://doi.org/10.1007/s12265-012-9404-5

McElhinny, A. S., Perry, C. N., Witt, C. C., Labeit, S., & Gregorio, C. C. (2004). Muscle-specific RING finger-2 (MURF-2) is important for microtubule, intermediate filament and sarcomeric M-line maintenance in striated muscle development. In *Journal of Cell Science* (Vol. 117, Issue 15, pp. 3175–3188). https://doi.org/10.1242/jcs.01158

Metzger, M. B., Pruneda, J. N., Klevit, R. E., & Weissman, A. M. (2014). RING-type E3 ligases: Master manipulators of E2 ubiquitin-conjugating enzymes and ubiquitination. In *Biochimica et Biophysica Acta - Molecular Cell Research* (Vol. 1843, Issue 1, pp. 47–60). https://doi.org/10.1016/j.bbamcr.2013.05.026

Miles, L., Miles, M. V., Horn, P. S., Degrauw, T. J., Wong, B. L., & Bove, K. E. (2012). Importance of muscle light microscopic mitochondrial subsarcolemmal aggregates in the diagnosis of respiratory chain deficiency. *Human Pathology*, *43*(8), 1249–1257. https://doi.org/10.1016/j.humpath.2011.09.016

Milone, M., & Wong, L. J. (2013). Diagnosis of mitochondrial myopathies. In *Molecular Genetics and Metabolism* (Vol. 110, Issues 1–2, pp. 35–41). https://doi.org/10.1016/j.ymgme.2013.07.007

Min, K. D., Asakura, M., Shirai, M., Yamazaki, S., Ito, S., Fu, H. Y., Asanuma, H., Asano, Y., Minamino, T., Takashima, S., & Kitakaze, M. (2021). ASB2 is a novel E3 ligase of SMAD9 required for cardiogenesis. *Scientific Reports*, *11*(1). https://doi.org/10.1038/s41598-021-02390-0

Mishra, P., Varuzhanyan, G., Pham, A. H., & Chan, D. C. (2015). Mitochondrial Dynamics Is a Distinguishing Feature of Skeletal Muscle Fiber Types and Regulates Organellar Compartmentalization. *Cell Metabolism*, *22*(6), 1033–1044. https://doi.org/10.1016/j.cmet.2015.09.027

Moraes, C. T., Ricci,$', E., Bonilla, E., Dimauro, S., Schon*'t', E. A., & Houston, H. (1992). The Mitochondrial tRNALeU(UUR) Mutation in Mitochondrial Encephalomyopathy, Lactic Acidosis, and Strokelike Episodes

(MELAS): Genetic, Biochemical, and Morphological Correlations in Skeletal Muscle. In *Am. J. Hum. Genet* (Vol. 50).

Moriscot, A. S., Baptista, I. L., Bogomolovas, J., Witt, C., Hirner, S., Granzier, H., & Labeit, S. (2010). MuRF1 is a muscle fiber-type II associated factor and together with MuRF2 regulates type-II fiber trophicity and maintenance. *Journal of Structural Biology*, *170*(2), 344–353. https://doi.org/10.1016/j.jsb.2010.02.001

Mrosek, M., Labeit, D., Witt, S., Heerklotz, H., Castelmur, E., Labeit, S., & Mayans, O. (2007). Molecular determinants for the recruitment of the ubiquitin-ligase MuRF-1 onto M-line titin. *The FASEB Journal*, *21*(7), 1383–1392. https://doi.org/10.1096/fj.06-7644com

Murphy, E., & Steenbergen, C. (2008). Mechanisms Underlying Acute Protection From Cardiac Ischemia-Reperfusion Injury. *Physiological Reviews*, *88*(2), 581–609. https://doi.org/10.1152/physrev.00024.2007

Nilsson, M. I., Nissar, A. A., Al-Sajee, D., Tarnopolsky, M. A., Parise, G., Lach, B., Fürst, D. O., van der Ven, P. F. M., Kley, R. A., & Hawke, T. J. (2013). Xin is a marker of skeletal muscle damage severity in myopathies. *American Journal of Pathology*, *183*(6), 1703–1709. https://doi.org/10.1016/j.ajpath.2013.08.010

Nilwik, R., Snijders, T., Leenders, M., Groen, B. B. L., van Kranenburg, J., Verdijk, L. B., & van Loon, L. J. C. (2013). The decline in skeletal muscle mass with aging is mainly attributed to a reduction in type II muscle fiber size. *Experimental Gerontology*, *48*(5), 492–498. https://doi.org/10.1016/j.exger.2013.02.012

Noguchi, S., Tsukahara, T., Fujita, M., Kurokawa, R., Tachikawa, M., Toda, T., Tsujimoto, A., Arahata, K., & Nishino, I. (2003). cDNA microarray analysis of individual Duchenne muscular dystrophy patients. *Human Molecular Genetics*, *12*(6), 595–600. https://doi.org/10.1093/hmg/ddg065

Nowak, M., Suenkel, B., Porras, P., Migotti, R., Schmidt, F., Kny, M., Zhu, X., Wanker, E. E., Dittmar, G., Fielitz, J., & Sommer, T. (2019). DCAF8, a novel MuRF1 interaction partner, promotes muscle atrophy. *Journal of Cell Science*. https://doi.org/10.1242/jcs.233395

Ogata, T., & Yamasaki, Y. (1997). Ultra-high-resolution scanning electron microscopy of mitochondria and sarcoplasmic reticulum arrangement in human red, white, and intermediate muscle fibers. *Anatomical Record*, *248*(2), 214–223. https://doi.org/10.1002/(SICI)1097-0185(199706)248:2<214::AID-AR8>3.0.CO;2-S

Olivé, M., Abdul-Hussein, S., Oldfors, A., González-Costello, J., van der Ven, P. F. M., Fürst, D. O., González, L., Moreno, D., Torrejón-Escribano, B., Alió, J., Pou, A., Ferrer, I., & Tajsharghi, H. (2015). New cardiac and skeletal protein aggregate myopathy associated with combined MuRF1 and MuRF3 mutations. *Human Molecular Genetics*, *24*(13), 3638–3650. https://doi.org/10.1093/hmg/ddv108

Olsen, S. K., & Lima, C. D. (2013). Structure of a Ubiquitin E1-E2 Complex: Insights to E1-E2 Thioester Transfer. *Molecular Cell*, *49*(5), 884–896. https://doi.org/10.1016/j.molcel.2013.01.013

Opitz, C. A., & Linke, W. A. (2005). Plasticity of cardiac titin/connectin in heart development. *Journal of Muscle Research and Cell Motility*, *26*(6–8), 333–342. https://doi.org/10.1007/s10974-005-9040-7

Pandit, A., Vadnal, J., Houston, S., Freeman, E., & McDonough, J. (2009). Impaired regulation of electron transport chain subunit genes by nuclear respiratory factor 2 in multiple sclerosis. *Journal of the Neurological Sciences*, *279*(1–2), 14–20. https://doi.org/10.1016/j.jns.2009.01.009

Papanicolaou, K. N., Khairallah, R. J., Ngoh, G. A., Chikando, A., Luptak, I., O'Shea, K. M., Riley, D. D., Lugus, J. J., Colucci, W. S., Lederer, W. J., Stanley, W. C., & Walsh, K. (2011). Mitofusin-2 Maintains Mitochondrial Structure and Contributes to Stress-Induced Permeability Transition in Cardiac Myocytes. *Molecular and Cellular Biology*, *31*(6), 1309–1328. https://doi.org/10.1128/mcb.00911-10

Park, J. B., Zhang, H., Lin, C. Y., Chung, C. P., Byun, Y., Park, Y. S., & Yang, V. C. (2012). Simvastatin maintains osteoblastic viability while promoting differentiation by partially regulating the expressions of estrogen receptors α. *Journal of Surgical Research*, *174*(2), 278–283. https://doi.org/10.1016/j.jss.2010.12.029

Park, Y. M., Keller, A. C., Runchey, S. S., Miller, B. F., Kohrt, W. M., Van Pelt, R. E., Kang, C., Jankowski, C. M., & Moreau, K. L. (2019). Acute estradiol treatment reduces skeletal muscle protein breakdown markers in early- but not late-postmenopausal women. *Steroids*, *146*, 43–49. https://doi.org/10.1016/j.steroids.2019.03.008

Peng, J., Schwartz, D., Elias, J. E., Thoreen, C. C., Cheng, D., Marsischky, G., Roelofs, J., Finley, D., & Gygi, S. P. (2003). A proteomics approach to understanding protein ubiquitination. In *NATURE BIOTECHNOLOGY VOLUME* (Vol. 21). http://www.nature.com/naturebiotechnology

Perera, S., Mankoo, B., & Gautel, M. (2012). Developmental regulation of MURF E3 ubiquitin ligases in skeletal muscle. *Journal of Muscle Research and Cell Motility*, *33*(2), 107–122. https://doi.org/10.1007/s10974-012-9288-7

Pérez-Schindler, J., Summermatter, S., Salatino, S., Zorzato, F., Beer, M., Balwierz, P. J., van Nimwegen, E., Feige, J. N., Auwerx, J., & Handschin, C. (2012). The Corepressor NCoR1 Antagonizes PGC-1α and Estrogen-Related Receptor α in the Regulation of Skeletal Muscle Function and Oxidative Metabolism. *Molecular and Cellular Biology*, *32*(24), 4913–4924. https://doi.org/10.1128/mcb.00877-12

Petruzzella, V., Vergari, R., Puzziferri, I., Boffoli, D., Lamantea, E., Zeviani, M., & Papa, S. (2001). A nonsense mutation in the NDUFS4 gene encoding the 18 kDa (AQDQ) subunit of complex I abolishes assembly and activity of the complex in a patient with Leigh-like syndrome. In *Human Molecular Genetics* (Vol. 10, Issue 5).

Pham, A. D., & Sauer, F. (2000). Ubiquitin-activating/conjugating activity of TAF(II)250, a mediator of activation of gene expression in Drosophila. *Science*, *289*(5488), 2357–2360. https://doi.org/10.1126/science.289.5488.2357

Picard, M., Hepple, R. T., & Burelle, Y. (2012). Mitochondrial functional specialization in glycolytic and oxidative muscle fibers: tailoring the organelle for optimal function. *Am J Physiol Cell Physiol*, *302*, 629–641. https://doi.org/10.1152/ajpcell.00368.2011.-In

Picard, M., White, K., & Turnbull, D. M. (2013). Mitochondrial morphology, topology, and membrane interactions in skeletal muscle: A quantitative three-dimensional electron microscopy study. *Journal of Applied Physiology*, *114*(2), 161–171. https://doi.org/10.1152/japplphysiol.01096.2012

Picard, M., Zhang, J., Hancock, S., Derbeneva, O., Golhar, R., Golik, P., O'Hearn, S., Levy, S., Potluri, P., Lvova, M., Davila, A., Lin, C. S., Perin, J. C., Rappaport, E. F., Hakonarson, H., Trounce, I. A., Procaccio, V., & Wallace, D. C. (2014). Progressive increase in mtDNA 3243A>G heteroplasmy causes abrupt transcriptional reprogramming. *Proceedings of the National Academy of Sciences of the United States of America*, *111*(38), E4033–E4042. https://doi.org/10.1073/pnas.1414028111

Pierce, N. W., Kleiger, G., Shan, S. O., & Deshaies, R. J. (2009). Detection of sequential polyubiquitylation on a millisecond timescale. *Nature*, *462*(7273), 615–619. https://doi.org/10.1038/nature08595

Pizon, V., Iakovenko, A., van der Ven, P. F. M., Kelly, R., Fatu, C., Fürst, D. O., Karsenti, E., & Gautel, M. (2002). Transient association of titin and myosin with microtubules in nascent myofibrils directed by the MURF2 RING-finger protein. In *Journal of Cell Science* (Vol. 115, Issue 23, pp. 4469–4482). https://doi.org/10.1242/jcs.00131

Plechanovov, A., Jaffray, E. G., Tatham, M. H., Naismith, J. H., & Hay, R. T. (2012). Structure of a RING E3 ligase and ubiquitin-loaded E2 primed for catalysis. *Nature*, *489*(7414), 115–120. https://doi.org/10.1038/nature11376

Polge, C., Cabantous, S., Deval, C., Claustre, A., Hauvette, A., Bouchenot, C., Aniort, J., Béchet, D., Combaret, L., Attaix, D., & Taillandier, D. (2018). A muscle-specific MuRF1-E2 network requires stabilization of MuRF1-E2 complexes by telethonin, a newly identified substrate. *Journal of Cachexia, Sarcopenia and Muscle*, *9*(1), 129–145. https://doi.org/10.1002/jcsm.12249

Porrello, E. R., Mahmoud, A. I., Simpson, E., Hill, J. A., Richardson, J. A., Olson, E. N., & Sadek, H. A. (2011). Transient regenerative potential of the neonatal mouse heart. *Science*, *331*(6020), 1078–1080. https://doi.org/10.1126/science.1200708

Reddy, B. A., Etkin, L. D., & Freemont, P. S. (1992). A novel zinc finger coiled-coil domain in a family of nuclear proteins. *Trends in Biochemical Sciences*, *17*(9), 344–345. https://doi.org/10.1016/0968-0004(92)90308-V

Reichmann, H., Vogler, L., & Seibel, P. (1996). Ragged Red or Ragged Blue Fibers. *European Neurology*, *36*(2), 98–102. https://doi.org/10.1159/000117217

Ribas, V., Drew, B. G., Zhou, Z., Phun, J., Kalajian, N. Y., Soleymani, T., Daraei, P., Widjaja, K., Wanagat, J., Vallim, T. Q. D. A., Fluitt, A. H., Bensinger, S., Le, T., Radu, C., Whitelegge, J. P., Beaven, S. W., Tontonoz, P., Lusis, A. J., Parks, B. W., … Hevener, A. L. (2016). Skeletal muscle action of estrogen receptor a is critical for the maintenance of mitochondrial function and metabolic homeostasis in females. *Science Translational Medicine*, *8*(334). https://doi.org/10.1126/scitranslmed.aad3815

Rodríguez, J. E., Liao, J. Y., He, J., Schisler, J. C., Newgard, C. B., Drujan, D., Glass, D. J., Frederick, C. B., Yoder, B. C., Lalush, D. S., Patterson, C., & Willis, M. S. (2015). The ubiquitin ligase MuRF1 regulates PPARα activity in the heart by enhancing nuclear export via monoubiquitination. *Molecular and Cellular Endocrinology*, *413*, 36–48. https://doi.org/10.1016/j.mce.2015.06.008

Romanello, V., Guadagnin, E., Gomes, L., Roder, I., Sandri, C., Petersen, Y., Milan, G., Masiero, E., Del Piccolo, P., Foretz, M., Scorrano, L., Rudolf, R., & Sandri, M. (2010). Mitochondrial fission and remodelling

contributes to muscle atrophy. *EMBO Journal*, *29*(10), 1774–1785.
https://doi.org/10.1038/emboj.2010.60

Rosenkranz, A. C., Hood, S. G., Woods, R. L., Dusting, G. J., & Ritchie, R. H. (2003). B-Type Natriuretic Peptide
Prevents Acute Hypertrophic Responses in the Diabetic Rat Heart Importance of Cyclic GMP. In
Diabetes (Vol. 52). http://diabetesjournals.org/diabetes/article-
pdf/52/9/2389/650087/db0903002389.pdf

Ross, J. M. (2011). Visualization of mitochondrial respiratory function using cytochrome C oxidase/succinate
dehydrogenase (COX/SDH) double-labeling histochemistry. *Journal of Visualized Experiments*, *57*.
https://doi.org/10.3791/3266

Rubinstein, J. L., Walker, J. E., & Henderson, R. (2003). Structure of the mitochondrial ATP synthase by
electron cryomicroscopy. *EMBO Journal*, *22*(23), 6182–6192. https://doi.org/10.1093/emboj/cdg608

Russell, A. P., Foletta, V. C., Snow, R. J., & Wadley, G. D. (2014). Skeletal muscle mitochondria: A major player
in exercise, health and disease. In *Biochimica et Biophysica Acta - General Subjects* (Vol. 1840, Issue 4,
pp. 1276–1284). Elsevier. https://doi.org/10.1016/j.bbagen.2013.11.016

Sabnis, G. J., Goloubeva, O., Chumsri, S., Nguyen, N., Sukumar, S., & Brodie, A. M. H. (2011). Functional
activation of the estrogen receptor-α and aromatase by the HDAC inhibitor entinostat sensitizes ER-
negative tumors to letrozole. *Cancer Research*, *71*(5), 1893–1903. https://doi.org/10.1158/0008-
5472.CAN-10-2458

Sahebkar, A., Cicero, A. F. G., Di Giosia, P., Pomilio, I., Stamerra, C. A., Giorgini, P., Ferri, C., von Haehling, S.,
Banach, M., & Jamialahmadi, T. (2020). Pathophysiological mechanisms of statin-associated
myopathies: possible role of the ubiquitin-proteasome system. In *Journal of Cachexia, Sarcopenia and
Muscle* (Vol. 11, Issue 5, pp. 1177–1186). Wiley Blackwell. https://doi.org/10.1002/jcsm.12579

Saks, V., Dzeja, P., Schlattner, U., Vendelin, M., Terzic, A., & Wallimann, T. (2006). Cardiac system
bioenergetics: Metabolic basis of the frank-starling law. In *Journal of Physiology* (Vol. 571, Issue 2, pp.
253–273). https://doi.org/10.1113/jphysiol.2005.101444

Salmeen, A., Andersen, J. N., Myers, M. P., Meng, T.-C., Hinks, J. A., Tonks, N. K., & Barford, D. (2003). Redox
regulation of protein tyrosine phosphatase 1B involves a sulphenyl-amide intermediate. *Nature*,
423(6941), 769–773. https://doi.org/10.1038/nature01680

Sandri, M., Lin, J., Handschin, C., Yang, W., Arany, Z. P., Lecker, S. H., Goldberg, A. L., & Spiegelman, B. M.
(2006). PGC-1α protects skeletal muscle from atrophy by suppressing FoxO3 action and atrophy-
specific gene transcription. *Proceedings of the National Academy of Sciences*, *103*(44), 16260–16265.
https://doi.org/10.1073/pnas.0607795103

Sandri, M., Sandri, C., Gilbert, A., Skurk, C., Calabria, E., Picard, A., Walsh, K., Schiaffino, S., Lecker, S. H., &
Goldberg, A. L. (2004). Foxo Transcription Factors Induce the Atrophy-Related Ubiquitin Ligase Atrogin-
1 and Cause Skeletal Muscle Atrophy IGF-1 or insulin (Sacheck et al. In *Cell* (Vol. 117).

Santel, A., & Fuller, M. T. (2001). Control of mitochondrial morphology by a human mitofusin. *Journal of Cell
Science*, *114*(5), 867–874. https://doi.org/10.1242/jcs.114.5.867

Schägger, H., & Pfeiffer, K. (2000). Supercomplexes in the respiratory chains of yeast and mammalian mitochondria. *EMBO Journal*, *19*(8), 1777–1783. https://doi.org/10.1093/emboj/19.8.1777

Schiaffino, S., & Reggiani, C. (2011). Fiber Types In Mammalian Skeletal Muscles. *Physiol Rev*, *91*, 1447–1531. https://doi.org/10.1152/physrev.00031.2010.-Mammalian

Schirris, T. J. J., Renkema, G. H., Ritschel, T., Voermans, N. C., Bilos, A., Van Engelen, B. G. M., Brandt, U., Koopman, W. J. H., Beyrath, J. D., Rodenburg, R. J., Willems, P. H. G. M., Smeitink, J. A. M., & Russel, F. G. M. (2015). Statin-induced myopathy is associated with mitochondrial complex III inhibition. *Cell Metabolism*, *22*(3), 399–407. https://doi.org/10.1016/j.cmet.2015.08.002

Sciacco, M., Bonilla, E., Schon, E. A., Dimauro, S., Moraes, C. T., & Houston, H. (1994). Distribution of wild-type and common deletion forms of mtDNA in normal and respiration-deficient muscle fibers from patients with mitochondrial myopathy. In *Human Molecular Genetics* (Vol. 3, Issue 1). http://hmg.oxfordjournals.org/

Sciacco, M., Prelle, A., Comi, G. P., Napoli, L., Battistel, A., Bresolin, N., Tancredi, L., Lamperti, C., Bordoni, A., Fagiolari, G., Ciscato, P., Chiveri, L., Perini, M. P., Fortunato, F., Adobbati, L., Messina, S., Toscano, A., Martinelli-Boneschi, F., Papadimitriou, A., … Ferrari, D. (2001). Retrospective study of a large population of patients affected with mitochondrial disorders: clinical, morphological and molecular genetic evaluation. In *J Neurol* (Vol. 248).

Segura, A. M., Frazier, O. H., & Buja, L. M. (2014). Fibrosis and heart failure. *Heart Failure Reviews*, *19*(2), 173–185. https://doi.org/10.1007/s10741-012-9365-4

She, H., Yang, Q., Shepherd, K., Smith, Y., Miller, G., Testa, C., & Mao, Z. (2011). Direct regulation of complex I by mitochondrial MEF2D is disrupted in a mouse model of Parkinson disease and in human patients. *Journal of Clinical Investigation*, *121*(3), 930–940. https://doi.org/10.1172/JCI43871

Shoffner, J. M., Lorrt, M. T., Voljavect, A. S., Soueidan, S. A., Costigan, D. A., & Wallace, D. C. (1989). Spontaneous Kearns-Sayre/chronic external ophthalmoplegia plus syndrome associated with a mitochondrial DNA deletion: A slip-replication model and metabolic therapy (oxidative phosphorylation/polymerase chain reaction/coenzyme Q10/succinate). In *Proc. Nati. Acad. Sci. USA* (Vol. 86). https://www.pnas.org

Short, K. M., & Cox, T. C. (2006). Subclassification of the RBCC/TRIM superfamily reveals a novel motif necessary for microtubule binding. *Journal of Biological Chemistry*, *281*(13), 8970–8980. https://doi.org/10.1074/jbc.M512755200

Skilving, I., Eriksson, M., Rane, A., & Ovesjö, M. L. (2016). Statin-induced myopathy in a usual care setting—a prospective observational study of gender differences. *European Journal of Clinical Pharmacology*, *72*(10), 1171–1176. https://doi.org/10.1007/s00228-016-2105-2

Small, E. M., Thatcher, J. E., Sutherland, L. B., Kinoshita, H., Gerard, R. D., Richardson, J. A., Dimaio, J. M., Sadek, H., Kuwahara, K., & Olson, E. N. (2010). Myocardin-related transcription factor-a controls myofibroblast activation and fibrosis in response to myocardial infarction. *Circulation Research*, *107*(2), 294–304. https://doi.org/10.1161/CIRCRESAHA.110.223172

Smirnova, E., Shurland, D.-L., Ryazantsev, S. N., & van der Bliek, A. M. (1998). A Human Dynamin-related Protein Controls the Distribution of Mitochondria. In *The Journal of Cell Biology* (Vol. 143, Issue 2). http://www.jcb.org

Smith, A. C., & Robinson, A. J. (2016). MitoMiner v3.1, an update on the mitochondrial proteomics database. *Nucleic Acids Research*, *44*(D1), D1258–D1261. https://doi.org/10.1093/nar/gkv1001

Smith, E. F., Shaw, P. J., & de Vos, K. J. (2019). The role of mitochondria in amyotrophic lateral sclerosis. In *Neuroscience Letters* (Vol. 710). Elsevier Ireland Ltd. https://doi.org/10.1016/j.neulet.2017.06.052

Smolina, N., Khudiakov, A., Knyazeva, A., Zlotina, A., Sukhareva, K., Kondratov, K., Gogvadze, V., Zhivotovsky, B., Sejersen, T., & Kostareva, A. (2020). Desmin mutations result in mitochondrial dysfunction regardless of their aggregation properties. *Biochimica et Biophysica Acta - Molecular Basis of Disease*, *1866*(6). https://doi.org/10.1016/j.bbadis.2020.165745

Song, Z., Ghochani, M., Mccaffery, J. M., Frey, T. G., Chan, D. C., & Shaw, J. M. (2009). Mitofusins and OPA1 Mediate Sequential Steps in Mitochondrial Membrane Fusion. *Molecular Biology of the Cell*, *20*, 3525–3532. https://doi.org/10.1091/mbc.E09

Soonpaa, M. H., & Field, L. J. (1998). Survey of Studies Examining Mammalian Cardiomyocyte DNA Synthesis. *Circulation Research*, *83*(1), 15–26. https://doi.org/10.1161/01.RES.83.1.15

Spencer, J. A., Eliazer, S., Ilaria, R. L., Richardson, J. A., & Olson, E. N. (2000). Regulation of Microtubule Dynamics and Myogenic Differentiation by MURF, a Striated Muscle RING-Finger Protein. In *The Journal of Cell Biology* (Vol. 150, Issue 4). http://www.jcb.org

Spinazzi, M., Casarin, A., Pertegato, V., Salviati, L., & Angelini, C. (2012). Assessment of mitochondrial respiratory chain enzymatic activities on tissues and cultured cells. *Nature Protocols*, *7*(6), 1235–1246. https://doi.org/10.1038/nprot.2012.058

Staron, R. S., & Hikida, R. S. (1992). Histochemical, biochemical, and ultrastructural analyses of single human muscle fibers, with special reference to the C-fiber population. *Journal of Histochemistry & Cytochemistry*, *40*(4), 563–568. https://doi.org/10.1177/40.4.1552189

Staron, R. S., & Pette, D. (1986). Histochemistry Correlation between myofibrillar ATPase activity and myosin heavy chain composition in rabbit muscle fibers. In *Histochemistry* (Vol. 86).

Staron, R. S., & Pette, D. (1993). The continuum of pure and hybrid myosin heavy chain-based fibre types in rat skeletal muscle. In *Histochemistry* (Vol. 100).

Strauss, K. A., Williams, K. B., Carson, V. J., Poskitt, L., Bowser, L. E., Young, M., Robinson, D. L., Hendrickson, C., Beiler, K., Taylor, C. M., Haas-Givler, B., Hailey, J., Chopko, S., Puffenberger, E. G., Brigatti, K. W., Miller, F., & Morton, D. H. (2020). Glutaric acidemia type 1: Treatment and outcome of 168 patients over three decades. *Molecular Genetics and Metabolism*, *131*(3), 325–340. https://doi.org/10.1016/j.ymgme.2020.09.007

Stringer, H. A. J., Sohi, G. K., Maguire, J. A., & Côté, H. C. F. (2013). Decreased skeletal muscle mitochondrial DNA in patients with statin-induced myopathy. *Journal of the Neurological Sciences*, *325*(1–2), 142–147. https://doi.org/10.1016/j.jns.2012.12.023

Suomi, T., & Elo, L. L. (2017). Enhanced differential expression statistics for data-independent acquisition proteomics. *Scientific Reports*, *7*(1). https://doi.org/10.1038/s41598-017-05949-y

Taegtmeyer, H. (2002). Switching metabolic genes to build a better heart. In *Circulation* (Vol. 106, Issue 16, pp. 2043–2045). https://doi.org/10.1161/01.CIR.0000036760.42319.3F

Tajsharghi, H., Thornell, L.-E., Lindberg, C., Lindvall, B., Henriksson, K.-G., & Oldfors, A. (2003). Myosin storage myopathy associated with a heterozygous missense mutation in MYH7. *Annals of Neurology*, *54*(4), 494–500. https://doi.org/10.1002/ana.10693

Terra, L. F., Wailemann, R. A. M., dos Santos, A. F., Gomes, V. M., Silva, R. P., Laporte, A., Meotti, F. C., Terra, W. R., Palmisano, G., Lortz, S., & Labriola, L. (2019). Heat shock protein B1 is a key mediator of prolactin-induced beta-cell cytoprotection against oxidative stress. *Free Radical Biology and Medicine*, *134*, 394–405. https://doi.org/10.1016/j.freeradbiomed.2019.01.023

Tokunaga, F., Sakata, S. I., Saeki, Y., Satomi, Y., Kirisako, T., Kamei, K., Nakagawa, T., Kato, M., Murata, S., Yamaoka, S., Yamamoto, M., Akira, S., Takao, T., Tanaka, K., & Iwai, K. (2009). Involvement of linear polyubiquitylation of NEMO in NF-κB activation. *Nature Cell Biology*, *11*(2), 123–132. https://doi.org/10.1038/ncb1821

Torres, M. J., Kew, K. A., Ryan, T. E., Pennington, E. R., Lin, C. te, Buddo, K. A., Fix, A. M., Smith, C. A., Gilliam, L. A., Karvinen, S., Lowe, D. A., Spangenburg, E. E., Zeczycki, T. N., Shaikh, S. R., & Neufer, P. D. (2018). 17β-Estradiol Directly Lowers Mitochondrial Membrane Microviscosity and Improves Bioenergetic Function in Skeletal Muscle. *Cell Metabolism*, *27*(1), 167-179.e7. https://doi.org/10.1016/j.cmet.2017.10.003

Turco, E., Savova, A., Gere, F., Ferrari, L., Romanov, J., Schuschnig, M., & Martens, S. (2021). Reconstitution defines the roles of p62, NBR1 and TAX1BP1 in ubiquitin condensate formation and autophagy initiation. *Nature Communications*, *12*(1). https://doi.org/10.1038/s41467-021-25572-w

Ulfig, N. (2005a). *Kurzlehrbuch Histologie* (N. Ulfig, Ed.; 2nd ed., pp. 53–60). Georg Thieme Verlag. 3.5. Das Muskelgewebe: 53-60 https://doi.org/10.1055/b-003-120843

Ulfig, N. (2005b). *Kurzlehrbuch Histologie* (N. Ulfig, Ed.; 2nd ed., p. 81). Georg Thieme Verlag. Das Herz: 81 https://doi.org/10.1055/b-003-120843

Van Rooij, E., Fielitz, J., Sutherland, L. B., Thijssen, V. L., Crijns, H. J., Dimaio, M. J., Shelton, J., De Windt, L. J., Hill, J. A., & Olson, E. N. (2010). Myocyte enhancer factor 2 and class ii histone deacetylases control a gender-specific pathway of cardioprotection mediated by the estrogen receptor. *Circulation Research*, *106*(1), 155–165. https://doi.org/10.1161/CIRCRESAHA.109.207084

Vanderheyden, M., Paulus, W. J., Voss, M., Knuefermann, P., Sivasubramanian, N., Mann, D., & Baumgarten, G. (2005). Myocardial cytokine gene expression is higher in aortic stenosis than in idiopathic dilated cardiomyopathy. *Heart*, *91*(7), 926–931. https://doi.org/10.1136/hrt.2004.035733

Vega, R. B., Huss, J. M., & Kelly, D. P. (2000). The Coactivator PGC-1 Cooperates with Peroxisome Proliferator-Activated Receptor in Transcriptional Control of Nuclear Genes Encoding Mitochondrial Fatty Acid Oxidation Enzymes. In *MOLECULAR AND CELLULAR BIOLOGY* (Vol. 20, Issue 5). https://journals.asm.org/journal/mcb

Verma, R., Aravind, L., Oania, R., McDonald, W. H., Yates, J. R., Koonin, E. v., & Deshaies, R. J. (2002). Role of Rpn11 metalloprotease in deubiquitination and degradation by the 26S proteasome. *Science*, *298*(5593), 611–615. https://doi.org/10.1126/science.1075898

Vicart, P., Caron, A., Guicheney, P., Li, Z., Prévost, M.-C., Faure, A., Chateau, D., Chapon, F., Tomé, F., Dupret, J.-M., Paulin, D., & Fardeau, M. (1998). A missense mutation in the αB-crystallin chaperone gene causes a desmin-related myopathy. *Nature Genetics*, *20*(1), 92–95. https://doi.org/10.1038/1765

Vincent, A. E., Grady, J. P., Rocha, M. C., Alston, C. L., Rygiel, K. A., Barresi, R., Taylor, R. W., & Turnbull, D. M. (2016). Mitochondrial dysfunction in myofibrillar myopathy. *Neuromuscular Disorders*, *26*(10), 691–701. https://doi.org/10.1016/j.nmd.2016.08.004

Vincent, A. E., Ng, Y. S., White, K., Davey, T., Mannella, C., Falkous, G., Feeney, C., Schaefer, A. M., McFarland, R., Gorman, G. S., Taylor, R. W., Turnbull, D. M., & Picard, M. (2016). The Spectrum of Mitochondrial Ultrastructural Defects in Mitochondrial Myopathy. *Scientific Reports*, *6*. https://doi.org/10.1038/srep30610

Wang, J. hua, Wang, Q. jing, Wang, C., Reinholt, B., Grant, A. L., Gerrard, D. E., & Kuang, S. (2015). Heterogeneous activation of a slow myosin gene in proliferating myoblasts and differentiated single myofibers. *Developmental Biology*, *402*(1), 72–80. https://doi.org/10.1016/j.ydbio.2015.02.025

Wehner, R., & Gehring, W. (2007a). *Zoologie* (R. Wehner & W. Gehring, Eds.; 24th ed.). Georg Thieme Verlag. 8.1. Muskelbewegung: 471-476 https://doi.org/10.1055/b-002-99143

Wehner, R., & Gehring, W. (2007b). *Zoologie* (R. Wehner & W. Gehring, Eds.; 24th ed.). Georg Thieme Verlag. 1.8. Mitochondrien: 30-32 https://doi.org/10.1055/b-002-99143

Wehner, R., & Gehring, W. (2007c). *Zoologie* (R. Wehner & W. Gehring, Eds.; 24th ed.). Georg Thieme Verlag. 4.1.2. Energieübertragung in der Zelle: 307-312 https://doi.org/10.1055/b-002-99143

Westerblad, H., Bruton, J. D., & Katz, A. (2010). Skeletal muscle: Energy metabolism, fiber types, fatigue and adaptability. In *Experimental Cell Research* (Vol. 316, Issue 18, pp. 3093–3099). Academic Press Inc. https://doi.org/10.1016/j.yexcr.2010.05.019

White, J. P., Gao, S., Puppa, M. J., Sato, S., Welle, S. L., & Carson, J. A. (2013). Testosterone regulation of Akt/mTORC1/FoxO3a signaling in skeletal muscle. *Molecular and Cellular Endocrinology*, *365*(2), 174–186. https://doi.org/10.1016/j.mce.2012.10.019

Wijk, S. J. L., & Timmers, H. T. M. (2010). The family of ubiquitin-conjugating enzymes (E2s): deciding between life and death of proteins. *The FASEB Journal*, *24*(4), 981–993. https://doi.org/10.1096/fj.09-136259

Willis, M. S., Wadosky, K. M., Rodríguez, J. E., Schisler, J. C., Lockyer, P., Hilliard, E. G., Glass, D. J., & Patterson, C. (2014). Muscle ring finger 1 and muscle ring finger 2 are necessary but functionally redundant during developmental cardiac growth and regulate E2F1-mediated gene expression in vivo. *Cell Biochemistry and Function*, *32*(1), 39–50. https://doi.org/10.1002/cbf.2969

Winter, L., Kuznetsov, A. V., Grimm, M., Zeöld, A., Fischer, I., & Wiche, G. (2015). Plectin isoform P1b and P1d deficiencies differentially affect mitochondrial morphology and function in skeletal muscle. *Human Molecular Genetics*, *24*(16), 4530–4544. https://doi.org/10.1093/hmg/ddv184

Witt, C. C., Witt, S. H., Lerche, S., Labeit, D., Back, W., & Labeit, S. (2008). Cooperative control of striated muscle mass and metabolism by MuRF1 and MuRF2. *EMBO Journal*, *27*(2), 350–360. https://doi.org/10.1038/sj.emboj.7601952

Witt, S. H., Granzier, H., Witt, C. C., & Labeit, S. (2005). MURF-1 and MURF-2 target a specific subset of myofibrillar proteins redundantly: Towards understanding MURF-dependent muscle ubiquitination. *Journal of Molecular Biology*, *350*(4), 713–722. https://doi.org/10.1016/j.jmb.2005.05.021

Wollersheim, T., Woehlecke, J., Krebs, M., Hamati, J., Lodka, D., Luther-Schroeder, A., Langhans, C., Haas, K., Radtke, T., Kleber, C., Spies, C., Labeit, S., Schuelke, M., Spuler, S., Spranger, J., Weber-Carstens, S., & Fielitz, J. (2014). Dynamics of myosin degradation in intensive care unit-acquired weakness during severe critical illness. *Intensive Care Medicine*, *40*(4), 528–539. https://doi.org/10.1007/s00134-014-3224-9

Wu, M., Gu, J., Guo, R., Huang, Y., & Yang, M. (2016). Structure of Mammalian Respiratory Supercomplex I1III2IV1. *Cell*, *167*(6), 1598-1609.e10. https://doi.org/10.1016/j.cell.2016.11.012

Wu, Z., Puigserver, P., Andersson, U., Zhang, C., Adelmant, G., Mootha, V., Troy, A., Cinti, S., Lowell, B., Scarpulla, R. C., & Spiegelman, B. M. (1999). Mechanisms Controlling Mitochondrial Biogenesis and Respiration through the Thermogenic Coactivator PGC-1. *Cell*, *98*(1), 115–124. https://doi.org/10.1016/S0092-8674(00)80611-X

Xu, P., Duong, D. M., Seyfried, N. T., Cheng, D., Xie, Y., Robert, J., Rush, J., Hochstrasser, M., Finley, D., & Peng, J. (2009). Quantitative Proteomics Reveals the Function of Unconventional Ubiquitin Chains in Proteasomal Degradation. *Cell*, *137*(1), 133–145. https://doi.org/10.1016/j.cell.2009.01.041

Yang, J., He, J., Ismail, M., Tweeten, S., Zeng, F., Gao, L., Ballinger, S., Young, M., Prabhu, S. D., Rowe, G. C., Zhang, J., Zhou, L., & Xie, M. (2019). HDAC inhibition induces autophagy and mitochondrial biogenesis to maintain mitochondrial homeostasis during cardiac ischemia/reperfusion injury. *Journal of Molecular and Cellular Cardiology*, *130*, 36–48. https://doi.org/10.1016/j.yjmcc.2019.03.008

Yao, T., & Cohen, R. E. (2002). A cryptic protease couples deubiquitination and degradation by the proteasome. *Nature*, *419*(6905), 403–407. https://doi.org/10.1038/nature01071

Zhao, J., Jung, Y. H., Jang, C. G., Chun, K. H., Kwon, S. W., & Lee, J. (2015). Metabolomic identification of biochemical changes induced by fluoxetine and imipramine in a chronic mild stress mouse model of depression. *Scientific Reports*, *5*. https://doi.org/10.1038/srep08890

Zhong, Y., Ahmed, S., Grupp, I. L., & Matlib, M. A. (2001). Altered SR protein expression associated with contractile dysfunction in diabetic rat hearts. *American Journal of Physiology-Heart and Circulatory Physiology*, *281*(3), H1137–H1147. https://doi.org/10.1152/ajpheart.2001.281.3.H1137

Zhou, J., Li, A., Li, X., & Yi, J. (2019). Dysregulated mitochondrial Ca 2+ and ROS signaling in skeletal muscle of ALS mouse model. In *Archives of Biochemistry and Biophysics* (Vol. 663, pp. 249–258). Academic Press Inc. https://doi.org/10.1016/j.abb.2019.01.024

Zile, M. R., & Brutsaert, D. L. (2002). New concepts in diastolic dysfunction and diastolic heart failure: Part I: Diagnosis, prognosis, and measurements of diastolic function. *Circulation*, *105*(11), 1387–1393. https://doi.org/10.1161/hc1102.105289

Zinn, A. R., Alagappan,', R. K., Brown,', L. G., Wool, I., & Page', D. C. (1994). Structure and Function of Ribosomal Protein S4 Genes on the Human and Mouse Sex Chromosomes. In *MOLECULAR AND CELLULAR BIOLOGY*. https://journals.asm.org/journal/mcb

10. Figure index

11. Table index

12. Acknowledgments

13. Supplement

13.1. LC-MS and Spectronaut Parameters

Table 16. LC-MS/MS parameter heart. Data independet mode, quantitative data

Data independent analyses (DIA)	
reversed phase liquid chromatography	**Ultimate 3000 RSLC (Thermo Scientific)**
Trap column	75 µm inner diameter, packed with 3 µm C18 particles (Acclaim PepMap100, Thermo Scientific)
Analytical column	75 µm inner diameter, packed with 2.6 µm C18 particles (Accucore, 25 cm, Thermo Scientific)
Flow rate	300 nl/min
column oven temperature	40°C
buffer system	binary buffer system consisting of 0.1% acetic acid in HPLC-grade water (buffer A) and 100% ACN in 0.1% acetic acid (buffer B)
gradient	gradient of buffer B: 2min 2% to 5 %, 8min 5%, 120min 5% to 25%, 5min 25 to 40%, 2 min 40% to 90%, 5 min 90%, 1 min 90% to 2%, 7 min 2%
Mass spectrometer	Q Exactive Plus mass spectrometer (Thermo Scientific)
operation mode	data-independent
electrospray	Nanospray Flex Ion Source
Full MS	
MS scan resolution	70,000
Full MS AGC target	5.00E+06
maximum ion injection time for the MS scan	120 ms
Scan range	350 to 1650 *m/z*
Spectra data type	profile
dd-MS2	
Resolution	35,000

MS/MS AGC target	3.00E+06
maximum ion injection time for the MS/MS scans	auto
Spectra data type	profile
selection for MS/MS	1
isolation window	19 windows *m/z* 24-222
Fixed first mass	200
dissociation mode	higher energy collisional dissociation (HCD)
normalized collision energy	fixed, 27.5%
dissociation mode	HCD

Table 17. LC-MS/MS parameter TA. Data independent mode, quantitative data

Data independent analyses (DIA)	
reversed phase liquid chromatography	**Ultimate 3000 RSLC (Thermo Scientific)**
Trap column	75 µm inner diameter, packed with 3 µm C18 particles (Acclaim PepMap100, Thermo Scientific)
Analytical column	75 µm inner diameter, packed with 2.6 µm C18 particles (Accucore, 25 cm, Thermo Scientific)
Flow rate	300 nl/min
column oven temperature	40°C
buffer system	binary buffer system consisting of 0.1% acetic acid in HPLC-grade water (buffer A) and 100% ACN in 0.1% acetic acid (buffer B)
gradient	gradient of buffer B: 2min 2% to 5 %, 8min 5% to 7%, 60min 7% to 25%, 5min 25 to 40%, 2 min 40% to 90%, 6 min 90%, 2 min 90% to 2%, 10 min 2%
Mass spectrometer	Exploris 480 mass spectrometer (Thermo Scientific)
operation mode	data-independent

electrospray	Nanospray Flex Ion Source
Full MS	
MS scan resolution	120,000
Normalized AGC target	300 %
maximum ion injection time mode	custom
Scan range	350 to 1200 *m/z*
Spectra data type	profile
dd-MS2	
Resolution	35,000
MS/MS AGC target	3.00E+06
maximum ion injection time for the MS/MS scans	auto
Spectra data type	profile
selection for MS/MS	1
isolation window	65 windows *m/z* 13, overlap *m/z* 2
Fixed first mass	200
dissociation mode	higher energy collisional dissociation (HCD)
normalized collision energy	fixed, 30%
dissociation mode	HCD

Table 18. Spectronaut parameters heart. Peptide/Protein identification and intensity extraction.

Spectronaut 14.3.200701.47784	
Computer Name: AGVOE-SPECTRONA	
User Domain Name: AGVOE-SPECTRONA	
User Name: spectronaut	
Analysis Mode: UI	
Analysis Type: directDIA	

Settings Used:	
Pulsar Search\Peptides	
Toggle N-terminal M:	True
Min Peptide Length:	7
Max Peptide Length:	52
Missed Cleavages:	2
Digest Type:	Specific
Enzymes / Cleavage Rules:	Trypsin/P
DIA Analysis\Data Extraction	
MS1 Mass Tolerance Strategy:	Dynamic
Correction Factor:	1
MS2 Mass Tolerance Strategy:	Dynamic
Correction Factor:	1
Intensity Extraction MS1:	Maximum Intensity
Intensity Extraction MS2:	Maximum Intensity
DIA Analysis\XIC Extraction	
XIC IM Extraction Window:	Dynamic
Correction Factor:	1
XIC RT Extraction Window:	Dynamic
Correction Factor:	1
Pulsar Search\Modifications	
Max Variable Modifications:	5
Database	
Original File:	Uniprot_04_2020.fasta (*Mus musculus*)
Select Modifications:	
Fixed Modifications::	Carbamidomethyl (C)
Variable Modifications: :	Acetyl (Protein N-term), Oxidation (M)
DIA Analysis\Calibration	
MS1 Mass Tolerance Strategy:	System Default
MS2 Mass Tolerance Strategy:	System Default
DIA Analysis\Identification	
Machine Learning:	Per Run
Protein Qvalue Cutoff (Experiment):	0.01
Protein Qvalue Cutoff (Run):	0.05

Exclude Single Hit Proteins:	False
PTM localization	True
Probability cut-off	0.75
Pvalue Estimator:	Kernel Density Estimator
Precursor Qvalue Cutoff:	0.001
Single Hit Definition:	By Stripped Sequence
DIA Analysis\Quantification	
Amino acids	False
Interference Correction:	True
MS1 Min:	2
MS2 Min:	3
Fragment ions:	
Best N fragments per peptide	True
Min	6
Max	10
Ion Charge	False
Ion Type	False
Protein LFQ Method:	Automatic
Major (Protein) Grouping:	by Protein Group Id
Minor (Peptide) Grouping:	by Stripped Sequence
Modifications	None
Minor Group Top N:	False
Minor Group Quantity:	Sum precursor quantity
Major Group Top N:	True
Min:	2
Max:	3
Major Group Quantity:	Mean peptide quantity
Quantity MS-Level:	MS2
Quantity Type:	Area
Proteotypicity Filter:	None
Data Filtering:	Qvalue sparse
Imputing Strategy:	No Imputing
Cross Run Normalization:	False
DIA Analysis\Workflow	

MS2 DeMultiplexing:	False
Run Limit for directDIA Library:	-1
Method Evaluation:	False
Profiling Strategy:	iRT Profiling
Profiling Row Selection:	Minimum Qvalue Row Selection
Qvalue Threshold:	0.001
Profiling Target Selection:	Profile only non-identfied Precursor
Identification Criterion:	Qvalue
Threshold:	0.001
Carry-over exact Peak Boundaries:	False
Unify Peptide Peaks Strategy:	Select corresponding Peak
DIA Analysis\Post Analysis	
Calculate Sample Correlation Matrix:	True
Calculate Explained TIC:	None
Differential Abundance Grouping:	Major Group (Quantification Settings)
Smallest Quantitative Unit:	Precursor Ion (Quantification Settings)
Use All MS-Level Quantities:	False
Differential Abundance Testing:	Paired t-test
Group-Wise Testing Correction:	False
Run Clustering:	True
Distance Metric:	Manhattan Distance
Linkage Strategy:	Ward's Method
Z-score transformation:	False
Order Runs by Clustering:	True
DIA Analysis\Pipeline Mode	
Post Analysis Reports:	
Scoring Histograms:	True
Data Completeness Bar Chart:	True
Run Identifications Bar Chart:	True
CV Density Line Chart:	True
CVs Below X Bar Chart:	True
Generate SNE File:	True
Store Iontraces in SNE:	False
Report Schema:	C_FunGene_complex (Normal)

Reporting Unit:	Across Experiment

Table 19. Spectronaut parameters TA. Peptide/Protein identification and intensity extraction

Spectronaut 14.10.201222.47784	
Computer Name: AGVOE-SPECTRONA	
User Domain Name: AGVOE-SPECTRONA	
User Name: spectronaut	
Analysis Mode: UI	
Analysis Type: directDIA	
Settings Used:	
Pulsar Search\Peptides	
Toggle N-terminal M:	True
Min Peptide Length:	7
Max Peptide Length:	52
Missed Cleavages:	2
Digest Type:	Specific
Enzymes / Cleavage Rules:	Trypsin/P
DIA Analysis\Data Extraction	
MS1 Mass Tolerance Strategy:	Dynamic
Correction Factor:	1
MS2 Mass Tolerance Strategy:	Dynamic
Correction Factor:	1
Intensity Extraction MS1:	Maximum Intensity
Intensity Extraction MS2:	Maximum Intensity
DIA Analysis\XIC Extraction	
XIC IM Extraction Window:	Dynamic
Correction Factor:	1
XIC RT Extraction Window:	Dynamic
Correction Factor:	1
Pulsar Search\Modifications	
Max Variable Modifications:	5
Database	
Original File:	Uniprot_02_2021.fasta (Mus musculus)

Select Modifications:	
Fixed Modifications::	Carbamidomethyl (C)
Variable Modifications: :	Acetyl (Protein N-term), Oxidation (M)
DIA Analysis\Calibration	
MS1 Mass Tolerance Strategy:	System Default
MS2 Mass Tolerance Strategy:	System Default
DIA Analysis\Identification	
Machine Learning:	Per Run
Protein Qvalue Cutoff (Experiment):	0.01
Exclude Single Hit Proteins:	False
PTM localization	True
Probability cut-off	0.75
Pvalue Estimator:	Kernel Density Estimator
Precursor Qvalue Cutoff:	0.001
Single Hit Definition:	By Stripped Sequence
DIA Analysis\Quantification	
Amino acids	False
Interference Correction:	True
MS1 Min:	2
MS2 Min:	3
Fragment ions:	
Best N fragments per peptide	True
Min	6
Max	10
Ion Charge	False
Ion Type	False
Protein LFQ Method:	Automatic
Major (Protein) Grouping:	by Protein Group Id
Minor (Peptide) Grouping:	by Stripped Sequence
Modifications	None
Minor Group Top N:	False
Minor Group Quantity:	Sum precursor quantity
Major Group Top N:	True
Min:	2

Max:	3
Major Group Quantity:	Mean peptide quantity
Quantity MS-Level:	MS2
Quantity Type:	Area
Proteotypicity Filter:	None
Data Filtering:	Qvalue
Imputing Strategy:	No Imputing
Cross Run Normalization:	False
DIA Analysis\Workflow	
MS2 DeMultiplexing:	False
Run Limit for directDIA Library:	-1
Method Evaluation:	False
Profiling Strategy:	iRT Profiling
Profiling Row Selection:	Minimum Qvalue Row Selection
Qvalue Threshold:	0.001
Profiling Target Selection:	Profile only non-identfied Precursor
Identification Criterion:	Qvalue
Threshold:	0.001
Carry-over exact Peak Boundaries:	False
Unify Peptide Peaks Strategy:	Select corresponding Peak
DIA Analysis\Post Analysis	
Calculate Sample Correlation Matrix:	True
Calculate Explained TIC:	None
Differential Abundance Grouping:	Major Group (Quantification Settings)
Smallest Quantitative Unit:	Precursor Ion (Quantification Settings)
Use All MS-Level Quantities:	False
Differential Abundance Testing:	Paired t-test
Group-Wise Testing Correction:	False
Run Clustering:	True
Distance Metric:	Manhattan Distance
Linkage Strategy:	Ward's Method
Z-score transformation:	False
Order Runs by Clustering:	True
DIA Analysis\Pipeline Mode	

Post Analysis Reports:	
Scoring Histograms:	True
Data Completeness Bar Chart:	True
Run Identifications Bar Chart:	True
CV Density Line Chart:	True
CVs Below X Bar Chart:	True
Generate SNE File:	True
Store Iontraces in SNE:	False
Report Schema:	C_FunGene_complex (Normal)
Reporting Unit:	Across Experiment

13.2. Plasmid charts

pcDNA™3.1/myc-His(-) (Invitrogen,Carlsbad, CA, USA) is a mammalian overexpression vector, which contains the sequence of the myc and six histidine epitomes. To ensure a high replication of the inserted gene in mammal cells, the multiple cloning side (MCS) is regulated by the Cytomegalovirus-Promotor. The SV40-, pUC- and f1-origin of replication enable replication in mammal cells, *E. coli* and of single stranded DNA. Via the coding sequences (CDS) for neomycin and ampicillin selection in mammal and bacterial cells is possible.

pcDNA™3.1(+)Flag (Invitrogen,Carlsbad, CA, USA) is a mammalian overexpression vector, which contains the sequence of the flag epitome. To ensure a high replication of the inserted gene in mammal cells, the multiple cloning side (MCS) is regulated by the Cytomegalovirus-Promotor. The SV40-, pUC- and f1-origin of replication enable replication in mammal cells, *E. coli* and of single stranded DNA. Via the coding sequences (CDS) for neomycin and ampicillin selection in mammal and bacterial cells is possible.

pEGFP-N3 Plasmid (gift from AG Cammann) is a mammalian overexpression vector, which contains the sequence of EGEFP. To ensure a high replication of the inserted gene in mammal cells, the multiple cloning side (MCS) is regulated by the Cytomegalovirus-Promotor. The SV40- and f1-origin of replication enable replication in mammal cells, *E. coli* and of single stranded DNA. Via the coding sequences (CDS) for neomycin and kanamycin selection in mammal and bacterial cells is possible.

pMP71 IRES GFP (gift from Prof. Dr. Il-Kang Na, Charité Berlin) is a retroviral overexpression vector, which contains the sequence of EGFP. To ensure a high replication of the inserted gene in mammal cells, the multiple cloning side (MCS) is regulated by the Lac-Promotor. Via the coding sequence (CDS) for ampicillin selection in bacterial cells is possible.

13.3. MuRF interaction partners

Table 20. Possible MuRF interaction partners.

	TA			Heart		
	All	Male	Female	All	Male	Female
	log2 ratio (DKO vs control)					
Actin, alpha	**-0,71**	-1,10	-0,47	-0,34	-0,44	-0,29
ADSS	0,07	0,00	0,08	0,10	0,19	-0,08
ATPMB						
BRD4						
Calsarcin-2/Myozenin 1						
Cardiac troponin I				**-0,45**	-0,40	**-0,52**
CARP						
COX4I1	**-0,35**	**-0,49**	-0,25	**-0,68**	**-0,73**	**-0,50**
Creatine kinase, brain						
Creatine kinase, muscle						
CTNNB1	-0,11	-0,24	0,85	-0,24	-0,39	-0,21
DAXX						
DCAF8				-0,52	-0,86	-0,18
Desmin	**0,97**	**1,06**	**0,87**	-0,23	-0,08	-0,25
DOCK7						
DVL3						
DYNLL1						
EEF1G	**0,17**	0,12	**0,26**	-0,04	-0,09	0,01
EIF2C2						
Enoyl Co-A hydratase I						
Fast skeletal troponin I						
FHL2				**-1,96**	-1,22	**-2,32**
Filamin A+B+C						
FRMD6						
GATA3						
GMEB-1						
GMF1/EFG1						
HNRPLL						
HSPB1	**1,94**	**1,91**	**2,05**	**0,40**	**0,49**	**0,46**

IGF2						
ILF3						
INT6/elF3S6						
IQWD1/NRIP						
KCTD15						
KIF1B						
LMCD1/Dyxin	**1,36**	**1,42**	**1,28**	0,23	0,03	0,45
MICAL2						
MRL-LP2						
MRP-L19						
MRP-L41				-0,38	-0,20	-0,30
Myosin binding protein C 1/3						
Myotilin	0,16	0,05	**0,24**	0,31	-0,33	**0,80**
NDUFA1						
Nebulette				**-0,38**	-0,39	**-0,38**
Nebulin						
NEDD8	0,03	0,04	0,01	0,22	0,32	0,11
NEFL	0,09	-0,72	0,81			
NOMO	**-0,58**	**-0,53**	-0,30	-0,33	-0,29	-0,37
NR1D2						
ODF2						
p62/SQSTM1	**0,83**	1,03	0,59	**0,89**	0,71	**1,07**
PABPC3						
PAFAH1B2	**0,22**	**0,33**	0,10	0,26	0,22	0,04
PIAS-1+3+X						
PKM2						
PLXNA3						
PRDX5	**-0,41**	**-0,61**	-0,22	-0,25	-0,19	-0,36
PRKACA	**0,25**	**0,32**	**0,20**	-0,07	-0,14	-0,08
PRMT5	**0,39**	0,15	**0,63**			
RBM15B						
RPL27A	**0,37**	0,33	**0,48**	0,02	0,03	0,01
RPS26	**0,53**	**0,56**	**0,51**	0,10	0,05	0,15

RPS4X	**0,66**	**0,63**	**0,53**	0,06	-0,01	-0,01
SEC23B						
SERBP1	0,27	0,23	0,27	0,18	0,23	0,05
Slow skeletal troponin T1						
SNW1						
SNX18						
Telethonin	-0,17	**-0,38**	0,03	-0,13	-0,14	-0,27
Titin M8-M10						
TRIM23						
TRIM41						
TSC22D4						
UQCRC1	**-0,65**	**-0,80**	**-0,47**	**-0,63**	-0,49	**-0,73**
UXT/ART-27						
VCP	0,15	0,12	0,15	**0,23**	0,22	0,23
ZNF655						

List of possible MuRF interaction partners, created with the yeast two-hybrid screening data of Nowak et al. 2019 and Witt et al. 2008. Bold marked proteins are significantly upregulated or downregulated in heart or TA.

14. Conference contributions and Publications

Conference contributions:

6th Young DZHK Retreat, Potsdam, 11-12.09.2019; poster presentation

8th Young DZHK Retreat, Potsdam, 14-15.09.2019; poster presentation

Publications:
SPSB1-mediated inhibition of TGF-β receptor-II impairs myogenesis in inflammation, Journal of Cachexia, Sarcopenia and Muscle (2023), Coauthor (Position 5)